Contact Analysis of CNT-Based Nanocomposites

Thesis submitted by

RAKESH BHADRA

Doctor of

Philosophy

(Engineering)

DEPARTMENT OF MECHANICAL ENGINEERING

FACULTY COUNCIL OF ENGINEERING &TECHNOLOGY

JADAVPUR UNIVERSITY

KOLKATA, INDIA

July, 2025

JADAVPUR UNIVERSITY

KOLKATA-700032, INDIA

INDEX NO. 286/21/E

1. Title of the Thesis: Contact Analysis of CNT-Based Nanocomposites

2. Name, Designation & Institution of the Supervisor(s):

i. Prof. Prasanta Sahoo,

Professor, Department of Mechanical Engineering,

Jadavpur University, Kolkata-700032

ii. Dr. Anirban Mitra

Associate Professor, Department of Mechanical Engineering,

Jadavpur University, Kolkata-700032

3. List of Publications (Referred Journals):

i. **Bhadra, R.,** Jana, T., Mitra, A., & Sahoo, P. (2022). Flattening cylindrical contact analysis of single walled carbon nanotube (SWCNT) nanocomposite. ***International Journal of Surface Engineering and Interdisciplinary Materials Science (IJSEIMS)***, *10*(1), 1-22. **(Scopus)**

ii. **Bhadra, R.**, Jana, T., Mitra, A., & Sahoo, P. (2023). Effect of CNT radius on flattening contact behaviour of CNT-Al nanocomposite: A numerical approch. ***Reports in Mechanical Engineering*****,** *4*(1), 121-130. **(Scopus)**

iii. **Bhadra, R.,** Jana, T., Mitra, A., & Sahoo, P. (2024). Contact analysis of CNT-FGM nanocomposite using indentation contact model. ***Procedia Structural Integrity***, *60*, 149-164. **(Scopus)**

iv. **Bhadra, R**., Jana, T., Mitra, A., & Sahoo, P. (2024). Finite element based indentation contact analysis of SWCNT nano-composite. ***Proceedings of the Institution of Mechanical Engineers, Part C: Journal of Mechanical Engineering Science***, *238*(4), 1125-1141. **(SCI)**

v. **Bhadra, R**., Jana, T., Mitra, A., & Sahoo, P. (2024). Loading-unloading contact analysis of functionally graded carbon nanotube reinforced composite (FG-CNTRC). ***Physica Scripta*****,** *99*(10), 105050, 1-17. **(SCI)**

vi. **Bhadra, R**., Jana, T., Mitra, A., & Sahoo, P. (2025). Carbon nanotube (CNT) reinforced functionally graded material matrix composite (CNTR-FGMMC) under flattening contact. ***Physica Scripta*****,** *100***,** 095022, 1-15. **(SCI)**

4. List of Book Chapters

i. **Bhadra, R.**, Jana, T., Mitra, A., & Sahoo, P. (2024). Contact analysis of functionally graded carbon nanotubes reinforced composite (FG-CNT). *In: Sahoo, P. and Barman, T. K. (Eds.),* ***Advances in Materials, Manufacturing and Design. Singapore: Springer Nature*****,** 793-805.

5. List of Publications in Proceeding

i. **Bhadra, R.,** Jana, T., Mitra, A., & Sahoo, P. (2024). Unloading analysis of functionally graded carbon nanotubes reinforced composite (FG-CNT), Proceedings of INCOM 2024, Jan 5-6, Kolkata, 287-290, J. U. Press, (ISBN: 978-81-954806-6-1).

6. List of Patents: Nil

7. List of Presentations in National/International Conferences:

i. **Bhadra, R.**, Jana, T., & Mitra, A. Indentation based contact simulation of CNT based nano-composite. In: National Conference on Sustainable Development and Circular Economy in Civil Engineering (SDCE 2021), Kolkata 2021.

ii. **Bhadra, R.**, Jana, T., Mitra, A., & Sahoo, P. Effect of CNT radius on flattening contact behaviour of CNT-Al nanocomposite. In: 1st International Conference On Mechanical Design and Manufacturing (ICMDM 2023), Howrah-2023.

iii. **Bhadra, R.**, Jana, T., Mitra, A., & Sahoo, P. Indentation-based contact analysis of CNT-FGM nanocomposite. In: The 3rd International Conference on Structural Integrity (ICONS 2023), Kalpakkam (Anupuram)-2023.

iv. **Bhadra, R.,** Jana, T., Mitra, A., & Sahoo, P. Unloading analysis of functionally graded carbon nanotubes reinforced composite (FG-CNT), In: 2nd International Conference on Mechanical Engineering (INCOM-2024), Jadavpur-2024.

STATEMENT OF ORIGINALITY

I, **Rakesh Bhadra** registered on 30.07.2021 do hereby declare that this thesis entitled **"Contact Analysis of CNT-Based Nanocomposites"** contains literature survey and original research work done by the undersigned candidate as part of Doctoral studies.

All information in this thesis have been obtained and presented in accordance with existing academic rules and ethical conduct. I declare that, as required by these rules and conduct, I have fully cited and referred all materials and results that are not original to this work.

I also declare that I have checked this thesis as per the "Policy on Anti Plagiarism, Jadavpur University, 2019", and the level of similarity as checked by iThenticate software is **1%.**

Rakesh Bhadra

Signature of Candidate: … … … … … … … … … … … … … … …

(Rakesh Bhadra)

Date: 14-07-2025

Certified by Supervisors:

Prasanta Sahoo 13/7/2025

Prof. Prasanta Sahoo
(Signature with date, seal)
Professor
Dept. of Mechanical Engineering
Jadavpur University, Kolkata-32

Anirban Mitra 14/07/2025

Dr. Anirban Mitra
(Signature with date, seal)
Associate Professor
Dept. of Mechanical Engineering
Jadavpur University, Kolkata-32

This page is left blank intentionally

CERTIFICATE FROM THE SUPERVISORS

This is to certify that the thesis entitled **"Contact Analysis of CNT-Based Nanocomposites"** submitted by **Rakesh Bhadra**, who got his name registered on **30. 07. 2021** for the award of Ph.D. (Engineering) degree of Jadavpur University is absolutely based upon his own work under our supervision and that neither his thesis nor any part of the thesis has been submitted for any degree/diploma or any other academic award anywhere before.

Signature of the Supervisors……

Prasanta Sahoo 14/07/2025

(Prof. Prasanta Sahoo)

Date with Office Seal

Professor
Dept. of Mechanical Engineering
Jadavpur University, Kolkata-32

Anirban Mitra 14/07/2025

(Dr. Anirban Mitra)

Date with Office Seal

Associate Professor
Dept. of Mechanical Engineering
Jadavpur University, Kolkata-32

This page is left blank intentionally

Acknowledgement

The journey toward completing my PhD thesis work has been an incredibly enriching experience. This path would not have been as pleasant and complete without the support of certain individuals. I would like to take this opportunity to express my heartfelt gratitude to those who stood by me whenever I needed them throughout this journey.

First and foremost, I am immensely grateful to my supervisors, Prof. Prasanta Sahoo and Dr. Anirban Mitra, for their generous assistance, constant encouragement, insightful inputs and unwavering belief in my abilities. Every interaction with them has been a valuable learning experience. Without their guidance, I could not have successfully completed my thesis work. I consider myself extremely fortunate to have had the opportunity to work under their guidance. Their vast knowledge and commitment to excellence have consistently inspired me throughout this journey.

I extend my sincere gratitude to AICTE for initiating the QIP-PhD scheme for faculty to pursue their Ph.D. and for granting me this opportunity. I am also deeply grateful to the Head of the Department of Mechanical Engineering, Tezpur University for permitting me to pursue my Ph.D. under the QIP scheme.

My heartfelt thanks go to the HoD, as well as all the academic and technical staff of the Mechanical Engineering Department, Jadavpur University, particularly the faculty members and lab-in-charge of the Machine Elements Laboratory, for their assistance in completing my thesis work.

I am deeply thankful to Dr. Tamonash Jana for his pivotal role in facilitating my understanding of contact analysis in ANSYS. His guidance and support were invaluable at every stage of my journey, specially when overcoming challenges related to ANSYS and my research. His assistance was crucial during difficult times throughout this journey.

I would like to thank all my friends, juniors, seniors and colleges during my academic journey, particularly Dr. Arpan Kumar Mondal, Dr. Sanjib Banerjee, Dr. Satya Sundar Bhattacharya, Dr. Polash Pratim Dutta, Dr. Sushen Kirtania, Dr. Paragmoni Kalita, Dr. Biraj Kumar Kakati, Dr. Angshuman Roy, Dr. Sushanta Ghuku, Dr. Palash Biswas, Dr. Manik Barman, Dr. Suswagata Poria, Dr. Sudip Banerjee, Dr. Abhishek Mondal, Mr. Rakesh Sikder, Mr. Md Rakim, Mr. Sudipta Roy, Mr. Soumyabrata Chakravarty, Mr. Kumar Abanindra Jana, Mr. Sagnik Ghatak, Mr. Rajesh Roy, Mr. Sudip Halder and Mr.(Late) Suman Nihar .

I also like to thank my all the teachers, particularly Prof. (Late) Asish Bandyopadhyay, Mr. (Late) Swapan Kumar Das, Prof. Apurbo Kishor Dutta, Prof. Bijan Kumar Mondal and Dr. Ashim Guha.

I would like to express my deepest appreciation to my wife, Dr. Rituparna Das, for her understanding, support, help, and patience throughout this entire journey. Her unwavering support made it possible for me to complete this work successfully. I also want to extend my love to our sweet and beautiful daughter, Ritisha Bhadra, who has been a source of inspiration in pursuing this endeavor.

Finally, I am profoundly thankful to my parents, Mr. Raimohan Bhadra and Mrs. Suniti Bhadra, my brothers, Mr. Rajat Bhadra and Mr. Rajib Bhadra, my brother-in-law, Mr. Deb Gopal Das, and all my family members for their unwavering love, patience, and support.

Above all, I am thankful to the Almighty.

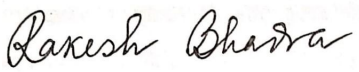

RAKESH BHADRA

Abstract

Carbon nanotubes (CNTs), when used as reinforcement materials in nanocomposites, significantly enhance these overall properties. When combined with a suitable matrix, demonstrate superior performance compared to other nanocomposites. This improvement is primarily due to CNTs' high strength-to-weight ratio, excellent electrical conductivity, and outstanding thermal characteristics. Another advanced material of interest is functionally graded material (FGM). CNTs reinforced FGM—either through graded distribution of CNTs in the elasto-plastic material or uniform dispersion within the FGM matrix—are attracting substantial research focus. These materials offer promising possibilities for applications requiring gradual changes in material properties. While the use of CNTs as reinforcement is rapidly expanding across various industries, most research has focused on determining the mechanical properties of CNT-based nanocomposites through numerical, analytical, or experimental methods. Understanding contact behavior is crucial for CNT-based nanocomposite applications. Experimental challenges make finite element (FE) analysis a preferred approach. FE models simulate indentation and flattening contacts effectively. These simulations help predict contact performance in complex conditions. Such insights are valuable for optimizing industrial nanocomposite designs.

This study investigates both indentation and flattening contact behavior of CNT-based nanocomposites through single-asperity contact model. Contact analyses are performed for three types of material configurations: (1) CNTs uniformly distributed in an aluminum matrix composite, (2) graded distribution of CNTs within the homogeneous matrix, and (3) CNTs uniformly distributed in a functionally graded material (FGM) matrix composite (CNTR-FGMMC). The single-asperity contact models (Indentation and flattening) are developed in ANSYS using APDL code. During flattening and indentation, the summit (in flattening) and indenter (in indentation) are treated as rigid bodies, with downward displacement applied for loading and upward movement used to observe contact behavior through unloading.

To carry out the present simulations, several assumptions have been made regarding the interaction between the embedded CNTs and the surrounding matrix material. It is assumed that a perfect bond exists between the CNTs and the matrix, implying no interfacial slip. Additionally, a frictionless (full slip) contact condition is considered between the indenter/summit and the substrate to simplify the contact interaction. The contact behavior in the simulation is implemented using a pure Lagrange multiplier contact algorithm, ensuring accurate enforcement of contact constraints. To capture the onset of plastic deformation, the

von Mises yield criterion is employed, with the material's post-elastic response modeled using bilinear isotropic hardening. Model validation is achieved by comparing results with published literature, and convergence analyses are conducted to optimize computational time.

The preliminary analysis focuses on the effects of CNT thickness and radius within the CNT-reinforced Al matrix composite using indentation based contact model. Key contact parameters such as contact force, contact area, contact pressure, and deformation behavior are extracted by varying the wall thickness of CNTs. Detailed examination of these results reveals the presence of sink-in and pile-up behavior in specific cases and CNTs thickness affect significantly. The flattening action is simulated using a rigid flat. It is observed that beyond a certain CNT thickness, an increase in volume fraction of CNTs enhances both the contact force and contact area. Furthermore, a higher percentage of CNTs causes more matrix material within the asperity to yield plastically.

The present work also explores the spherical indentation contact behavior of a functionally graded CNT reinforced composite (FG-CNTRC) substrate. The composite gradation is achieved by varying the distribution of CNTs within the aluminium matrix. A comprehensive investigation is performed for three CNT distribution types—uniform, increasing, and decreasing with depth—to assess their influence on various contact parameters. This study aims to assist in the modeling and fabrication of FG-CNTRC substrates tailored for specific and damage-resistant contact performance.

The study extends to simulate the flattening contact of a CNT-reinforced functionally graded material (CNTR-FGMMC) using a finite element-based cylindrical model. This analysis emphasizes the impact of matrix gradation index, modeled as an elastically graded material where the modulus of elasticity and tangent modulus vary while yield strength remains constant. The flattening simulations are performed by varying the elastic inhomogeneity while keeping the CNT wall thickness constant. The results demonstrate how changes in the gradation parameter significantly affect contact behaviour of the composite. To further explore the indentation contact behavior of CNTR-FGMMC, a 3D finite element model is developed using APDL in ANSYS. Results show that positive gradation improves both contact force and contact area when compared with other graded and without graded systems, although it demonstrates a higher force but lower area when compared to the only matrix material. These findings offer critical insights for designing nanocomposites with specific performance goals.

About the Author

Sri Rakesh Bhadra was born in the village of Chowberia in the North 24 Parganas district of West Bengal in 1984. He holds both B.E. and M.E. in Mechanical Engineering from Bengal Engineering and Science University, Shibpur (now the Indian Institute of Engineering Science and Technology, Shibpur), West Bengal.

He has previously served as an Assistant Professor in the Department of Mechanical Engineering, Durgapur Institute of Advanced Technology and Management, Durgapur, West Bengal and Academy of Technology, Adisaptagram, West Bengal.

Currently, he is an Assistant Professor in the Department of Mechanical Engineering, Tezpur University, located in Tezpur, Assam, India. Additionally, he holds an honorary position as Senior Engineering Consultant at Resolin Technologies, Jorhat, India.

He was granted QIP-PhD fellowship from AICTE for pursuing this thesis work at Jadavpur University for three years (2020-2023). The present thesis is the outcome of that research study performed at Department of Mechanical Engineering, Jadavpur University.

His research primarily focuses on the numerical and experimental analysis of materials, welding, contact mechanics and environmental sustainability. He has contributed to 15 peer-reviewed journal articles, 8 conferences, and 3 book chapters. He has successfully completed one project (as P.I.) funded by the Research and Innovation Grant, Tezpur University, and is currently working on three (as P.I. & Co-P.I.) ongoing projects funded by the external funding agency.

This page is left blank intentionally

Dedicated to

My Parents,

Teachers,

Wife

&

Daughter

This page is left blank intentionally

Table of Contents

This page is left blank intentionally

List of Figures

List of Tables

This page is left blank intentionally

Chapter 1

Introduction

1.1 Introduction

Carbon Nanotube (CNT) based nanocomposites have gained significant attention in modern technology due to their advanced properties and potential applications. Carbon nanotubes, with their exceptional mechanical, electrical and thermal properties, have garnered significant interest in various engineering applications, including structural materials, electronics and biomedical devices (Nieto et al., 2021; Saba et al., 2016). When incorporated into a composite matrix, CNTs can significantly enhance mechanical properties such as stiffness, strength, and toughness, making them promising candidates for next-generation materials (Zuberi and Esat, 2015).

Selection of appropriate material is crucial for modern industrial applications, which often involve contact between surfaces. Engineering surfaces are inherently rough in nature and due consideration is necessary in this regard to analyse real-life contact situations. Presence of relative motion between contacting surfaces, such as belts, bearings, gears, and cam-follower mechanisms (Song et al., 2013) introduce additional complexities. Contact effects can lead to the failure of components, making contact analysis essential before choosing materials for specific applications. Contact between rough surfaces is often modeled as single asperity contact, where, a solitary peak is considered in contact with a flat and behaviour of the single asperity is representative the contact behaviour of the rough surface as a whole. The other alternative in analysing contact of rough surfaces is multi-asperity contact, where, a number of asperities or peaks in contact with a flat is considered. However, due to ease of analysis, single asperity analysis is, by far, the more popular option.

In the context of CNT-based nanocomposites, examining the effect of carbon nanotubes within the matrix material as the composite contacts other surfaces, whether rigid or deformable, is an important consideration. Understanding this interaction is vital for predicting the overall mechanical response of the composite material. Several factors influence the behavior of CNT-based nanocomposites in contact, including the geometry and properties of the contacting surfaces, as well as the orientation and density of carbon nanotubes within the matrix. Theoretical models, computational simulations and experimental techniques are employed by different research groups across the world to

investigate these interactions, providing insights into phenomena such as adhesion, friction, wear, and deformation mechanisms at the nanoscale.

In the present thesis, single asperity contact of CNT-based nanocomposites is simulated with the objective of understanding their behavior and performance. Such an analysis offers valuable insights into the material's tribological properties, which are critical for applications where friction and wear resistance play a significant role (such as in aerospace components, automotive parts and biomedical implants). Furthermore, the present analysis provides a stepping stone that might aid in future studies for optimizing design and manufacturing processes to harness the full potential of CNT-based nanocomposites in various engineering applications and thus contributing to the advancement of materials science and technology.

1.2 Nanocomposite

Nanocomposites combine nanoscale components (Such as CNTs, B_4C) with a matrix material (Such as Al, Mg, Functionally Graded Material (FGM)) to achieve enhanced properties or functionalities. Their unique combination of properties results from the synergistic effects between the nanoscale fillers and the matrix. Compared to their conventional counterparts, nanocomposites can be engineered to exhibit improved mechanical, thermal, electrical, optical and barrier properties.

1.2.1 CNT

Carbon nanotubes (CNTs) are cylindrical structure, composed of carbon atoms arranged in hexagonal patterns, exhibiting exceptional mechanical, electrical, thermal and optical properties. They come in single-walled (SWCNTs) or multi-walled (MWCNTs) forms, with diameters ranging from 0.4 to several nanometres. CNTs possess extraordinary tensile strength, surpassing that of steel and high electrical conductivity, making them promising candidates for applications in electronics, such as transistors and interconnects. Additionally, their outstanding thermal conductivity and stability enable utilization in thermal management systems and composite materials for aerospace and automotive industries. CNTs are also explored for energy storage and biomedical applications due to their high surface area, chemical stability and biocompatibility. Despite their remarkable properties, challenges persist in large-scale synthesis, purification and dispersion, as well as concerns regarding their toxicity and environmental impact, requiring continued research and development efforts.

1.2.2 CNT-Aluminium (Al) Nanocomposites

Al is widely used in nanocomposites due to its excellent properties such as low density, high strength-to-weight ratio, good corrosion resistance and excellent thermal and electrical conductivity. When combined with nanoparticles like CNTs, Al-based nanocomposites exhibit significantly enhanced mechanical, thermal and electrical properties (Kirtania & Chakraborty, 2018). For instance, studies have demonstrated that incorporating CNTs into an Aluminium matrix can substantially improve the composite's mechanical strength and stiffness. This is primarily due to the superior mechanical properties of CNTs and their ability to effectively transfer load within the composite. Additionally, the high thermal conductivity of CNTs enhances the overall thermal performance of the Al nanocomposite, making it suitable for applications requiring efficient heat dissipation (Yang et al., 2013).

Some research has looked at how the amount of carbon nanotubes (CNTs) in nanocomposites affects their properties, including the issue of CNT agglomeration. Rubel et al. (2019) point out that even small amounts of CNTs can have noticeable effects, which become worse as their volume increases. Hassanzadeh-Aghdam et al. (2019) created a micromechanical model that shows how CNT agglomeration can lower the creep resistance of polymer nanocomposites, highlighting the importance of considering how well the CNTs are dispersed. Kumar (2023) used a multiscale finite element model to demonstrate the strong impact of CNT agglomeration on the elastic properties of these materials. Zeinedini et al. (2018) discovered that while well-dispersed CNTs can enhance the fracture toughness of epoxy nanocomposites, agglomeration can reduce it, and this was backed up by a theoretical model. Lastly, Yousefi et al. (2020) studied how CNT agglomeration affects the vibration characteristics of laminated conical shells using various theoretical and numerical methods.

There are various methods for developing nanocomposites using Aluminium (Al) as the matrix material, with carbon nanotubes (CNTs) as the reinforcing agent. The distribution of CNTs within the matrix is typically random. As the volume percentage of CNTs increases, significant improvements in material properties are observed; however, beyond a certain threshold, agglomeration effects, as reported in the literature (Rubel et al., 2019; Kumar, 2023; Yousefi et al., 2020), may occur. To simplify analytical and numerical modelling, researchers often assume uniform distribution of CNTs throughout the Aluminium matrix, providing consistent reinforcement across the material. In other approaches, CNTs are arranged in specific patterns or distributed randomly within the nanocomposite.

1.2.3 CNT-FGM Nanocomposites

Functionally graded materials (FGMs) are engineered materials designed with a gradual variation in composition, microstructure or properties over their volume, providing tailored performance suited to specific applications. Unlike traditional homogeneous materials, FGMs exhibit unique combinations of mechanical, thermal, electrical and optical properties that vary systematically from one end to another. This gradient design allows for optimized performance under varying environmental conditions or loading scenarios, minimizing stress concentrations and enhancing durability. FGMs find applications in diverse fields, including aerospace, automotive, biomedical and energy industries, where they are utilized in components such as turbine blades, heat shields, dental implants and battery electrodes. Research in FGMs focuses on optimizing fabrication methods, understanding the underlying material behavior and exploring novel applications to harness their full potential in addressing complex engineering challenges.

Functional gradation in CNT reinforced nanocomposites can be obtained through two distinct approaches. In the first approach CNTs are distributed and oriented within the matrix material in a way that enables the overall nanocomposite to exhibit graded behavior. In this case the matrix material itself is homogeneous in nature. But, strategic arrangement of CNTs significantly enhances the mechanical properties, resulting in a composite that not only maintains structural integrity but also optimizes performance under various conditions. The second approach utilizes the FGM itself as the matrix material, with CNTs uniformly distributed throughout this matrix. This uniform distribution is intended to provide consistent reinforcement, maximizing the interaction between the CNTs and the matrix. As a result, such CNT reinforced FGM nanocomposite may lead to notable improvements in thermal, mechanical and electrical properties, making the composite more versatile and effective for various applications. Fabrication of both types of CNT-FGM nanocomposite is a challenging task.

1.3 Contact Analysis

Contact between surfaces of machine components is associated with certain phenomena (such as adhesion, abrasion, wear etc.) that greatly affect the lifespan of these parts. The inherent roughness or undulations of the surfaces enhances the complexity and makes it even more critical. The overall effect is that the actual behavior at the contact interface differs significantly from large-scale engineering assumptions.

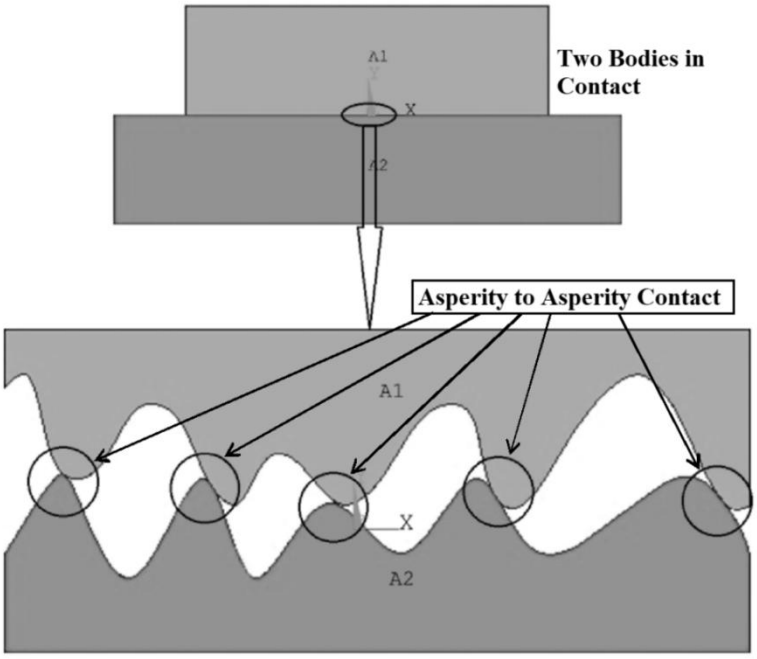

Figure 1.1: Magnified view of the contact surface.

The presence of surface roughness leads to a much smaller actual contact area compared to the apparent contact area (Figure 1.1). As a result, the contact pressures and stresses at the contact points can be significantly higher, while they remain relatively low at other areas of the surface. Furthermore, the contact situation is further complicated by factors such as friction, adhesion, varying loading conditions, and different material behaviors. Complexities involved in contact phenomenon makes modelling and analysing the contact behavior a challenge and these characteristics create considerable opportunities for research aimed at gaining deeper insights into contact behavior.

Contact analysis involving both single- and multi-asperity contacts is essential for understanding the mechanical behavior of materials under various loading and unloading conditions. Single asperity contact refers to the interaction between two surfaces at a single point, where one microscopic protrusion (asperity) on one surface contacts a corresponding point on the other surface. In contrast, multi-asperity contact involves multiple contact points at the microscopic scale, accounting for the complex interactions between numerous asperities on the surfaces in contact. This concept is fundamental in understanding contact mechanics, as it simplifies the analysis of surface interactions and provides valuable insights into material behavior during loading and unloading.

There are two common approaches for analysing a single asperity contact and these are the indentation and flattening contact models.

- **Indentation Contact Analysis:** Indentation contact is used to study the behavior of materials under the influence of localized loads, typically represented by an indenter. The primary objective of an experimental indentation process is to understand how materials deform and respond to contact forces, such as those exerted by a sharp or blunt indenter. The simulation of the same process involves accurately capturing the interaction between the indenter and the material surface, considering factors such as material properties, indenter geometry, loading conditions and environmental effects. Simulation of such kind of contact is a popular domain of research as this type of contact is widely observed in various fields, including material science, mechanical engineering and nanotechnology and it also realistically acts as a tool for determination of important material properties. Finite element analysis (FEA) and molecular dynamics (MD) simulations are commonly employed techniques for conducting such analyses. Usually, indentation simulation models consist of a deformable substrate and a rigid indenter capable of executing vertical movement (as shown in Figure 1.2(a)). Applications of indentation contact analysis range from characterizing the mechanical properties of bulk materials to assessing the performance of thin films, coatings and biomaterials. It is instrumental in material design, quality control and optimization of manufacturing processes, as well as in the development of advanced materials for specific applications.
- **Flattening Contact Analysis:** Flattening contact analysis is a technique used to study the behavior of materials when subjected to compressive forces that result in a significant area of contact and deformation. Unlike indentation contact analysis, where the focus is on localized loading by an indenter, flattening contact considers broader contact areas and the resulting deformation patterns. In flattening contact analysis, a compressive force is applied to the material, leading to the flattening of its surface and the redistribution of stresses within the material. Simulation of the flattening process is usually on the basis of a model with a deformable asperity (hemispherical or cylindrical) and a rigid flat able to execute up and down motion (Figure 1.2(b)). This analysis is essential for understanding the mechanical response of materials under conditions such as compression testing, forming processes, and surface treatments. Flattening contact analysis finds applications in various industries, including manufacturing, aerospace, automotive and biomechanics. It is used to optimize processes such as forming, stamping, forging and rolling, as well as to predict the performance of components under loading conditions encountered during service. Additionally, it aids in material selection, design optimization, and failure analysis to ensure the reliability and durability of engineering systems.

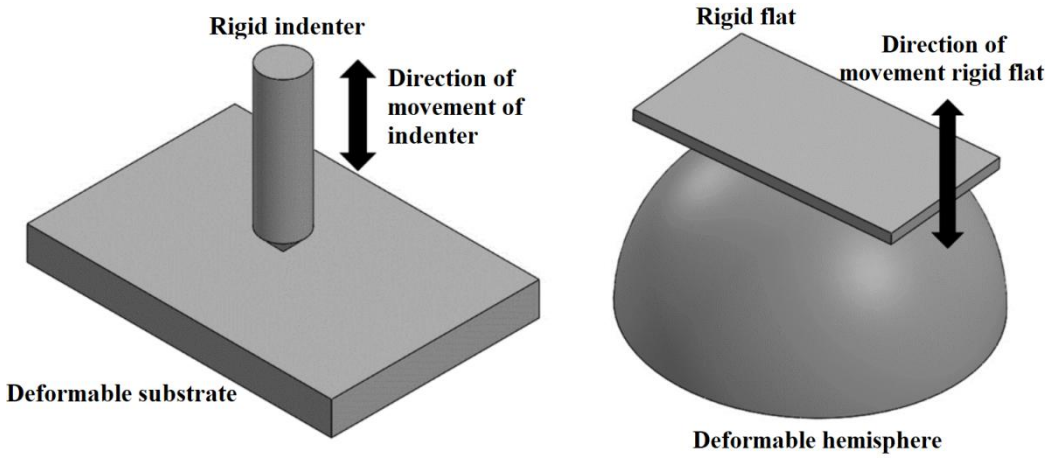

Figure 1.2: Schematic representation of (a) Indentation and (b) Flattening contact

1.4 Literature Review

To understand the context of the present thesis, it's very important to review past research in the relevant field. This helps clarify the study's goals and plan the work. The contact behavior of CNT-reinforced nanocomposites is the key focus area of the present research work. It warrants that literature survey should be taken up along two distinct verticals, contact analysis (covering both indentation and flattening) and CNT-based nanocomposites and also explore the overlap, if any, of the two above-mentioned vast domains. Research on mechanical properties of CNT-based nanocomposites, using numerical simulations with tensile and compression tests, has been ongoing since these materials were discovered. While Aluminium is important as matrix material for its mechanical and chemical properties, other materials are also being explored. On the other hand, contact analysis itself is a field of study that has seen over a century of research resulting in a massive body of work. Contact analysis, especially with CNTs as a reinforcing material in Aluminium and FGM matrix, is a relatively new but growing field. So, it is impractical, if not impossible, to exhaustively review all such work within the confines of a single chapter. Nor is that the goal of the following sections. The objective is to highlight the most relevant research papers and to set up the backdrop of the present thesis work. Hence, a structured and extensive literature review is taken up and described in the following sections. This literature review is divided into four sections: indentation contact analysis, flattening contact analysis, CNT-Al nanocomposites and CNT-FGM nanocomposites.

1.4.1 Literature on Indentation Contact Analysis

Indentation contact analysis is critical for advancing material science, especially in applications involving relative motion between contacting surfaces like belts, bearings, gears, and cam-follower mechanisms (Song et al., 2013). Shtaerman (1949) provided the first closed-form solution for conical indentation, with subsequent studies incorporating complexities like surface tension effects (Borodich et al., 2004; Vasiliev et al., 2017). Early work by Hardy et al. (1971) and Johnson (1985) laid the foundation for understanding sequential domains of contact behavior in indentation processes. Ramamurty and Jang (2014) reviewed experimental nanoindentation techniques and post-experiment data analysis, enhancing the understanding of molecular crystal mechanics. Further research by Song and Komvopoulos (2013, 2014) identified four distinct deformation regimes: linear elastic-plastic, nonlinear elastic-plastic, transient fully plastic, and steady-state fully plastic. The study of contact phenomena, particularly at different scales, is critical for advancing material science, including nanocomposites known for their superior properties. Research has shown that carbon nanotube (CNT) embedded matrix materials significantly enhance mechanical, thermal, and electrical properties (Kirtania & Chakraborty, 2018). Therefore, investigating the contact behavior of CNT-based nanocomposites and analysing variations in relevant contact parameters is essential. Bartier et al. (2010) developed analytical models for the contact radius between spherical indenters and elastic-plastic materials, noting friction's impact. Choi et al. (2004) used sharp-tip indentation to measure micromaterial hardness and elastic modulus, introducing a depth ratio indicator. Kogut et al. (2004) provided dimensionless relationships for frictionless spherical indentation. Jackson and Kogut (2006) compared single asperity contact models, showing condition-dependent model choice. Chudoba and Jennett (2008) improved force-displacement curve accuracy with new corrections. Feng et al. (2007) analysed stress distribution in the plastic zone using combined Hertzian and ECD fields.

Big-Alabo et al. (2015) presented a novel post-yield contact model for spherical indentation, introducing new force-indentation relationships. Finite element (FE) simulations have significantly contributed to the study of indentation contact analysis, with notable work by Komvopoulos and Ye (2001) and Kogut and Komvopoulos (2004). These simulations validated classical Hertzian solutions and experimental observations, revealing the detailed mechanics of the indentation process. Selecting appropriate materials is crucial for modern industrial applications involving relative motion between contacting surfaces. Daeinabi & Korayem (2011) used AFM to explore nanoparticle mechanics and adhesion. Song &

Komvopoulos (2014) examined elastic-plastic materials' unloading response, deriving dimensionless equations for residual depth and plastic work. Alaboodi & Hussain (2019) emphasized thin films' roles, using nanoindentation and FEM for property evaluation. Lyashenko et al. (2024) studied friction between steel indenters and elastomers, showing a power-law decrease in friction coefficient. Lyashenko & Popov (2020) analysed adhesive contact between indenters and rubber. Durst et al. (2022) proposed a new yield strength measurement method from spherical indentation curves. Jin et al. (2024) developed a method for conical indenter response on transversely isotropic, layered elastic half-spaces.

Numerical analyses have been instrumental in understanding the contact phenomena of various materials. Brake (2012) developed an elastic-plastic contact model for different materials and geometries, while Buczkowski et al. (2014) applied fractal theory to determine normal contact stiffness for rough surfaces. respectively. The study of indentation contact analysis is essential for understanding localized deformation behavior, surface roughness, and mechanical properties such as hardness and elastic modulus. Johnson (1985) pioneered analytical models for unloading contact behavior using a spherical indenter, and Tabor (1948) provided validation for these models, showing that unloading follows an elastic path despite significant plastic deformation. Hardy et al. (1971) advanced the field with a FEM model focusing on elastic-plastic deformation due to high contact forces. Subsequent research by Biwa et al. (1995), Hernot et al. (2006), and Kim et al. (2006) employed both numerical and analytical techniques to delve into deformation mechanics and stress distribution during indentation contact analysis. The interaction between contact surfaces during loading and unloading phases is crucial for determining the longevity of components. The rapid surge in stress during loading and its sudden decrease during unloading can lead to microcrack formation, presenting engineering challenges. Johnson (1985) developed analytical models to understand unloading contact behavior with a spherical indenter, while Tabor (1948) validated these models, highlighting the elastic path of unloading despite plastic deformation. Subsequent research by Biwa et al. (1995), Hernot et al. (2006), and Kim et al. (2006) utilized numerical and analytical techniques to delve into deformation mechanics and stress distribution during indentation contact analysis. Kogut & Etsion (2002) analysed elastic-plastic sphere-flat contact, providing dimensionless expressions across deformation stages. Borodich (2014) connected Hertz-type problems with depth-sensing indentation, covering anisotropic and adhesive contacts. N'Jock (2016) proposed a Vickers indentation method to assess elastic modulus, validated through FE analysis. Phani & Oliver (2019) optimized Berkovich indenter spacing for accurate material characterization. Gourgiotis & Zisis (2016)

derived solutions for plane strain contact using couple-stress elasticity, highlighting microstructural effects. Wu et al. (2016) revealed Hertz theory inaccuracies for large deformations through nanoindentation. Pau et al. (2006) studied plane contact using ultrasound and FEM, validating stress state reflection data. Larsson et al. (1996) provided formulae for Berkovich indentation, comparing elastic materials and metals. Váradi et al. (1999) used FE techniques to study composite indentation, revealing stress distribution variations based on fiber orientation. Yuan et al. (2021) used physical vapor deposition for multilayer coatings, assessing mechanical properties via nanoindentation and FEM.

1.4.2 Literature on Flattening Contact Analysis

Flattening contact analysis, particularly with spherical asperities, is vital for asperity contact modelling. FE simulations have been instrumental in validating classical solutions and experimental observations (Follansbee et al., 1984; Sinclair et al., 1985). Komvopoulos and Ye (2001) developed a constitutive dimensionless equation for modelling the contact behavior of an elastic-perfectly plastic half-space, while Kogut and Komvopoulos (2004) established the relationship between mean contact pressure and yield strength under fully plastic conditions. Contact between rough surfaces can be modeled as multi-asperity or single-asperity contact, with cylindrical contact models commonly used to reflect the behavior of rough surfaces (Sharma & Jackson, 2017). These models are particularly effective for elongated asperities in fibrous and anisotropic material structures. Johnson (1985) provided the first closed-form elastic solution for cylindrical contact, with subsequent enhancements by researchers like Green (2005), Sharma and Jackson (2017), and Xu et al. (2022). Chatterjee and Sahoo (2014) and Wang et al. (2019) further explored these concepts using finite element simulations to study non-adhesive, frictionless contact and the impact of peak load during flattening operations. Various analytical and numerical models have been developed to perform contact analysis and investigate different aspects of cylindrical contact interactions. Megalingam and Mayuram (2014) employed the Fast Fourier Transform (FFT) and FEM to create a 3D contact model for Gaussian rough surfaces, demonstrating different deformation behaviors based on surface roughness. These studies emphasize the importance of understanding cylindrical contact interactions, especially in the context of nanocomposite materials. Flattening contact models are crucial for understanding the behavior of surfaces with elongated asperities in fibrous and anisotropic materials. Xu et al. (2022) enhanced the cylindrical contact model, originally developed as a closed-form elastic solution by Johnson (1985). Additionally, Gandhi et al. (2012) used FE analysis to study the impact of tangent

modulus on frictionless elastic-plastic contact behavior. These studies highlight the importance of numerical modelling in predicting and analysing contact behavior across different material systems and conditions. Hertz (1881) pioneered flattening contact analysis, correlating force, contact area, and deformation. Ghaednia et al. (2016) integrated the yield strength ratio into elastic-plastic contact modelling. Researchers like Olsson et al. (2016), Kogut et al. (2002), and Zhao et al. (2015) have focused on flattening contact analysis through numerical and experimental approaches to understand material behavior.

1.4.3 Literature on CNT-Based Nanocomposites with Al as Matrix Material

A composite material is formed when two or more materials with different properties are combined without changing their individual mechanical properties. If one phase is at the nanoscale, the material is termed a nanocomposite. Composite materials retain the distinct properties of their constituents, allowing for tailored properties suited to specific applications (Gupta et al., 2015; Zhang et al., 2020). Common reinforcements include SiC, B_4C, Y_2O_3, Al_2O_3, TiC, BN, ZnO, and CNTs, with CNTs offering exceptional mechanical properties such as a Young's modulus of 1 TPa and tensile strength of 200 GPa (Thostenson et al., 2001; Al-Saleh et al., 2009). CNT-reinforced composites have been extensively researched since the early 2000s (Kirtania & Chakraborty, 2014). Studies on the mechanical properties of CNT-reinforced nanocomposites often employ finite element modelling (FEM) and molecular mechanics. Nahas (2012) described the fundamentals of FE modelling for CNT nanocomposites, while Liu and Chen (2003) evaluated mechanical properties using FEM and representative volume elements (RVE). Zuberi and Esat (2015) also used FE models to understand the effect of CNTs in nanocomposites. Molecular mechanics approaches, such as those by Asgari et al. (2015), have also been used to determine mechanical properties at the nanoscale. Al and its alloys are favored matrix materials for CNT-based nanocomposites due to their excellent mechanical properties. Research by Kwon et al. (2009), Isaza et al. (2016), and Esawi et al. (2010) demonstrated significant improvements in mechanical properties with CNT reinforcement. Thermo-mechanical properties were experimentally investigated by Zhan et al. (2003) and Zhang et al. (2009). Khanna et al. (2021) reviewed mechanical property enhancements in Al metal-matrix composites, concluding that proper combinations of CNT and Al significantly improve mechanical properties, though large volume fractions can lead to agglomeration and reduced improvements. Nanocomposites, which combine materials with differing properties, offer tailored characteristics for specific applications. CNT-reinforced composites have gained popularity due to their enhanced mechanical

properties. Early studies by Yoo et al. (2013), So et al. (2018), and Liu et al. (2021) focused on experimentally studies. Lusti and Gusev (2004), and Carneiro and Simoes (2020) contributing to the understanding of CNT nanocomposites. CNT-reinforced composites, known for their advanced mechanical, thermal, and electrical properties, have been extensively researched. Nahas and Alzahrani (2012) investigated the impact of CNT volume percentage on CNT/epoxy nanocomposites, while Zuberi and Esat (2015) used a finite element (FE) model to understand the role of CNTs in nanocomposites with an epoxy matrix. Hassanzadeh-Aghdam and Mahmoodi (2017) developed an analytical model to predict the elastic modulus, yield strength, and ultimate tensile strength of CNT-Al nanocomposites, considering various influencing factors. Abdullahi et al. (2013) fabricated CNT-reinforced aluminium nanocomposites via powder metallurgy, focusing on wear behavior using a pin-on-disc tribometer against AISI52100 steel under varying CNT contents and conditions. Sarkar and Das (2014) demonstrated that hot-pressed MWCNT/alumina nanocomposites exhibit improved flexural strength, hardness, and fracture toughness compared to pure alumina. Abdullahi et al. (2021) investigated the hardness behavior of CNT-reinforced aluminium using nanoindentation and Vickers micro hardness techniques, observing significant hardness enhancement at 1.5 wt% CNT. Yu et al. (2018) achieved a 13.5% enhancement in Young's modulus for 1.5 wt% CNT/Al, emphasizing precise measurement techniques. Ahmadi et al. (2019) employed a finite element micromechanical model to study the impact of the Al4C3 interphase on the elastic modulus of CNT-Al nanocomposites, highlighting its significant effect, particularly with smaller CNT diameters.

Kwon et al. (2009) and Esawi et al. (2010) explored the effective mechanical properties of CNT-reinforced nanocomposites. Studies by Zhan et al. (2003) and Zhang et al. (2009) determined the thermo-mechanical properties of CNT-reinforced nanocomposites experimentally. Khanna et al. (2021) discussed enhancements in Aluminium metal-matrix composites, and Ahmed et al. (2020) developed an FE model for Al-CNT nanocomposites to explore the impact of CNT wall thickness. Comprehensive reviews by Shokrieh and Rafiee (2010), Radhamani et al. (2018), and Kumar et al. (2021) provide in-depth insights into this topic.

1.4.4 Literature on CNT-FGM Nanocomposite

Functionally graded materials (FGMs), pioneered in Japan in the 1980s, are composite materials with controlled composition or structure that enable localized attributes tailored to specific requirements (Erdogan et al., 1995; Yang et al., 1997; Kokini et al., 1997). These

materials facilitate the production of components with specific local properties (Carvalho et al., 2015). Gunes et al. (2011) and Etemadi et al. (2009) developed models for FGMs using the Mori-Tanaka scheme, enhancing their structural integrity and functionality. Suresh et al. (1997) created a finite element-based model for analysing contact during indentation with a spherical indenter, highlighting their versatile mechanical behavior under varying loads. Chen et al. (2020) formulated a nonlinear contact force law for analysing indentation contact in FGM-coated elastic materials, demonstrating their robustness in different loading conditions. Incorporating carbon nanotubes (CNTs) into FGMs, as proposed by Shen (2009), enhances interfacial bonding strength and mechanical properties, making them suitable for demanding applications. While, CNT-FGM nanocomposites have not been extensively analysed in contact mechanics, several studies have focused on their behavior in other domains. Rashidifar and Ahmadi (2015) analysed CNT-reinforced functionally graded beams using finite element modelling for free vibration analysis. Nguyen and Duc (2024) studied nonlinear vibration of CNT-reinforced ceramic-metal shells using a new shear deformation theory. Kim et al. (2019) fabricated high-strength, ductile FGMs with Aluminium and CNTs via hot extrusion. Xue et al. (2024) developed a vibration model for CNT-reinforced FG plates for space applications, analysing reinforcement distribution and boundary conditions. Research on FG-CNT composites has explored their buckling behavior (Sears et al.; 2006; Sun et al.; 2008), free vibration characteristics (Maji et al., 2020; Rashidifar et al., 2015; Fallah et al.; 2018), and responses to low-velocity impacts (Zarei et al., 2017; Selim et al., 2017; Song et al., 2016).

1.4.5. Summary of Literature Review

The extensive literature review performed brings into focus the current state of knowledge and gaps in the field of contact analysis. It clearly reveals that substantial research has been carried out on the contact analysis of elastoplastic materials, graded materials and nanocomposites. Research work carried out in this domain encompasses both single asperity and multi-asperity contact scenarios, employing a variety of experimental, numerical and analytical methods to explore and understand these interactions. For elastoplastic materials, the literature demonstrates a comprehensive understanding of their contact behavior under different loading conditions. Similarly, significant efforts have been made to study graded materials, which exhibit variations in properties across their volume, providing insights into their performance under contact conditions. Nanocomposites, which integrate nanoparticles

to enhance material properties, have also been extensively studied, focusing on their contact mechanics.

Despite this broad research landscape, there is a notable gap when it comes to CNT-based nanocomposites. Most of the existing research on these materials have concentrated on evaluating their mechanical properties, such as hardness and tensile strength etc. Additionally, studies have explored their electrical and thermal properties, primarily through experimental methods. These investigations have provided valuable information on the fundamental characteristics of CNT-based nanocomposites. However, the literature review indicates a significant lack of research on the contact analysis of CNT-based nanocomposites. While some studies have addressed the contact behavior of functionally graded materials (FGMs), which are materials with gradually varying properties, there are very few studies focused on CNT-based FGMs. This highlights a critical gap in the research, as there is no substantial literature addressing specifically contact analysis of CNT-based FGMs. But, integration of vapor deposition and powder metallurgy techniques have enabled the development of functionally graded (FG) materials with carbon nanotubes (CNTs) uniformly dispersed within the FG material for innovative applications. Hence, research studies in the above mentioned domain are not only of academic interest, but have possibilities in terms of real-life applications in near future.

From the literature review three key areas can be highlighted where there is scope for further research work on involving contact analyses of CNT composites.

- Contact analysis of CNT-reinforced Al matrix nanocomposites
- Contact analysis of functionally distributed CNT-based nanocomposite
- Contact analysis of CNT-reinforced FGM matrix nanocomposites

In summary, while there is extensive research on the contact analysis of various materials, including elastoplastic materials, graded materials and general nanocomposites, there is a clear deficiency in studies specifically targeting the contact analysis of CNT-based nanocomposites and CNT-based FGMs. It presents an opportunity to explore and understand the unique contact behavior of these advanced materials.

1.5. Objective

Based on the literature review and the identified gaps in existing research, the objective of the present thesis is to analyze the contact behaviour of CNT-Al nanocomposites and CNT-based FGMs with a view to study the effects of various parameters on the said

behaviour. In order to fulfil the objective, following detailed and specific tasks are mapped out.

1. To develop a 2D FE model for the indentation contact analysis of CNT-Al nanocomposites using a Berkovich indenter.
2. To develop a 2D FE model for the flattening contact analysis of CNT-Al nanocomposites using a rigid flat.
3. To investigate the effects of CNT thickness on the indentation and flattening contact behavior of CNT-Al nanocomposites.
4. To develop a 3D finite element model (FEM) for the indentation contact analysis of functionally graded CNT-reinforced composites using a rigid spherical indenter.
5. To estimate the effect of CNTs distribution pattern in the composite (FG-CNTRC) on the indentation contact behaviour.
6. To evaluate the effect of the elastic gradation parameter on the indentation contact and flattening contact behavior of uniformly distributed CNTs in the FGM (CNTR-FGMMC).

1.6 Present Thesis

The present thesis is structured into seven chapters as follows:

- Chapter one provides an introduction to the thesis, including literature review, identification of the research domain and the objectives to be achieve.
- Chapter two details the 2D finite element simulation for a rigid Berkovic indenter, focusing on static analysis to understand the impact of CNTs on the contact behavior of the composite.
- Chapter three presents a 2D finite element-based static contact analysis of the flattening contact model involving a cylindrical substrate and a rigid flat.
- Chapter four explores the 3D spherical indentation model to analyze the significance of CNT distribution in the contact domain.
- Chapter five examines the effect of the elastic gradation parameter on material behavior in CNT-reinforced FGM matrix nanocomposites using a 3D indentation model with a spherical rigid indenter.
- Chapter six discusses the influence of CNT wall thickness and the elastic gradation parameter of the matrix material on contact behavior during flattening contact analysis.

- Chapter seven concludes the thesis by summarizing the findings, outlining future research directions, and highlighting the novel contributions of the work.

Chapter 2

Indentation Contact Analysis of Single Wall Carbon Nanotubes (SWCNTs) Nanocomposite

2.1 Introduction

A composite material, characterized by the combination of two or more materials with differing properties, offer tailored mechanical characteristics without altering the individual properties of its constituents. When one of these components is at the nanoscale, it forms a nanocomposite. Unlike alloys, where multiple phases merge to form a new substance, composite materials maintain distinct phases without dissolving or blending. The selection of matrix and reinforcement materials is pivotal in achieving desired properties for specific applications. Enhancements in mechanical properties are achieved through a variety of reinforcing materials, including carbon nanotubes (CNTs), prized for their exceptional mechanical attributes such as high Young's modulus and tensile strength (Saba et al., 2016). Incorporating CNTs into composites has garnered significant attention, leading to extensive research in the past decade. Understanding the mechanical properties of these materials is vital, prompting numerous studies utilizing diverse techniques. Finite element modelling (FEM) and molecular dynamics (MD) are preferred for their accuracy at micro and nano-scales. Representative volume element (RVE) analysis is commonly employed to simulate behavior (Song et al., 2014). Experimental investigation alongside simulation methods provides comprehensive insights. Among potential matrix materials, aluminium and its alloys stand out due to their favorable properties. Aluminium metal matrix composites (Al MMCs) offer low thermal expansion coefficients, high strength, and wear resistance. Various studies have explored the mechanical properties of CNT/Al nanocomposites (Zhan et al., 2003; Zhang et al., 2009; Khanna et al., 2021), revealing improvements in properties with increased CNT content. However, excessive CNT volume fractions may lead to diminished returns due to agglomeration effects.

Indentation techniques, particularly nanoindentation, serve as valuable tools for assessing mechanical properties such as hardness and Young's modulus. Experimental, analytical, and numerical approaches have been employed to study indentation contact behavior, primarily focusing on spherical indentation models (Borodich et al., 2004; Vasiliev et al., 2017). However, detailed indentation-based contact analysis of SWCNT-based nanocomposites remains unexplored.

This chapter undertakes finite element-based indentation contact analysis on CNT-reinforced Al matrix nanocomposites. A contact model has been developed using APDL code on the ANSYS platform to investigate the impact of CNT thickness on contact characteristics under loading and unloading conditions.

2.2 Finite Element Model

Detailed discussion on the finite element modelling of Indentation contact has been presented in chapter 2. A finite element (FE) model is developed using FEM software ANSYS to simulate the indentation of a rectangular block of Aluminium reinforced with single walled CNT (SWCNT). In order to reduce the analysis size and computational load on the available resources, 2D axisymmetric FE model (with the y-axis being the axis of symmetry) is adopted for the analysis instead of a 3D model (Jackson et al., 2005) (Figure 2.1). The indentation contact analysis is performed between a conical indenter which is assumed as rigid, and the deformable metal matrix with SWCNT reinforcement.

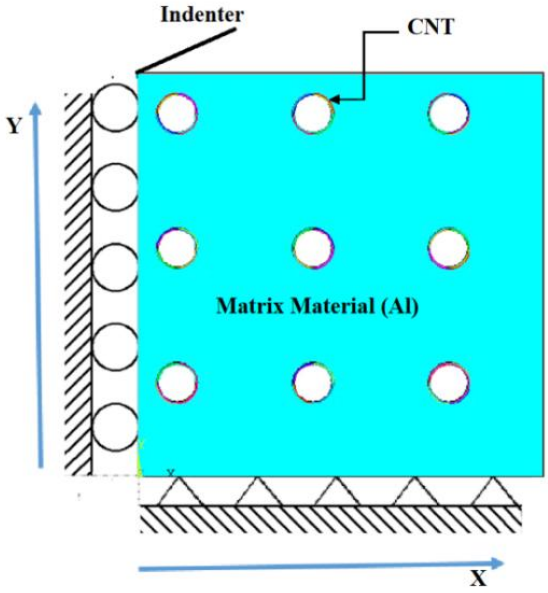

Figure 2.1: Schematic diagram of the axisymmetric indentation model

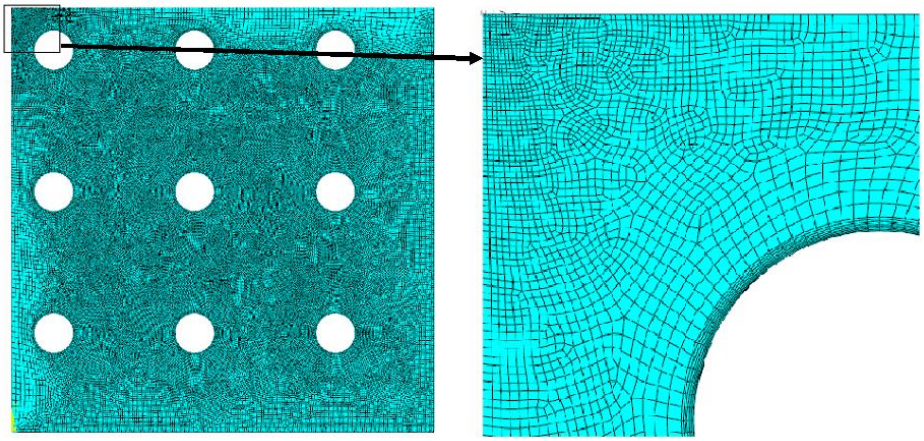

Figure 2.2: FE mesh of the model with magnified view of the near-contact zone.

The most commonly used semi-cone angle to reproduce the results of Berkovic indenter is 70.3º (Lichinchi et al., 1998; Wei et al., 2012), which results in same base area of contact at any indentation depth as the Berkovic indenter. However, some studies (Qin et al., 2009; Shi et al., 2010) have argued that the semi-cone angle equal to the pyramid indenter angle of the original Berkovic indenter (65.3º) results in better imitation of indentation results. In the present analysis, the later approach is adopted, i.e., the conical indenter's face makes an angle of 65.3º with the line of action of the applied load.

Table 2.1: Value of parameters (Ahmed et al., 2020 and Nouri et al., 2012)

Property	**Value**
Diameter of CNT	1 nm
Indenter tip displacement	0.78 nm
Number of CNT	9
Modulus of Elasticity of CNT, E_t	1000 GPa
Poisson's Ratio of CNT, $\boldsymbol{v_t}$	0.27
Modulus of Elasticity of Aluminium, E_m	7000 MPa
Poisson's Ration of Aluminium, $\boldsymbol{v_m}$	0.23
Wall thickness of CNT (t)	0.034 nm, 0.068 nm, 0.102 nm, 0.136 nm and 0.170 nm

The nanocomposite block has a dimension of 10 nm × 10 nm. Within the matrix material, total 9 SWCNTs are embedded and the distribution of these nanotubes is as shown in Figure 2.2. In view of the uniform distribution of nanotubes considered in the present model, it is apparent that it cannot capture the effect of inherent randomness of the CNT distribution inside the matrix material in an actual physical scenario. The composite is considered to be

defect-free. The nanotubes are assumed to be perfectly bonded with the metal matrix (Hallad et al., 2016; Kirtania and Chakraborty, 2014) and it ensures that the tubes do not slip, detach or become loose from the matrix material. However, this assumption, introduced for the sake of computational simplicity, imposes the condition that the phenomenon of interfacial slip cannot be analysed and the limiting force for the same cannot be estimated. It is to be mentioned here that frictionless (full slip) contact between the indenter and the material block is assumed for the present analysis. Practically for indentation with conical indenters, there exists the interfacial friction between the indenter and the substrate and the results are indeed influenced by it. However, it is found that in a significant number of numerical indentation studies with sharp ended indenter, the full-slip consideration (zero friction) was adopted and the results (Giannakopoulos et al., 1997; Carlsson et al., 2001) were found to be in acceptable range with experimental results.

It has been highlighted at the end of the introduction segment that the objective of the present work is to investigate the effect of variation of CNT wall thickness on loading and unloading behaviour of the composite. In order to do so, following 5 different thicknesses are considered - 0.034, 0.680, 0.102, 0.136 and 0.170 nm. Consequently, change in thickness corresponds to change in volume percentage on CNTs in the nano-composite. For the above-mentioned wall thicknesses, the volume percentage of the CNTs are as follows - 0.93 %, 1.86%, 2.79 %, 3.72 % and 4.65 %. PLANE183, a 2D quadrilateral element with quadratic displacement behaviour is used to mesh the matrix as well as the nanotubes. The top surface of the composite which comes in contact with the conical indenter is meshed with CONTA172 elements, while, TARGE169 elements are used to mesh the rigid indenter surface. With the objective of reducing the solution time without compromising the accuracy of the solution, gradient is applied in the mesh size in such way that the mesh becomes coarser to finer as it moves towards the point of indentation. The mesh size gradation is shown in the magnified view in Figure 2.2. Pure Lagrange multiplier contact algorithm is selected for the realization of the contact in the analysis. In any finite element simulation of a contact problem, it is extremely important to choose proper boundary conditions. In the present model all the nodes on the y-axis (Figure 2.1) are restricted to move along the x-direction, i.e., these nodes can only move vertically. On the other hand, the nodes placed on the x-axis are restricted from moving in the vertical direction (y-direction) (Ahmed et al., 2020). The von Mises yield criterion is adopted to determine the onset of post-elastic behaviour, which is modeled as bilinear isotropic hardening. Initially, the indenter is moved towards the nanocomposite substrate up to an indentation depth of 0.78 nm then slowly

withdrawn from the substrate. Table 2.1 shows the material properties and other measurements considered in the present model.

2.3 Results and Discussion

2.3.1 Mesh Convergence Study

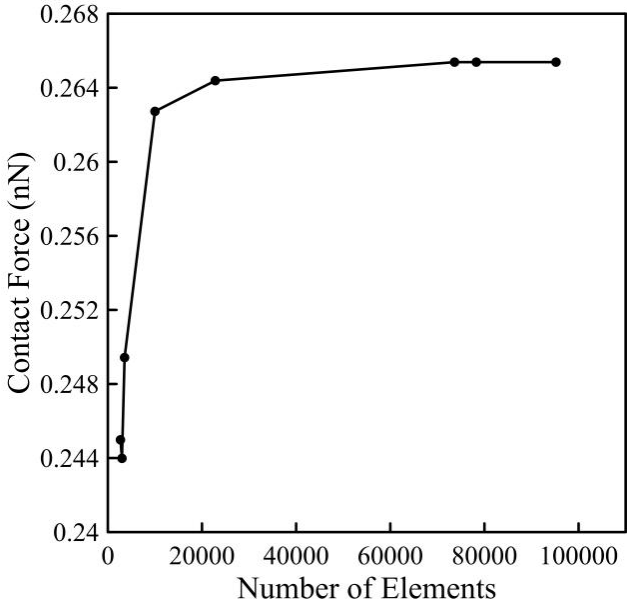

Figure 2.3: Mesh convergence plot in terms of contact force and numbers of elements.

Model accuracy in FEM is dependent on the size of the element, which in turn controls the mesh density. Smaller element size means a large number of elements in a FE model and it ensures high degree of accuracy in the simulated results. But it is obtained at the expense of large solution time. On the other hand, large size elements result in a sparse or coarse mesh and the accuracy of the results is not upto the mark. Although solution time is significantly less. A mesh convergence analysis provides optimum number of elements necessary in a model for sufficiently accurate results with minimum solution time. Hence, checking for mesh convergence is an important part of any finite element simulation study. Without a proper convergence analysis, the model accuracy is left open to question.

A system similar to the one explained in the previous section is adopted for the convergence study. The thickness of the CNTs embedded in the Aluminium (Al) metal matrix nano-composite substrate is considered to be 0.034 nm. For the mesh convergence analysis, the element size is reduced in steps (with corresponding increase in number of elements) and resulting contact force corresponding to interference value of 0.10 nm is extracted for each step. The process is continued until the change in resulting contact force corresponding to two

successive steps drops below 0.0004%. Figure 2.3 presents the mesh convergence plot and shows the contact force corresponding to the number of elements used for the analysis. The figure shows that at initial steps of mesh refinement, the change in resulting contact force is quite significant, whereas, after certain a level the change is found to be extremely small. It can be clearly observed from the convergence plot that the changes in numbers of element from 73654 to 78270 causes the changes in contact force is about 0.0003769% which is negligible. In this present analysis 73654 number of elements are considered.

2.3.2 Validation Study

The objective of this section is to graphically present the validation of the present method by comparing numerical results (contact force vs. indentation depth) produced by the present method against results published in established literature (Ahmed et al., 2020; Wagih and Fathy, 2016). Two different comparisons are performed for the present model – the first one compares the contact force vs. interference plot in case of loading and unloading of an Aluminium block by a sharp tip [Ahmed et al., 2020], while the second one compares the results of an indentation analysis performed on a CNT-based nanocomposite (Ahmed et al., 2020). Appropriate adjustments are made to the present model in order to make it equivalent to the systems analysed in the two above-mentioned papers (Ahmed et al., 2020; Wagih et al., 2016).

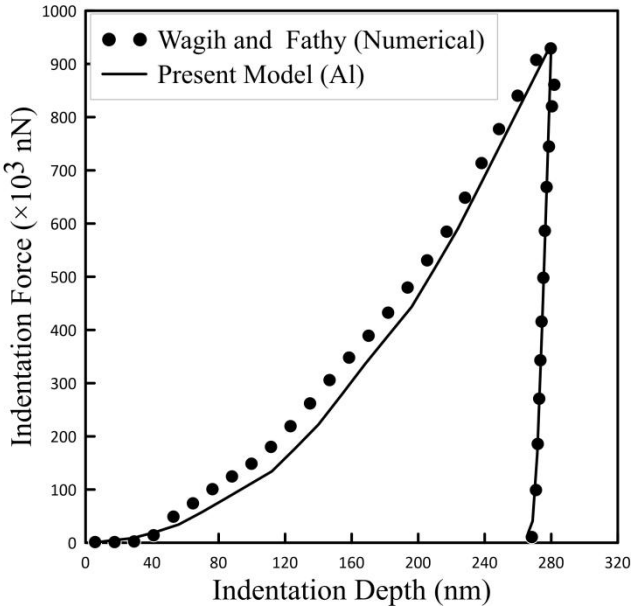

Figure 2.4: Validation of contact force with the results of Wagih and Fathy (2016).

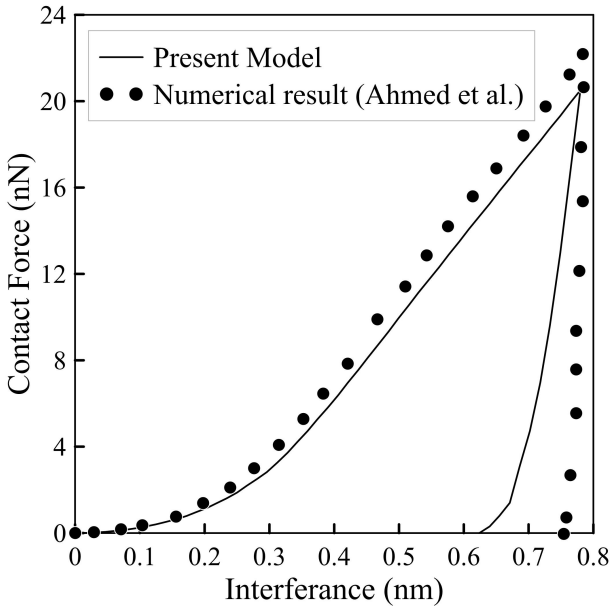

Figiure 2.5: Validation of the present model with the results of Ahmed et al. (2020).

Wagih and Fathy (2016) carried out an FE simulation to generate the load-indentation curve for pure Al indented by a sharp tip under loading-unloading condition. Figure 2.4 shows the comparison between results obtained by Wagih and Fathy (2016) and those generated through the present model (with appropriate material properties). Good matching between the two sets of data is observed from the figure. In Figure 2.5 force-indentation depth result obtained from Ahmed et al. (2020), who analysed the indentation process of a 10 ×10 nm CNT based nano-composite block for CNT wall thickness of 0.168 nm by a Berkovic indenter, is compared against simulated results provided by the present FE model. There is satisfactory agreement between the two curves and they follow the same pattern. From these comparisons validity of the present model can be established. It is to be noted that there is a sudden change in the indentation force vs. depth curve towards the end of the unloading stage. At the point of detachment of the indenter from the substrate, the elastic deformation part is recovered and as a result the material tends to ‘spring back' to some extent. It increases the rate of change of penetration depth with respect to the force, thus, resulting in a reduced slope near the end of the unloading phase.

2.3.3 FE Analysis Results

The present analysis is primarily focused on the effect of SWCNT wall thickness on nanocomposite behaviour during loading and unloading. Initially the indenter tip just touches the top surface of the substrate and from this position a downward displacement is imparted to it so that the substrate located beneath it is deformed. Once the interference achieves the

desired value relevant contact parameters (contact force, contact area etc.) are extracted This is followed by withdrawal of the indenter so that there is complete detachment between the two. This is the unloading phase of the indentation process. After the unloading is completed, contact parameter results are obtained in a similar manner as before. In the present chapter unloading of the indenter is carried out from three different interference values and these indentation depth values are 0.38, 0.58 and 0.78 nm, respectively.

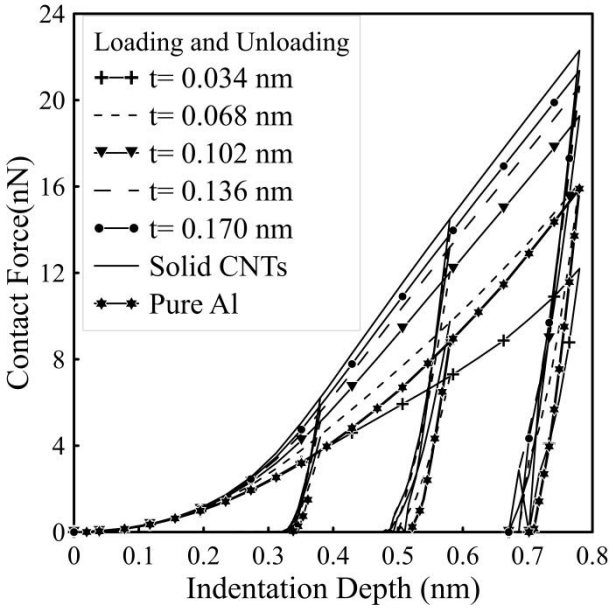

Figure 2.6: Indentation Depth vs. Contact Force plots for loading and unloading of SWCNT nano-composite with varying wall thickness

Different aspects of contact behaviour under loading and unloading conditions are studied with variation of CNT wall-thickness. Contact force is plotted against indentation depth or interference value for the entire loading-unloading phase in Figure 2.6. In this figure five different CNT thicknesses (0.034, 0.068, 0.102, 0.136 and 0.170 nm) have been considered along with three levels of indentation depth (0.38, 0.58 and 0.78 nm) from where unloading is performed. In order to provide a basis for comparison loading-unloading plots corresponding to a solid CNT based Aluminium nano-composite and a pure Aluminium substrate (without any embedded CNTs) are incorporated into the figure. It is clear from the figure that the contact force at the end of the loading phase (for all three indentation depths) increases with increase in SWCNT thickness. However, during the first part of the loading (up to 0.000125 μm of indentation), all the plots coincide, which indicates that there is no effect of thickness at this stage. This behaviour can be explained by the fact that initially only the matrix material located near the surface undergoes deformation, while the CNTs and the matrix at its

vicinity remain undeformed. After that point the individual curves diverge from one another with higher contact force corresponding to higher CNT thickness.

It is to be noted that the loading-unloading curve for CNT thickness 0.034 nm lies below that of pure Al in the higher interference zone. Embedding of CNT in this scenario diminishes the contact force. It may be due to buckling of SWCNT during the loading phase because of high diameter to thickness ratio of the tubes (Jackson et al., 2005). The figure also shows that the curve for CNT thickness 0.068 nm is very close to that of the pure Aluminium one. Here the maximum contact force at an interference of 0.78 nm is 0.0161 μN which is nearly same as that obtained for pure Al (0.0159 μN). There is considerable increase in maximum contact force values corresponding to CNT thicknesses higher than 0.068 nm, which is evident from the figure. At the higher end of thickness band, increase in contact force w.r.t. a certain interference is found to be lower. The gap between the two sets of loading curves corresponding to 0.136 nm and 0.170 nm is smaller than the gap between 0.068 nm and 0.102 nm. It is also observed that there isn't a considerable difference between the contact force-indentation depth plot for solid CNT and 0.170 nm thickness CNT nano-composite.

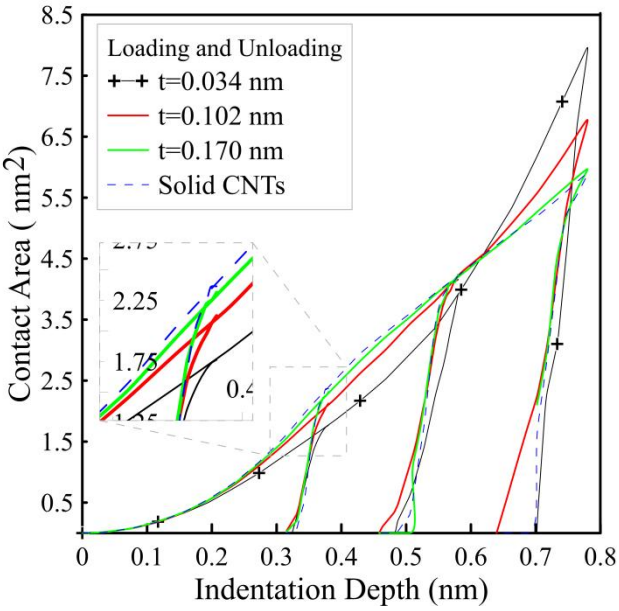

Figure 2.7: Indentation Depth vs. Contact Area plots for loading and unloading of SWCNT nanocomposite with varying wall thickness

Plots of contact area against indentation depth, for three different wall thickness values (0.034, 0.102, and 0.170 nm) along with a solid CNT, are presented in Figure 2.7. Similar to contact force behaviour at the initial stages of contact (low interference), the curves of contact area vs. indentation depth corresponding to different wall thickness of CNT do not exhibit any significant variation. This is due to the fact that at this stage there is almost no effect of the

indentation on the CNTs and its immediate neighbouring location. Beyond a particular interference, the curves start to differ from one another. In the medium interference zone the contact area corresponding to solid CNT is found to be the highest with wall thickness 0.034 nm being responsible for smallest contact area. However, in the high interference range this trend becomes opposite, as solid CNT nano-composite produces the minimum contact area for a given depth. Consequently, CNT nano-composite with low wall thickness (0.034 nm) has the maximum contact area. The reason for this type of behaviour is that, up to a certain indentation depth (around 0.62 nm in this case) the trend of the contact area is primarily governed by plastic deformation at the vicinity of the indenter contact zone (shown in later section). However, in the later stage, i.e. when indentation depth is higher and when the CNTs have started to deform, the trend is primarily governed by the compliance of the CNTs. Hence, lower wall thickness results in higher contact area.

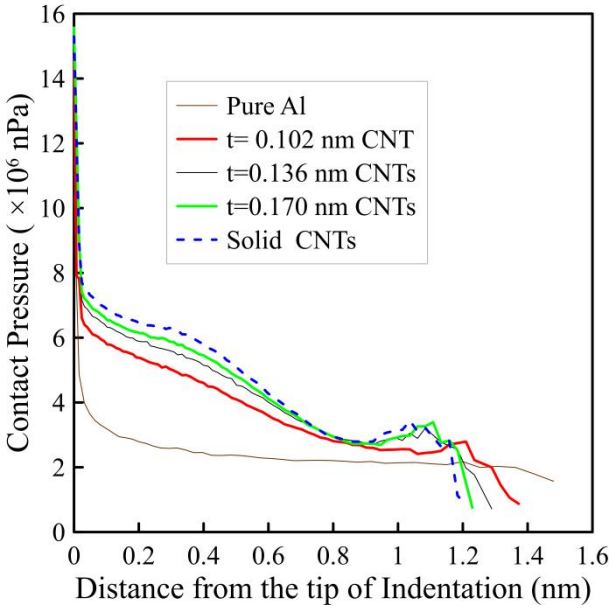

Figure 2.8: Contact pressure on the contacting edge of indenter at the end of loading stage for an indentation depth of 0.78 nm.

Figure 2.8 presents the contact pressure (at the end of the loading phase at an indentation depth of 0.78 nm) variation from the contacting edge of the indenter. The maximum contact pressure is observed at the tip of indenter but just away from the tip there is a sudden fall of pressure because in the present model straight edge is considered instead of a circular tip. It is clearly shown that the contact pressure is higher for high thickness of CNTs as high thickness CNTs require higher force to obtain the same deformation. It can be pointed out that the contact force decreases with distance from the tip of indenter but towards the end of the

contact edge there is an increase in contact pressure. It may be due to material flow at the edge of contact and this increase may result in pile-up.

2.3.3.1 Analysis of stresses

In any contact analysis, study and comprehension of the stress distribution is a crucial aspect. Contour plots of average von Mises stress for Al-SWCNT nano-composite corresponding to variation in CNT wall thickness are furnished in Figure 2.9. For each wall thickness, there are two contour plots – one considers the entire substrate including the embedded CNTs, while the other shows the stress distribution only in the Al matrix. The stress generated in the CNT is found to be much higher than that generated in the matrix and hence, it is necessary to provide the second contour plot so as to have a better understanding of the distribution of stresses in the matrix. In Figure 2.9., contour plots marked (i) are for the complete nano-composite including the CNTs, whereas, plots marked (ii) are for only the Al matrix.

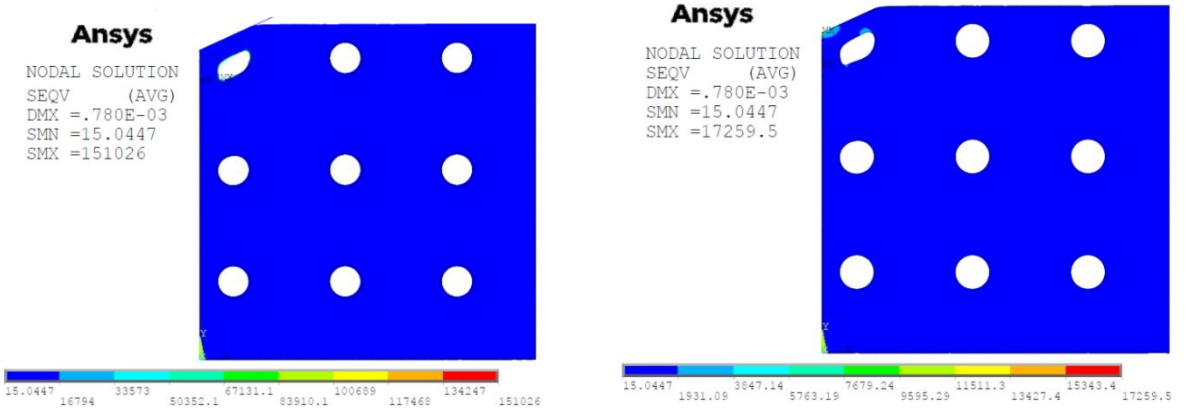

(i) (ii)

(a)

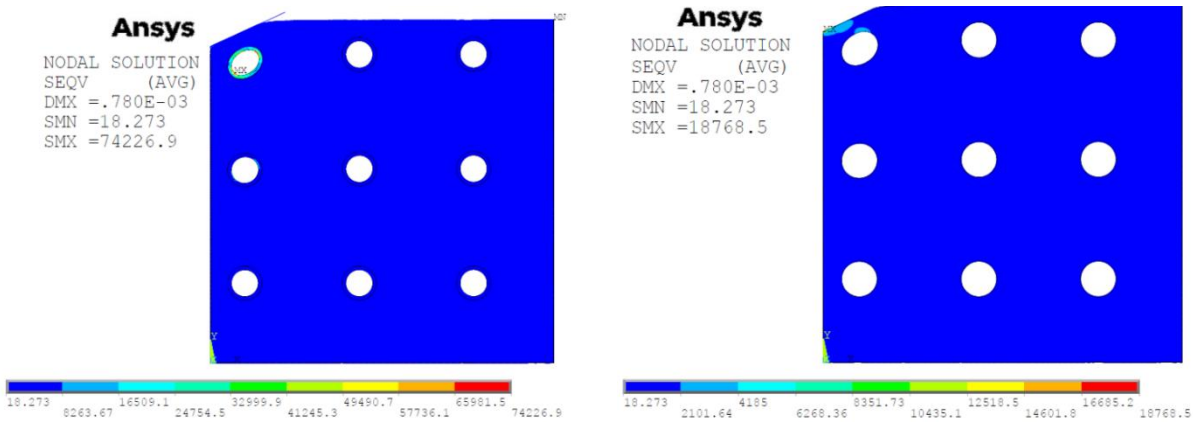

(i) (ii)

(b)

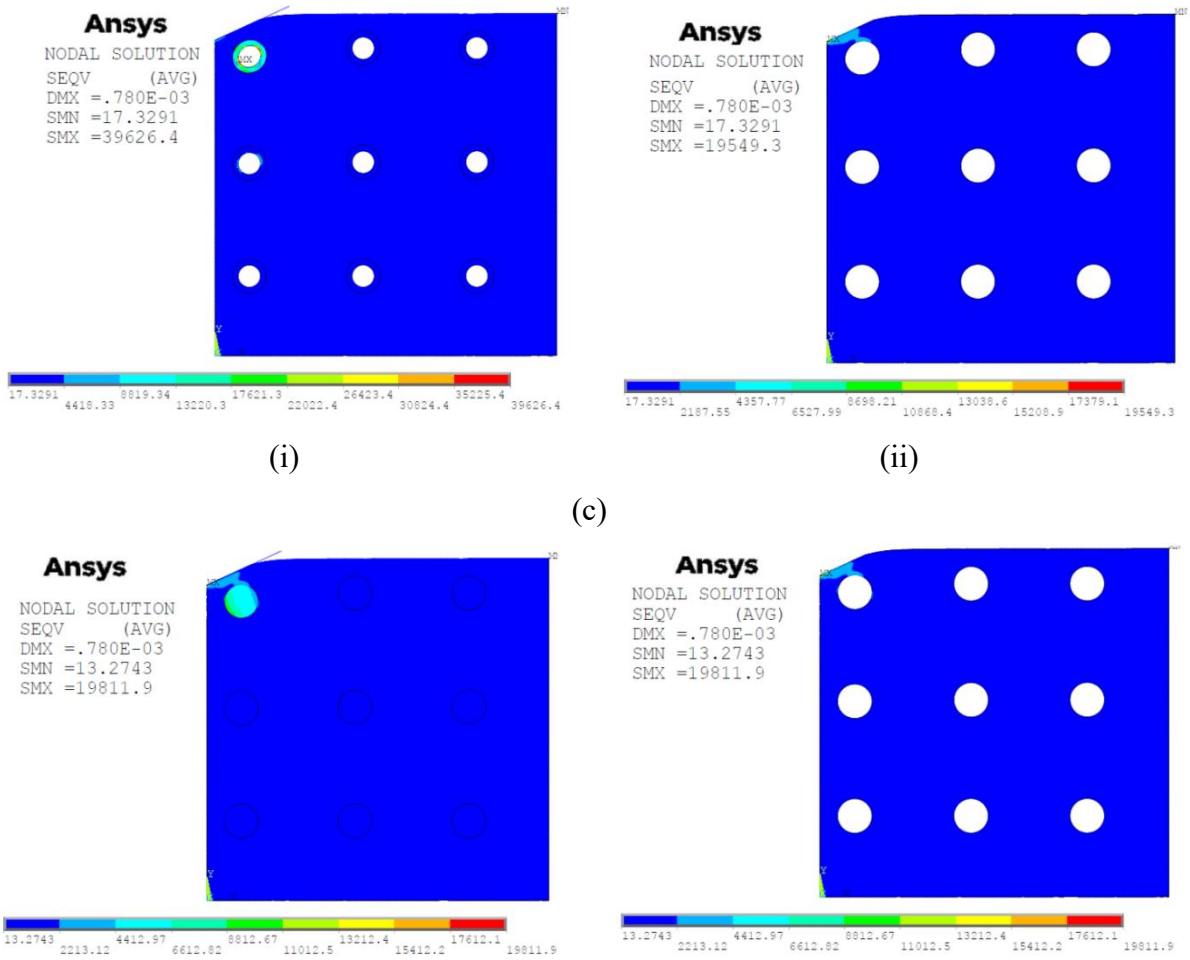

(i) (ii)

(c)

(i) (ii)

(d) Solid

Figure 2.9: Contour plot of von-Mises stresses at the end of loading phase at an indentation depth of 0.78 nm with varying wall thickness: (a) t = 0.034 nm, (b) t = 0.102 nm, (c) t = 0.170 nm and (d) Solid

Since, the Young's modulus of the CNT is much higher than that of the substrate, maximum stress in the system occurs in the CNTs, with lower wall thickness CNT generating the higher stresses. The distortion in shape of the CNT (nearest to the tip of the indenter) with lower thickness is naturally observed to be maximum [Figures 2.9(a-i)]. On the other hand, there is minimal distortion in shape of the CNT with 0.170 nm thickness [Figures 2.9(c-i)] and the solid CNT [Figures 2.9(d-i)]. For a certain indentation depth, higher distortion takes place in the CNTs with lower wall thickness, resulting in higher equivalent strain, hence inducing higher von Mises stress in the CNTs. On the other hand, with increasing distortion in the CNTs, equivalent strain, as well as stress in the matrix material decreases. Therefore, opposite trend is observed in terms of induced von Mises stress in the CNT and matrix material under varying CNT wall thickness. However, the variation of stress in the matrix is

of lower magnitude in comparison with that in the CNTs. There is no significant change in the distribution of stress in the matrix as well, as observed from Figures 2.9(a-ii) to 2.9(d-ii).

One important aspect of the indentation phenomena is to study the indented or deformed geometry and distribution of residual stresses after complete unloading, i.e., detachment of the indenter from the nano-composite substrate. Contour plots of residual Von Mises stress (unloaded from an interference of 0.78 nm) for Al-SWCNT nano-composite with varying wall thickness of CNT are presented in Figure 2.10. As in case of Figure 2.9., there are two separate plots for each CNT wall thickness. The first one (represented by (i)) provides the residual stress distribution of the entire substrate and the second one (represented by (ii)) gives the residual stress distribution of the Al matrix only. In all the cases [Figures 2.10(a) to 2.10(d)], the high residual stress zones are found to be directly below the contact location. It could be noted that the trend observed in the loaded condition persists in the unloaded condition as well, i.e. with higher CNT thickness, lower and higher residual stresses are observed in the CNTs and the matrix material, respectively.

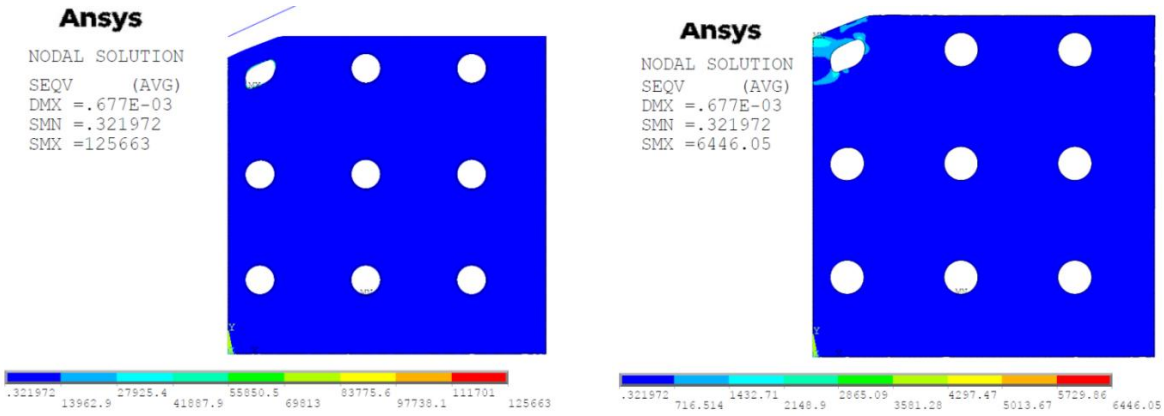

(i) (ii)

(a)

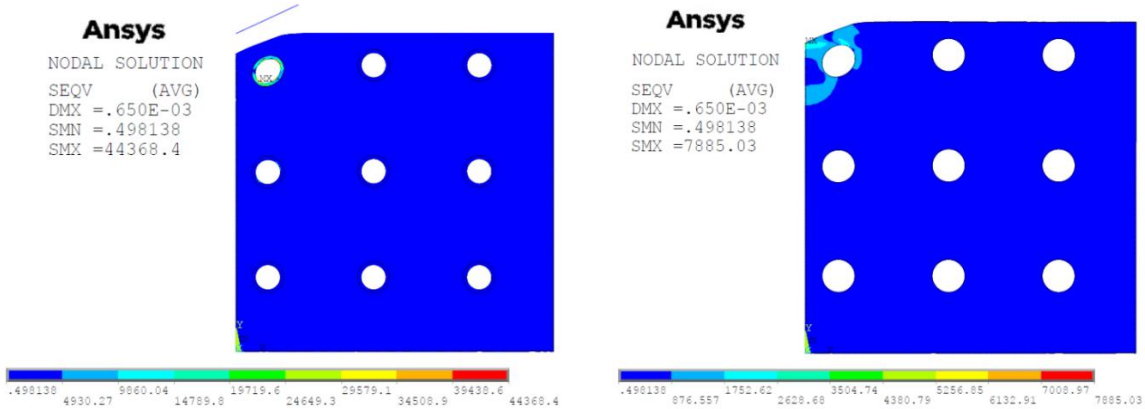

(i) (ii)

(b)

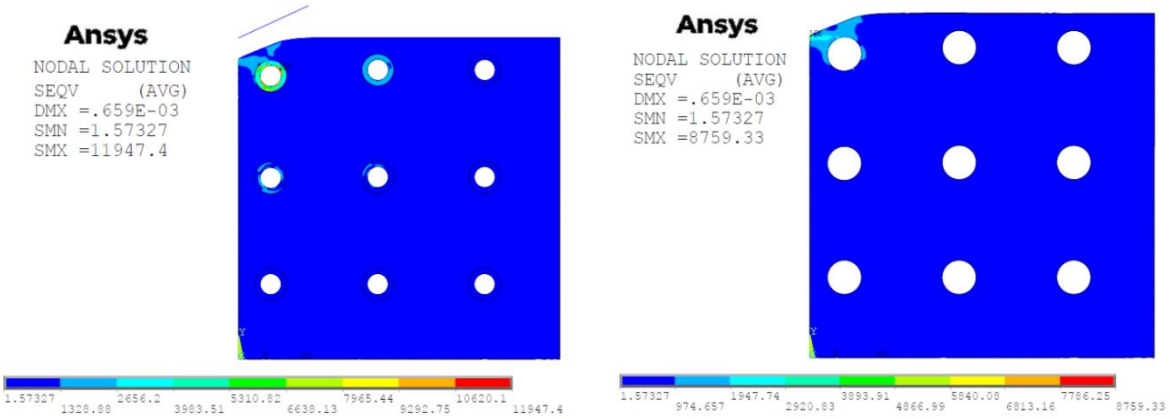

(i) (ii)

(c)

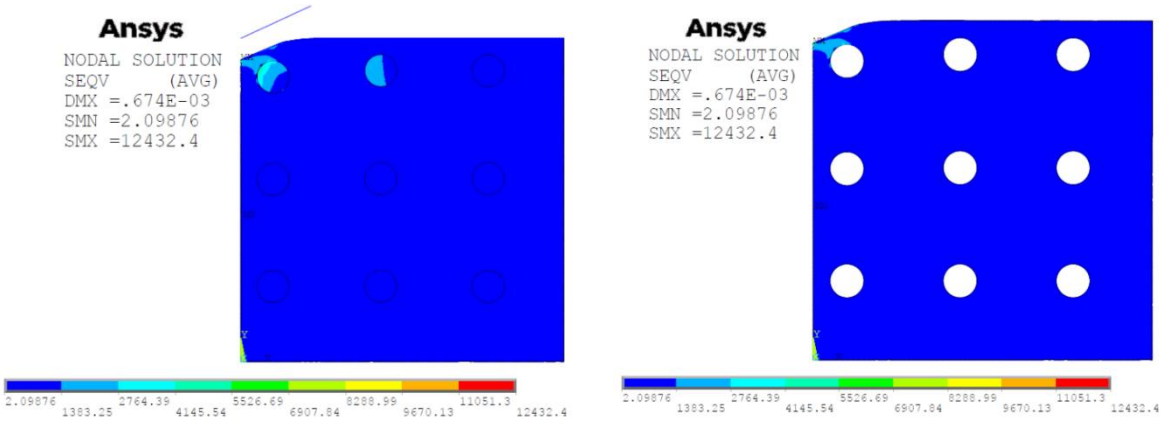

(i) (ii)

(d)

Figure 2.10: Contour plot of residual von-Mises stresses after unloading from an indentation depth of 0.78 nm with varying wall thickness: (a) t = 0.034nm, (b) t = 0.102 nm, (c) t = 0.170 nm and (d) Solid

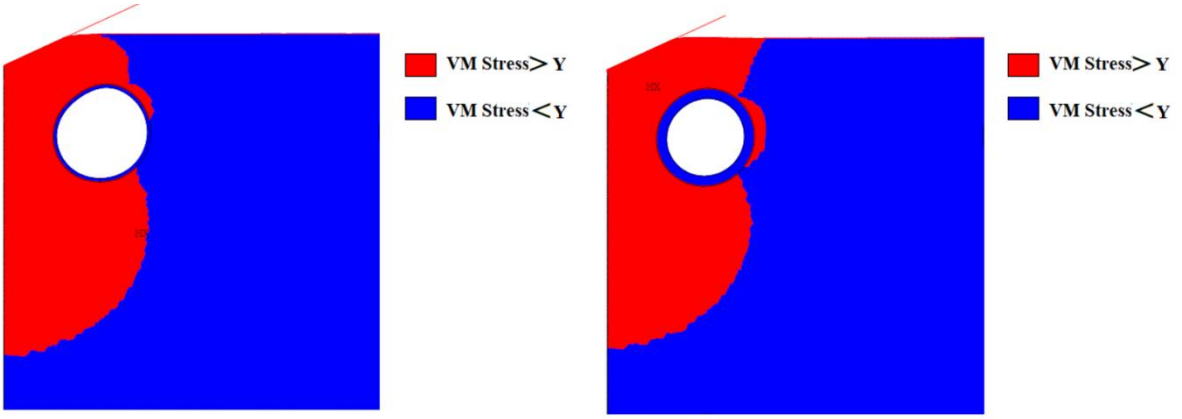

(a) (b)

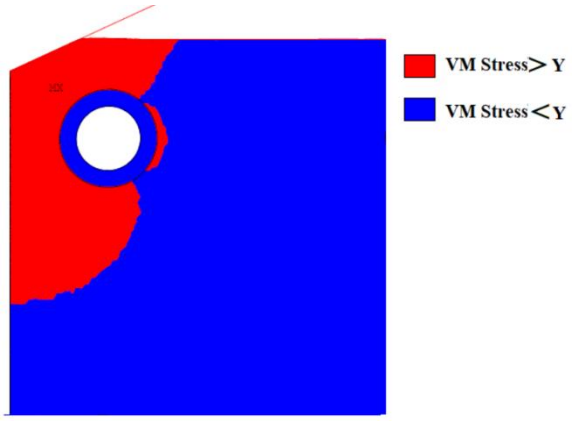

(c)

Figure 2.11: Stress-state contour plot of the near-contact zone comparing von-Mises stress to yield stress corresponding to indentation depth of 0.3354 nm with varying wall thickness: (a) t = 0.034nm, (b) t = 0.102 nm, (c) t= 0.170

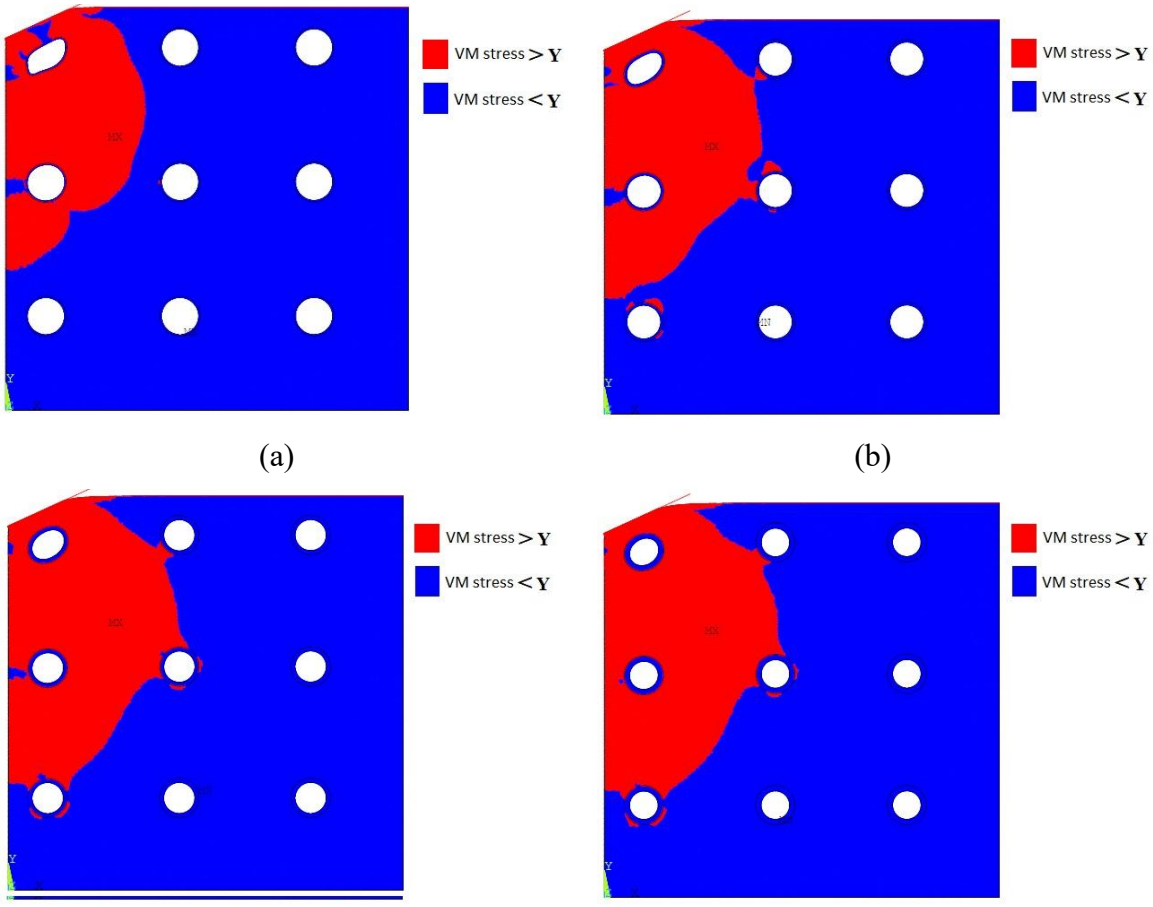

(a) (b)

(c) (d)

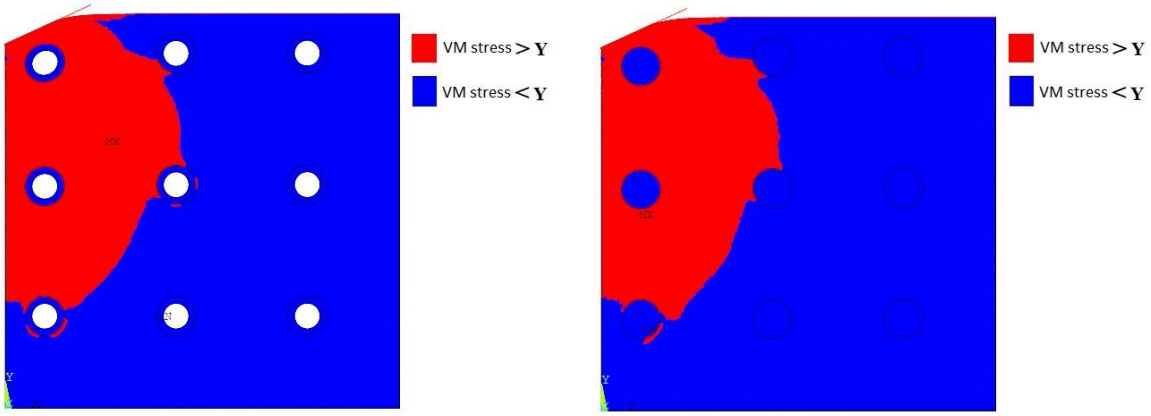

(e) (f)

Figure 2.12: Stress state contour plot comparing von-Mises stress to yield stress at the end of loading phase with indentation depth of 0.78 nm

Figure 2.11 provides the stress-state contour plots of the near contact zone of the Al-SWCNT nano-composite for three values of CNT wall thickness, corresponding to the indentation depth of 0.3354 nm. These plots are generated by comparing the von Mises stress values at each and every point with the yield strength of the material at that point. It provides a visual indication of the portion of the material that has gone into the post-elastic regime. Similar plots corresponding to the final indentation depth is furnished in Figure 2.12. It can be noted from these two figures that, at earlier stage of indentation, for thinner CNT, the yielded zone is larger and it propagates deeper into the nanocomposite. However, as far as yielding of the top surface is concerned, more surface gets yielded when CNT thickness is higher. This is the reason that causes higher contact area for higher CNT thickness at the earlier stage of indentation (Figure 2.7). In the plastically yielded zone, the matrix material undergoes plastic flow in the outward direction w.r.t. the axis of symmetry. As the indentation depth increases, CNTs with low wall thickness gets distorted in such way that the matrix material located at the neighbourhood of the CNTs gets displaced in the inward direction w.r.t. the axis of symmetry (towards left in the axisymmetric model). As a result, stress relaxation takes place in those locations causing partial unloading and creating a few unloaded elastic zones. Consequently, the volume of the yielded material shrinks. Therefore, at final stage of indentation, lower volume of yielded material is observed for thinner CNT wall, which is opposite to the trend observed at earlier level of indentation (0.3354 nm). It is noticeable that the volume of plastically yielded material increases with increases in the thickness of CNTs. However, the increase in volume of plastically yielded material is higher as wall thickness

increases from 0.034 nm to 0.102 nm, as compared to when it increases from 0.136 nm to 0.170 nm.

2.3.3.2 Analysis of Deformation

Examination of different aspects of deformation of Al-SWCNT nano-composite undergoing indentation is also an important feature. Primarily, the deformed shape of the Al-SWCNT substrate at the end of loading phase and after completion of unloading are studied in the present section. The changes in the deformed shape due to variation in the CNT wall thickness are observed at an interference of 0.78 nm once the loading cycle is completed [Figure 2.13(a)] and again after unloading to complete detachment of the indenter (from the above-mentioned interference level) [Figure 2.13(b)]. In each of the loading and unloading stage plots, there are three deformed shapes corresponding to three different wall thickness values (0.034, 0.102 and 0.170 nm). In both the figures a magnified view of the contact region is included. The undeformed shape (provided as a reference) is represented by a dashed line parallel to x-axis in the normal and magnified views in Figure 2.13. This line is the initial position of the top surface of the nano-composite prior to indentation process.

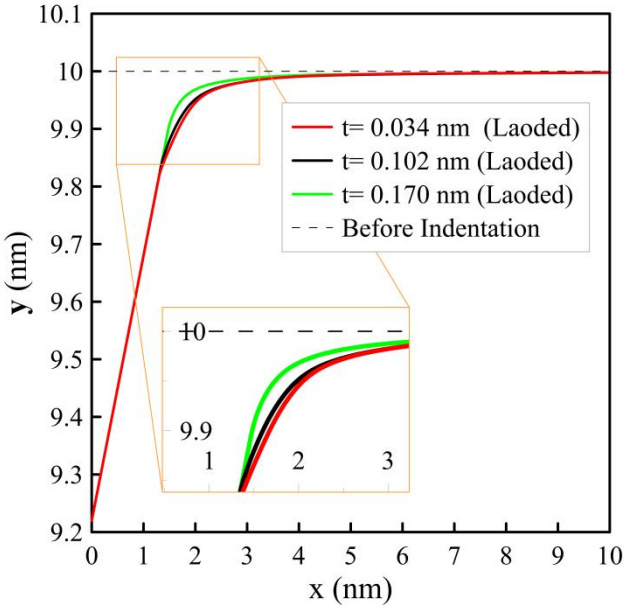

(a)

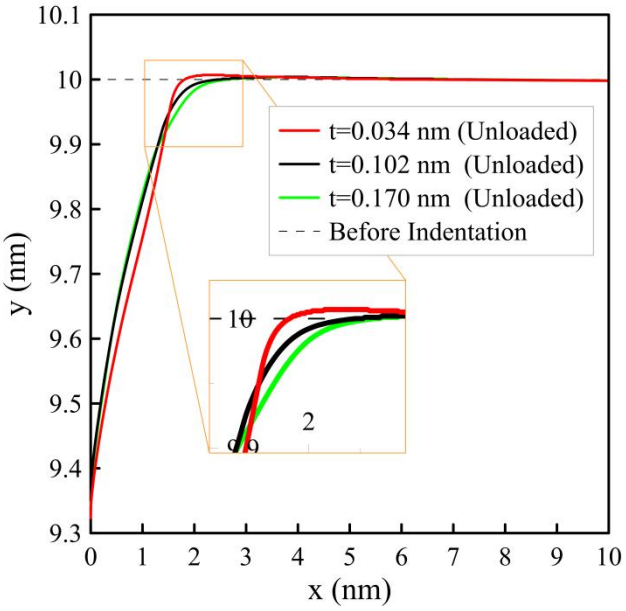

(b)

Figure 2.13: Deformed geometry of contact surface with indentation depth of 0.78 nm: (a) End of loading stage and (b) End of unloading stage.

At the completion of the loading phase, sink-in behaviour is observed which is in accordance with the indentation results of pure Al reported by Celentano et. al. (2012). It is also observed that the depth of sink-in increases with increase in thickness of CNTs. Aluminium is a soft material with low yield strength and as a result there exists a localized plastic deformation region (Figure 2.12) in the metal matrix below the contact area of the indenter. This may cause the material to exhibit sink-in behaviour. As already mentioned, Figure 2.13(b) shows the topography of the top surface of the nanocomposite once there is detachment of the indenter at the end of unloading stage. Significantly, pile-up phenomenon is observed in case of CNT wall thickness of 0.034 nm. Here, the deformed surface is above that of the initial undeformed surface after unloading. Similar pile-up condition has also been reported in case of experimental as well as numerical studies (Carlsson et al., 2001; El Moharrami et al., 2014 and Taljat et al., 2004) of indentation of pure Al substrate. Figure 2.12(a) shows that during loading, in the vicinity of the indenter an elastic zone is formed for low thickness of CNTs but for higher thickness, such elastic zone does not appear.

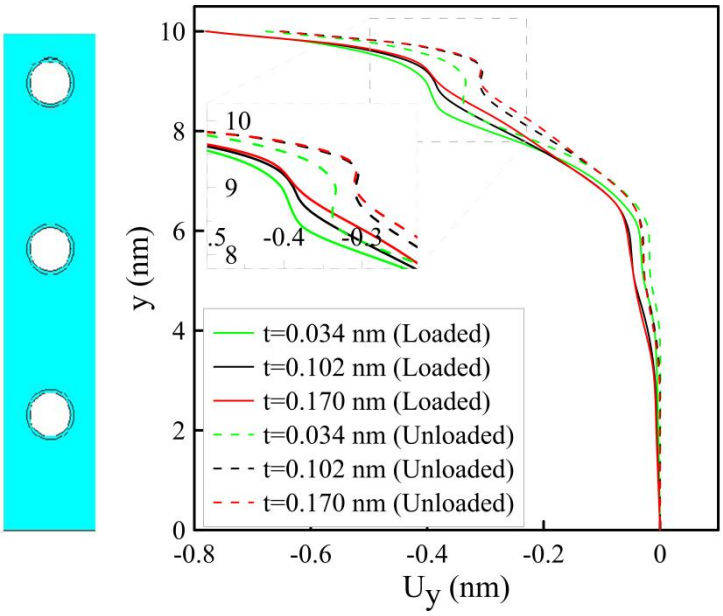

Figure 2.14: Displacement in the y direction of nodes on the line of symmetry for an indentation depth of 0.78 nm.

Figure 2.14 illustrates the nodal displacements in y-direction for the nodes situated on the vertical line of symmetry corresponding to variation of CNT wall thickness. At the end of loading step the indentation depth is 0.78 nm and from this level of interference the indenter is unloaded to complete detachment. The difference between the nodal displacement curves are more prominent at the location where the CNTs are present. The CNTs are able to get distorted under loading and hence, provide more space for the substrate material to deform as well. From the loading curve, it is clearly seen that the displacement of the nodes is larger in the case of low thickness of the CNTs. Lower wall thickness of the tubes provides lower stiffness and consequently more distortion in the shape. That is why the nodal displacements are found to be higher in such a scenario. The dotted line in the figure represented nodal residual displacement after unloading. The trend of the nodal displacement variation also persists in the unloaded state.

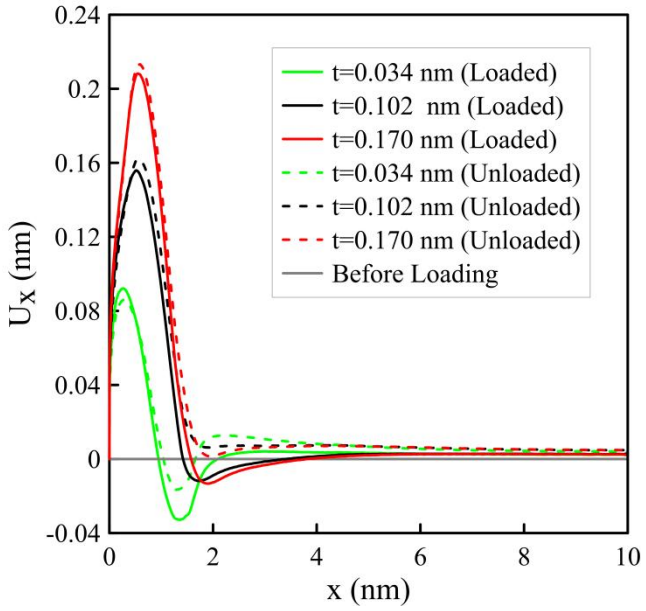

Figure 2.15: Nodal displacement in x direction of the nodes located on the surface

Nodal displacements in the horizontal (x) direction for the nodes located at the top surface of the substrate block are shown in Figure 2.15 for different values of wall thickness. For each thickness, plots for loaded (up to full indentation depth) and unloaded conditions are included. In the vicinity of the indenter tip positive x-direction displacement is observed due to plastic flow in an outward direction (away from y-axis). On the other hand, at the edge of the indenter there is displacement in negative x-direction. This is because, under the action of indentation, the material below the indenter sinks down while pulling the two edges towards each other. Since up to the end of the indentation, more plastic deformation takes place at the vicinity of the indenter (ref. to Figure 2.12), the outward (positive) displacement is higher for high wall thickness of CNTs. The displacement curves after unloading exhibit similar pattern as in case of loading phase. However, during the unloading process, for higher wall thickness of the CNTs, further outward displacement could be observed for the material located below the indenter. This behaviour could be attributed to secondary plastic flow which takes place during the unloading process. The phenomenon of secondary plastic flow of contact surface was previously reported by Kadin et al. (2006) and Etsion et al. (2005) during investigating flattening contact problem.

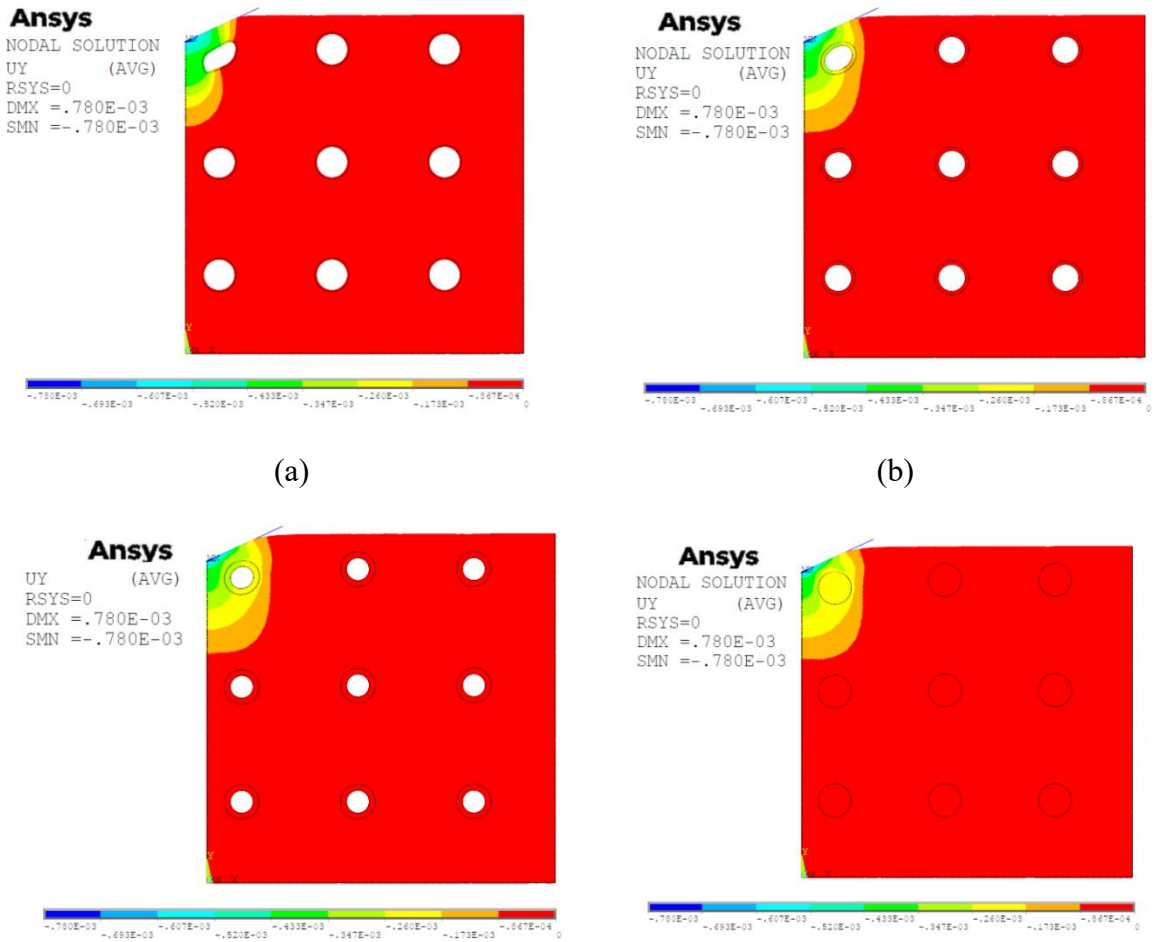

Figure 2.16: Contour plot of nodal displacement in the y-direction of SWCNT nanocomposite loading up to indentation depth of 0.78 nm for varying wall thickness: (a) t =0.034 nm, (b) t =0.102 nm (c) t =0.170 nm and (d) Solid.

Figures 2.16 and 2.17 show the contour plot of y-direction nodal displacement at the end of loading and unloading stages, respectively. As expected, the displacements near the vertical axis of symmetry are high and gradually decreases as one moves away from the point of indentation. Increase in the thickness of the CNTs causes the nodal displacements to also increase towards the positive x-direction. The zone of significant downward displacement is wider for higher thickness of SWCNTs. Similar trends are observed for residual displacement at the end of unloading stage.

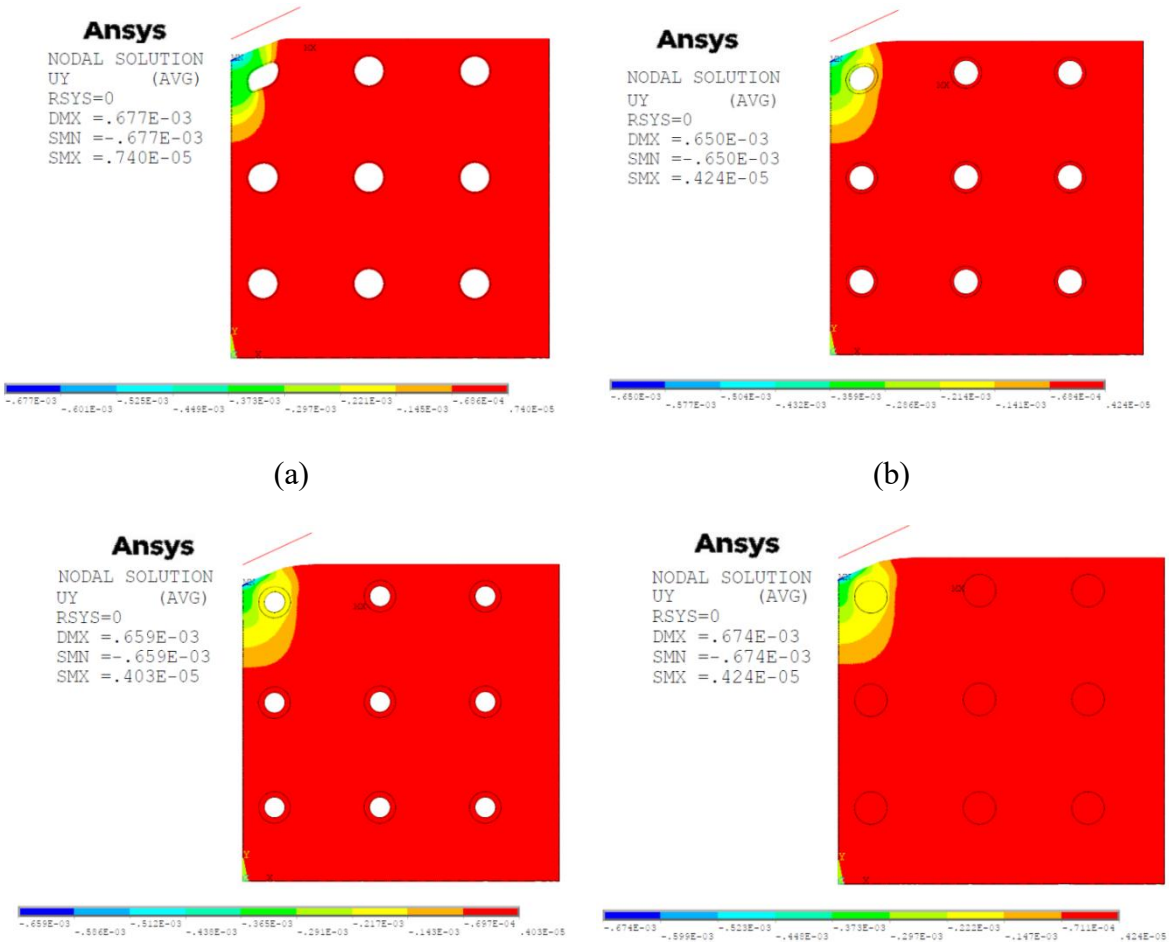

Figure 2.17: Contour plot of nodal displacement in y-direction after unloading from 0.78 nm for varying wall thickness of SWCNT nanocomposites: (a) t =0.034 nm, (b) t =0.102 nm (c) t =0.170 nm, (d) Solid CNT.

2.4 Summary

Chapter 2 presents a finite element-based loading and unloading analysis of Al-SWCNT nano-composites under indentation by a Berkovic indenter. The indentation problem is simulated using ANSYS, successfully developing the nanocomposite substrate model with SWCNTs embedded in an Al matrix. The simulated contact force results align well with published literature. The study varies the wall thickness of the embedded nanotubes, generating results for contact force, contact area, and contact pressure plotted against indentation depth. Stress distribution and deformation are extracted at different indentation stages to assess the wall thickness effect.

Key observations include:

- A change in the trend of contact area vs. indentation depth: lower thickness CNT nanocomposites show lower contact area at shallow depths but higher contact area at greater depths compared to thicker CNT nanocomposites.
- For low-thickness CNTs, significant deformation at high indentation depths causes material displacement toward the axis of symmetry, leading to partial unloading and small unloaded elastic zones in the matrix.
- Sink-in behavior is observed at the end of loading for all cases, with pile-up occurring at a CNT wall thickness of 0.034 nm.
- For high wall thickness CNTs, unloading causes outward displacement of material below the indenter, attributed to secondary plastic flow during unloading.

This page is left blank intentionally

Chapter 3

Flattening Contact Analysis of CNT-Al Nanocomposite

3.1 Introduction

Selecting appropriate materials for specific applications is crucial in modern industrial growth and the use of advanced machinery, where relative motion between contacting surfaces of different parts is inevitable. Contact phenomena are frequently encountered in belts, rolling element bearings, cam-follower mechanisms, gears, and other components. Hence, studying contact at various scales is an essential research domain, especially with advanced materials like nanocomposites. These materials have gained popularity due to their superior mechanical, thermal, and electrical properties, with carbon nanotube (CNT) embedded matrices showing significant improvements. Therefore, investigating the contact behavior of CNT-based nanocomposites and analysing the variation of relevant contact parameters is necessary.

Numerous scholars have recently focused on numerical analysis to understand contact phenomena in different materials. Brake (2012) developed an elastic-plastic contact model for various material qualities and contact geometries. Buczkowski et al. (2014) used fractal theory to determine normal contact stiffness for rough and smooth isotropic surfaces. Chatterjee and Sahoo (2014) used finite element simulation to study the effect of varying elastic modulus in non-adhesive frictionless bulk deformation contact. Wang et al. (2019) created the Gurson-Tvergaard-Needleman damage model and examined peak load impacts during flattening. Peng et al. (2013) investigated the impact of the yield stress to elasticity modulus ratio on contact behavior. Wang et al. (2022) developed an analytical contact model for predicting contact area and force for Gaussian rough surfaces. Ogar et al. (2021) created an analytical model for forecasting residual stress during flattening operations. Wang and Xiang (2013) examined tangential contact properties under normal elastic-plastic deformation. Gandhi et al. (2012) studied the impact of tangent modulus on frictionless elastic-plastic contact behavior.

The cylindrical contact model, efficiently modelling contact interactions in fibrous and anisotropic material structures, is widely used. Significant works on cylindrical contact interaction include those by Johnson (1985), Green (2005), Sharma and Jackson (2017), and others.

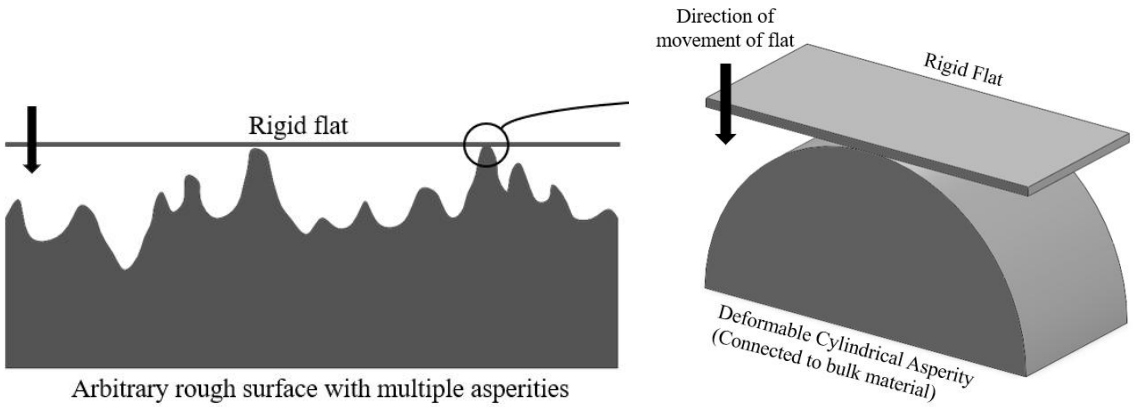

(a) (b)

Figure 3.1: (a) Rough surface in contact with a flat and (b) Schematic representation of cylindrical flattening contact

Contact between rough surfaces can be idealized as multi-asperity or single asperity contact, with cylindrical models representing elongated asperities. Research on CNT-based nanocomposites, such as those by Yoo et al. (2013) and Shin et al. (2016), highlights their enhanced properties. However, finite element modelling of CNT-based nanocomposites in contact analysis remains underexplored.

This chapter investigates the loading and unloading analysis of cylindrical flattening contact between SWCNT-reinforced Al nanocomposites and a rigid flat using ANSYS. The study examines the effects of varying CNT wall thickness and volume percentage, providing novel insights in the field. This finite element simulation model is a novel contribution and could potentially serve as benchmark results in the relevant area of research.

3.2 Finite Element Model

In the present study loading and unloading phases of a flattening type cylindrical contact between Al-SWCNT nanocomposite and a rigid flat are simulated on the basis of a finite element model. The description of the contact system consisting of a cylindrical asperity (Al-SWCNT nanocomposite) and a rigid flat plate is schematically represented in 3D in Figure

3.2. In order to reduce load on computation resources and consequently reduce computation time, a 2D quarter-circle model is used to equivalently represent a 3D half-cylinder [Jackson et al., 2005]. Circular nanotubes are embedded within this quarter-circular region, which has a diameter of 8 nm. So, the model consists of two separate material phases: an Aluminium (Al) matrix and reinforcement in the form of single walled carbon nanotubes (SWCNT).

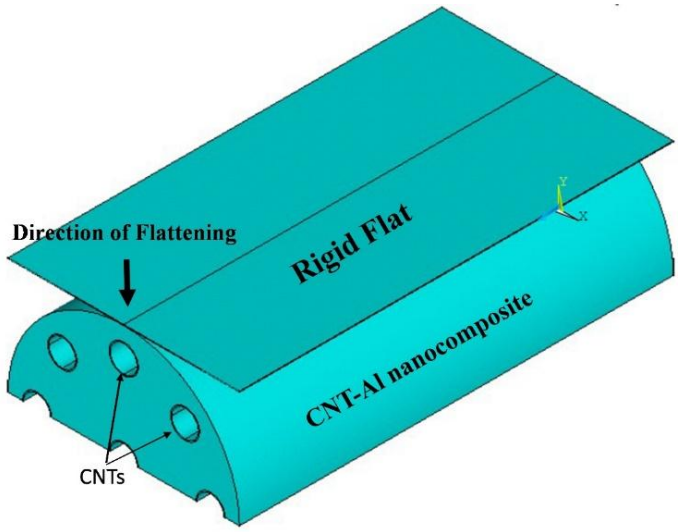

Figure 3.2: Al-SWCNT nanocomposite in contact with a rigid flat

The proposed objective of the present work is to observe the effect of volume percentage of CNT on contact behaviour and hence, provision for the same is provided in terms of variation in number and thickness of CNTs, while the radius is kept constant throughout. In the present model a constant diameter 1 nm is fixed for the CNTs (Yu et.al., 2007; Yuan et.al., 2018; Saito et.al., 1998). Figure 3.3 shows the different models with the varying number and orientation of CNTs within the Al matrix. In Model I there are 2.25 number of CNTs in the quarter-circle (as shown in Figure 3.3), which equates to a total of 9 CNTs in the cylinder. Similarly, Model II and Model III consist of, in total, 13 and 17 CNTs, respectively. For each of the three different models, four different wall thickness (0.034, 0.102, 0.170 nm and solid CNTs) are taken into consideration. The variations of SWCNT volume percentages with the different orientations (Model I, II and III) and wall thickness are shown in Table 3.1. The material properties of the SWCNTs and the matrix material are described in Table 3.2. It should be mentioned here that nanocomposite is assumed to be completely defect free and the interaction between the matrix and the nanotubes is taken into consideration as properly bound and linked.

While considering the different models (Figure 3.3), an important aspect that should be considered is the distance between the nanotubes. It is well established that the Van der

Waals forces between the SWCNTs prevent them from being in close proximity beyond a certain limit (Nouri et al., 2012).

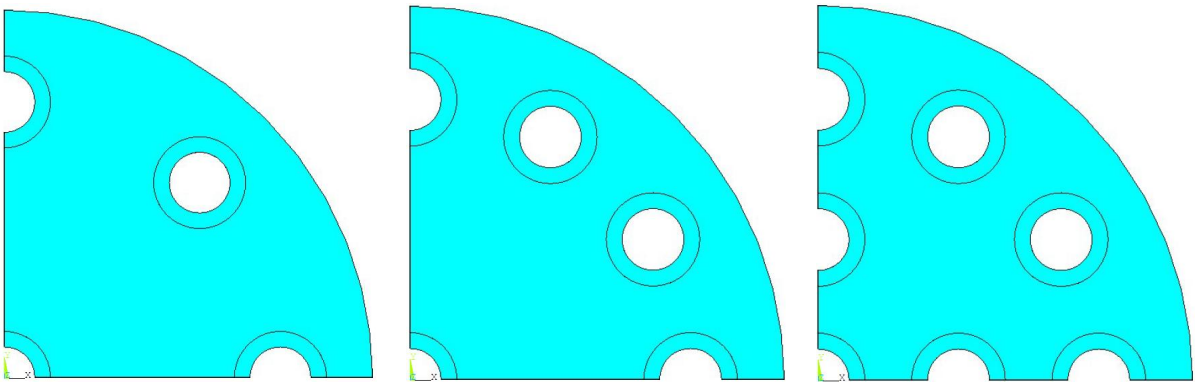

Model I Model II Model III

Figure 3.3: Number and orientation of embedded SWCNTs for different models

Table 3.1: Volume percentages of CNTs

Thickness of CNTs (nm)	**Vol. % of CNT**		
	Model I	**Model II**	**Model III**
0.034	1.85	2.67	3.49
0.102	5.15	7.44	9.73
0.170	7.94	11.47	14.10
Solid	14.06	20.31	26.56

Table 3.2: Value of parameters (Ahmed et al., 2020 and Nouri et al., 2012)

Property	**Value**
Diameter of CNT	1 nm
Interference	0.6 nm
Modulus of Elasticity of CNT, E_t	1000 GPa
Poisson's Ratio of CNT, v_t	0.27
Modulus of Elasticity of Aluminium, E_m	70 GPa
Poisson's Ration of Aluminium, v_m	0.23
Wall thickness of CNT (t)	0.034 nm, 0.102 nm, 0.170 nm and Solid CNT bar

This minimum distance between the nanotubes can be determined from molecular mechanics and it is reported by Nouri et al. (2012) as 3R, where R is the CNT radius. The minimum distance (3R) criterion between the center of two neighboring SWCNTs has been satisfied for the different orientations of the nanotubes. Figure 3.4 shows the quarter-circular model of the cylinder with embedded SWCNTs (Model I), representing a single-asperity, in contact with a rigid flat at the summit of the cylinder. As seen in the Figure 3.4, the rigid surface is represented by a straight line that is parallel to the X-axis. The rigid flat in its downward movement flattens the cylinder up to a given interference level. Once the loading stage is completed, the flat is slowly withdrawn by providing it with an upward movement till detachment and it makes up the unloading stage. The contact behaviour between the cylindrical surface and the rigid flat is regarded as a perfect slip condition, following Jackson et al. (2005). The orientations of the coordinate axes are also shown Figure 3.4. The model's Y-axis is positioned on the vertical axis of symmetry, while, X-axis is horizontal and coincides with the base of the quarter-circle.

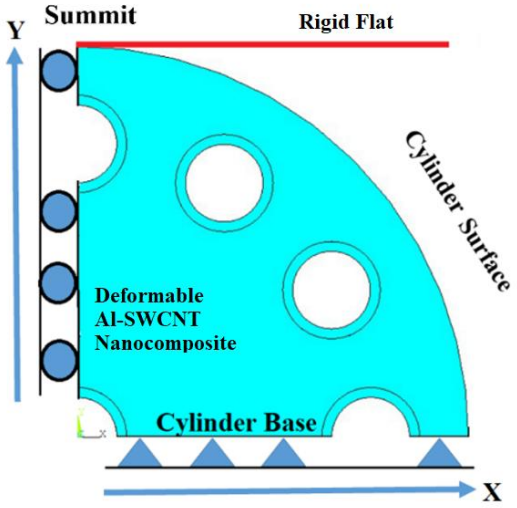

Figure 3.4: Schematic representation of the flattening model with coordinate axes and boundary conditions

The mesh generated for the present finite element model is shown in Figure 3.5. The quarter-circle and rigid flat are meshed using PLANE183, a 2D structural element, and TARGE169, respectively. The structural element has two degrees of freedom in its each node and these are the nodal x- and y-direction translations. The contact surface of the cylinder, i.e., the curved perimeter of the quarter-circle is meshed with CONTA172 elements, overlaying the PLANE183 elements. The mesh is created in such a way that there is fine mesh in and around the critical zones, i.e., the contact region and around the CNTs. Away from these areas, the

mesh is coarse in nature. A detailed convergence study (described later) is performed in order to finalize the mesh configuration and the number of elements. Coarse to fine transition of the mesh configuration helps in reducing computation time substantially. The analysis employs a pure Lagrange multiplier contact algorithm (Chatterjee and Sahoo, 2012; Jackson and Green, 2005), which is appropriate for the present analysis as it enforces zero penetration at the contact interface. In spite of the fact that this algorithm makes the solution computationally costlier, it is preferred for simulating flattening contact problem (Carpenter et al., 1991; Papadopoulos and Soldberg, 1998; Bourago and Kukudzhanov, 2005) because it provides provide the highest level of accuracy among the contact algorithms.

Another critical aspect of a finite element analysis is a proper choice of the boundary conditions. In the present model, the nodes on the Y-axis are restricted to move only in the vertical direction. The nodes present on the base of the quarter-circle, which are coincident on the X-axis, are completely constrained and cannot move in any direction (Brizmer et al., 2005, 2006). The basis for the above assumption is that the asperity is presumably connected to bulk material at its base. The von Mises yield criteria provides the threshold beyond which post-elastic behaviour needs to be implemented and bilinear isotropic hardening is utilized to model such behaviour.

As previously mentioned, the rigid flat simulates loading and unloading of the asperity by its downward displacement (in the negative Y-direction) till an interference of 0.60 nm and consequently moving upward until there is detachment. Various contact parameters, such as, contact force, contact area, stresses developed in the zone of contact and in the vicinity of the SWCNTs, describe the contact behaviour and are extracted through post-processing.

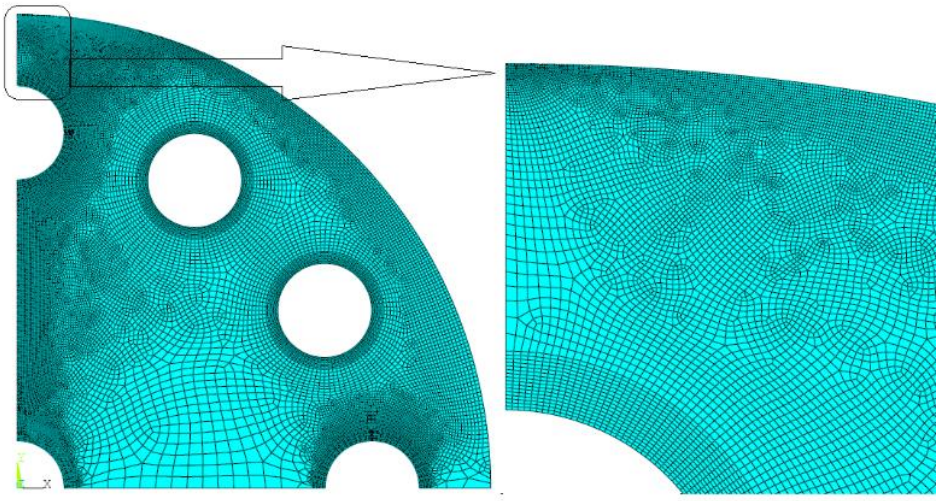

Figure 3.5: Mesh configuration with magnified view of the near-contact zone

3.3 Mesh Convergence Study

Determination of an appropriate mesh configuration is probably one of the most important aspects of a finite element analysis. It ensures that sufficient number of elements are present in the system to generate sufficiently accurate results, while keeping the computation time in check.

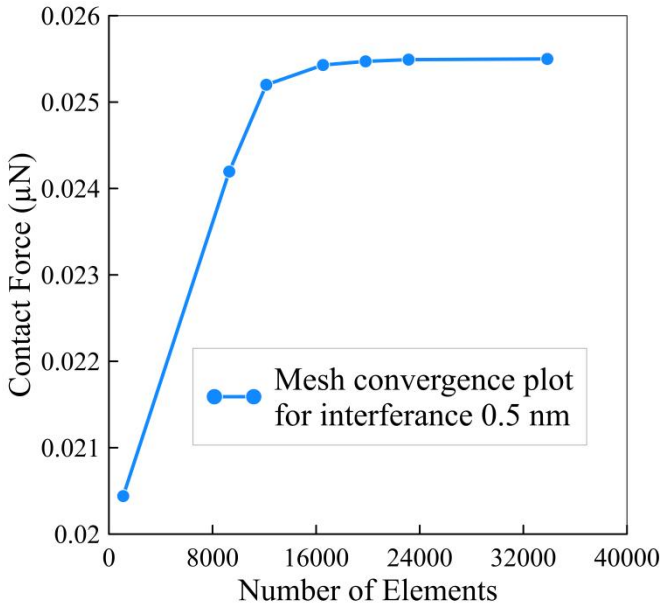

Figure 3.6: Mesh convergence plot: Contact force vs. numbers of elements.

For the present work, mesh convergence study is performed on Model I with an interference of 0.5 nm. Gradual increase in the number of elements is effected (to create progressively finer mesh), while keeping track of the contact force. the termination criterion is taken as 0.05% variation in contact force between subsequent iterations. It should be reiterated here that the mesh configuration is such that around the critical zones concentration of elements is high. Figure 3.6 displays the result of convergence study in terms of contact force vs. number of elements plot. It is perfectly clear from the figure that beyond a certain number of elements there is hardly any variation in contact force. Accordingly, an appropriate number of elements is selected for the present research work.

3.4 Validation Study

The validity of the developed finite element model must be established before generation of meaningful results and the best way to validate is to compare with published results for similar systems. However, to the best of authors' knowledge, there are no existing studies that deal with flattening of CNT based nanocomposites. In this scenario, the present model

can be tested against certain systems with reduced complexity or through comparison with a problem which has some similar aspects.

Contact force results generated through the present model is compared with two different previously published models. First, comparison is made with results of Jackson et al. (2005), where, a 2D semi-circular model for hemispherical flattening contact (with homogeneous material in absence of embedded CNTs) is analyzed. The radius of the semi-circle is considered as $1\mu m$, while, material properties used in this model are as follows: Young's modulus – 200 GPa, Poisson ratio – 0.32, Yield Stress – 0.210 GPa. Needless to say, in order to make the comparison, the SWCNT dimension and properties in the present model are set to zero. The comparative results are presented in Figure 3.7, where, normalized interference is plotted against normalized contact force. The normalization scheme followed here is exactly same as presented in Jackson et al. (2005). The figure demonstrates that the results of the current model have a significant degree of agreement with the established results.

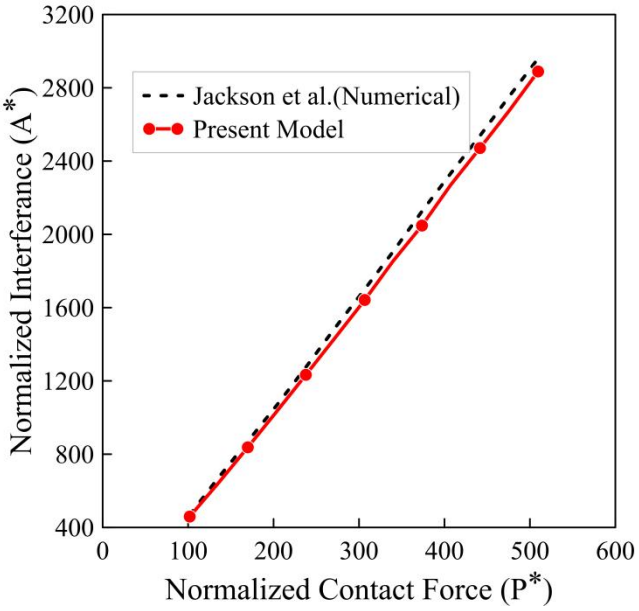

Figure 3.7: Validation Study: 2D hemispherical flattening contact with homogeneous material (Jackson et al, 2005)

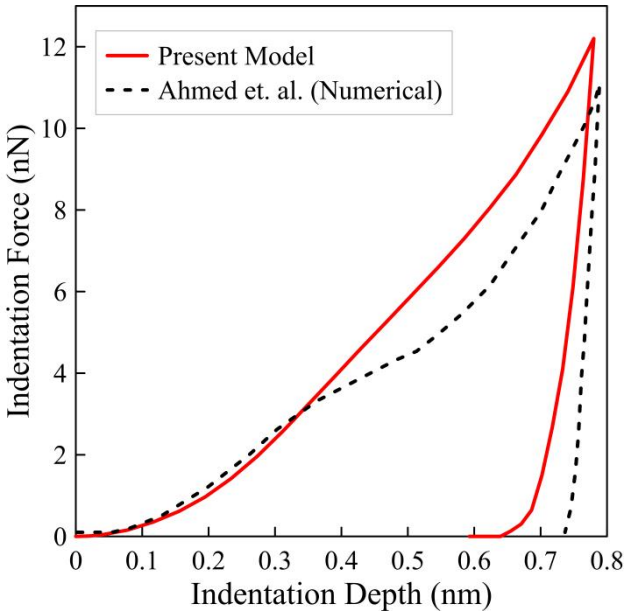

Figure 3.8: Validation Study: CNT-Al nanocomposite indentation with Berkovic indenter (Ahmed et al., 2020)

The second comparison is carried out for an indentation problem [Ahmed et al., 2020]. Here, instead of a rigid flat flattening a cylinder, indentation of a 10 × 10 nm CNT-Al nanocomposite substrate with a Berkovic indenter (modeled as a line that intersects the vertical axis at an angle of 65.30 degrees) is considered. The objective of this study is to check if the present model can accurately simulate CNT behaviour along with its interaction with the metal matrix. The contact force comparison corresponding to the two different models are furnished in Figure 3.8. It is apparent from the figure that the trend of contact force variation with respect to indentation depth is similar, with a maximum variation of less than 10%. These two comparative studies establish the validity of the present model albeit for systems with reduced complexity or slight variation in problem description.

3.5 Results and Discussion

Finite element based Loading-unloading analysis of cylindrical contact between SWCNT-Al nanocomposite and a rigid flat is conducted following the process explained in the preceding sections and the results are extracted in the post-processing step in the form of various contact parameters, such as contact force, contact area, stress distribution and deformations. SWCNT volume percentage is varied on the basis of the three models described before, which implies that change is enforced by considering different numbers of nanotubes with different wall thickness but constant diameter.

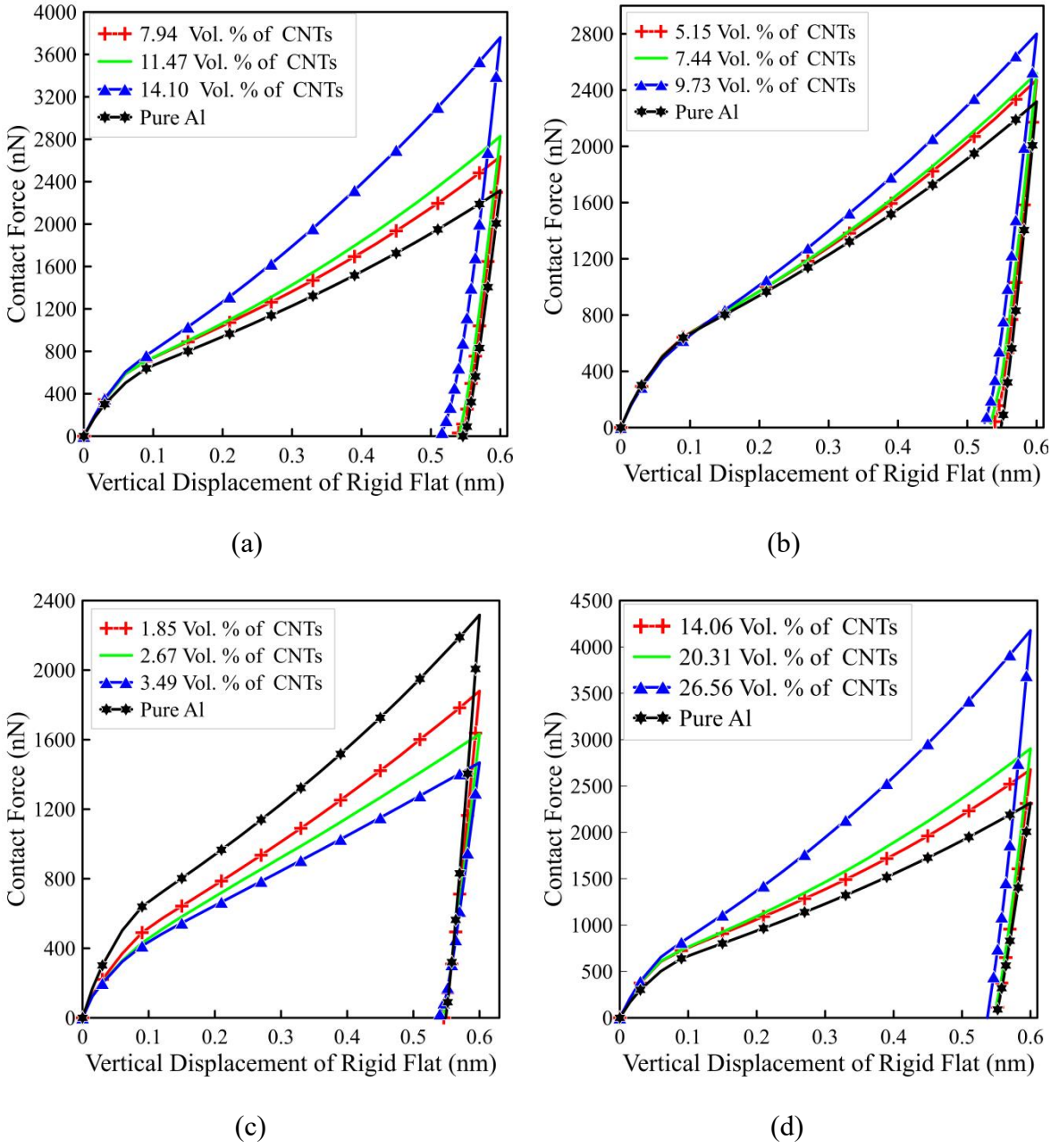

Figure 3.9: Interference vs. Contact Force plots for loading and unloading of SWCNT nano-composite with varying volume % and wall thickness of the SWCNTs: (a) 0.034 nm, (b) 0.102 nm (c) 0.170 nm and (d) Solid CNT.

The first set of data, shown in Figure 3.9, presents variation of contact force w.r.t. interference or vertical displacement of the rigid flat corresponding to three different wall thickness (0.034 nm, 0.102 nm and 0.170 nm) and Solid CNT. In each of these plots, there are three loading-unloading curves are presented for various volume percentages. These volume percentages are, of course, outcome of different number, distribution (Model I, II and III) and wall thickness of CNTs (Refer Table 1). In addition to these, each plot also

includes the loading-unloading curve for a pure Al specimen, without embedded CNTs. Interestingly, Figure 3.9(a) shows that contact force for pure Al quarter-cylinder flattening is greater than that obtained in case of nanocomposite with 0.034 nm thick SWCNTs. It is also observed that in this case (Figure 3.9(a)), contact force (for a given interference) reduces with increase in volume % of CNTs. It is natural to expect the contact force to increase with increase in volume % of reinforcement material, as the material becomes stiffer. However, it should be mentioned here that in an earlier experimental study [Liu et al., 2012], it was observed that a higher volume percentage of CNT resulted in lowering of yield strength of the material.

The trend shown in Figure 3.9(a) is completely opposite of what is observed for other three cases of wall thickness in Figures 3.9(b) to 3.9(d). Here, an increase in volume % results in an increase in contact force. It is also noted that at lower interference, the gap between contact force curves for different volume % is small, but increases substantially as contact moves towards high interference zone. At lower interference, there is hardly any deformation of the CNTs, as majority of the load is taken up by the matrix material. However, with increase in downward displacement of the flat, CNTs start to deform and provide resistance to flattening. As volume percentage of SWCNTs is raised, the strength of the nanocomposite increases, which affects the contact force during the loading and unloading stages.

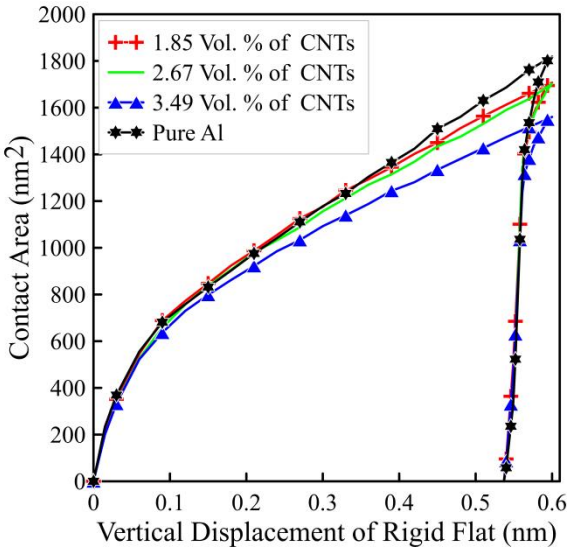

(a)

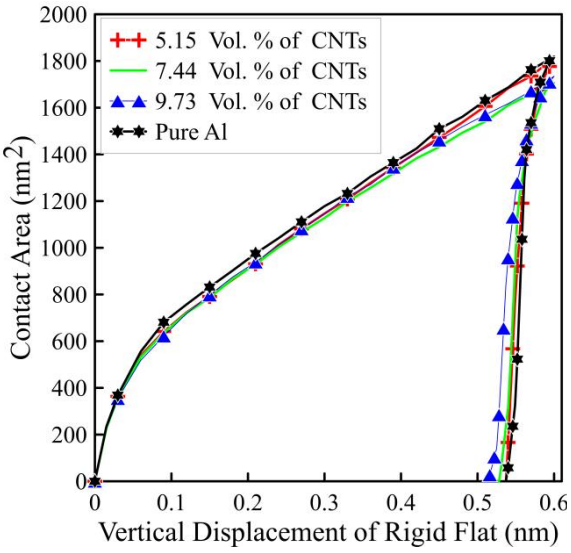

(b)

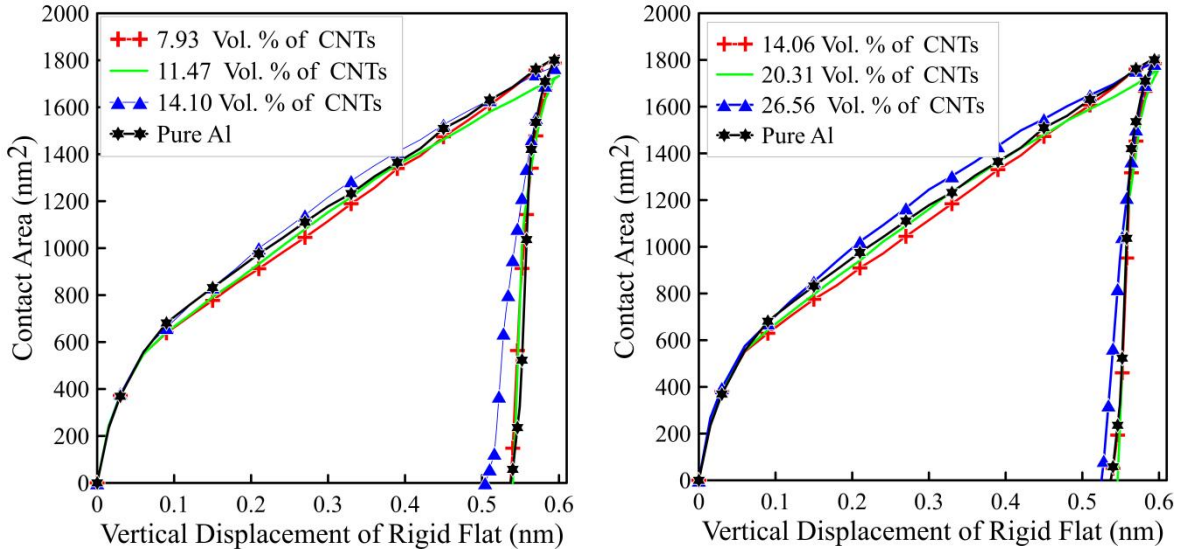

(c) (d)

Figure 3.10: Interference vs. Contact Area plots for loading and unloading of SWCNT nanocomposite with varying volume % and wall thickness of the SWCNTs: (a) 0.034 nm, (b) 0.102 nm (c) 0.170 nm and (d) Solid CNT.

Variation of contact area with vertical displacement of rigid flat during loading and unloading phases is presented in Figure 3.10. Similar to Figure 3.9, wall thickness of 0.034, 0.102, and 0.170 nm along with solid CNT are considered, while, variation of volume percentage takes place as per Table 1. In all the cases (Figs. 3.10(a) to 3.10(d)), the contact area curves are found to be close to one another and it seems volume % does not significantly effect this parameter. Closer inspection of Figure 3.10(a) shows that contact area for pure Al is higher than that of the CNT reinforced cases, with higher volume % of CNT corresponding to lower contact area. Similar to the previous figure, at lower interference contact area curves overlap one another as only the matrix material deforms at this stage.

3.5.1 Analysis of Stresses

Investigation into developed stresses and its distribution plays an important part in contact analysis. Figure 3.11 provides contour plots of average von Mises stress developed in the quarter-circle of nanocomposite corresponding to variation in the volume % of CNT. For stress analysis, Al-SWCNT nanocomposite with wall thickness of 0.034 nm is chosen. The choice is made due to the fact that this particular CNT wall-thickness exhibited opposite behaviour (as seen in Figure 3.9(a) and 3.10(a)) to the other cases.

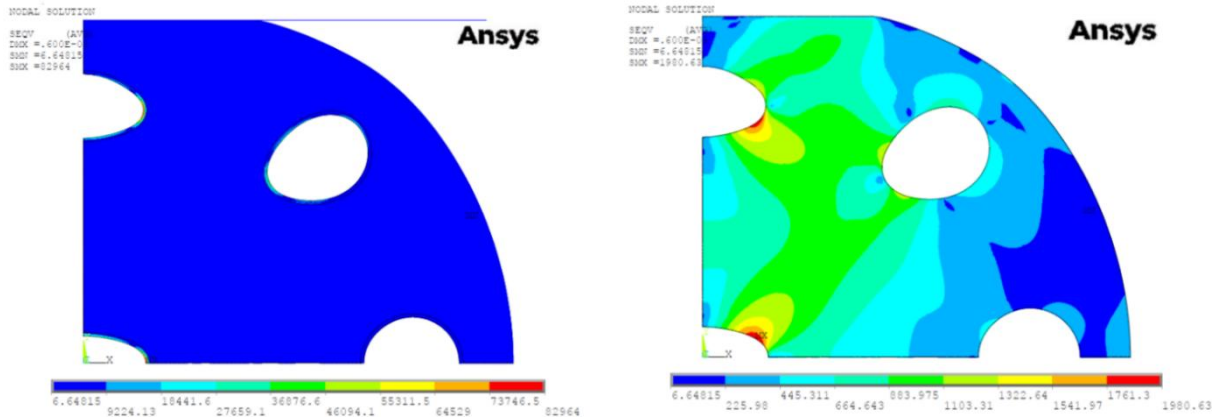

(i) (ii)

(a)

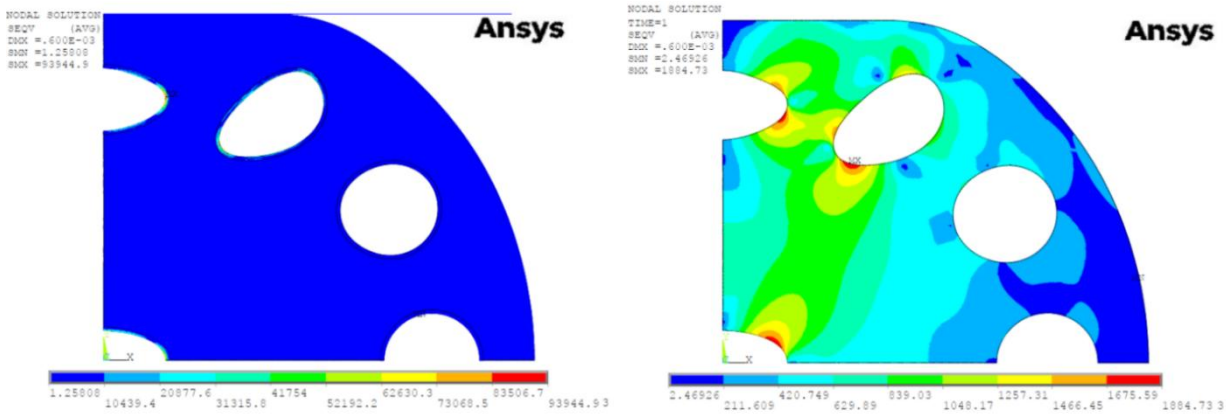

(i) (ii)

(b)

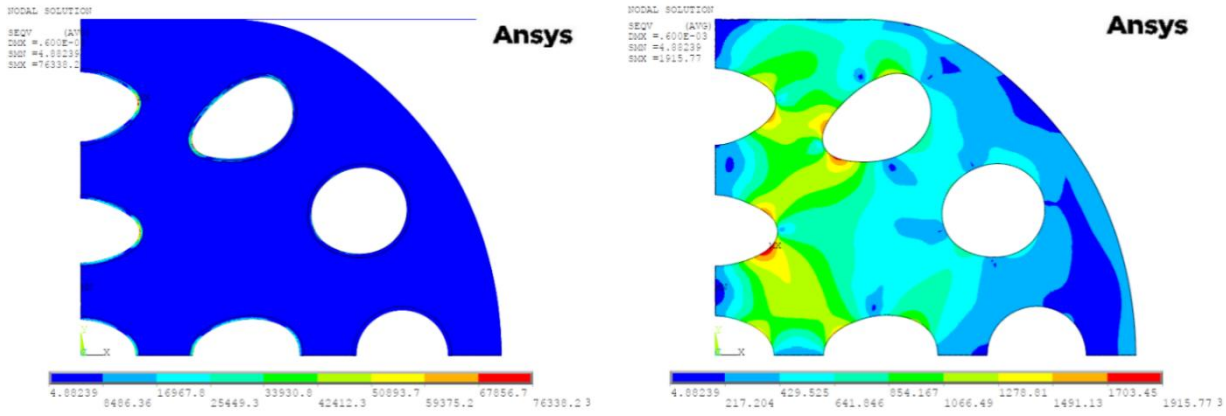

(i) (ii)

(c)

Figure 3.11: Contour plot of von-Mises stresses at the end of loading phase (interference of 0.6 nm) with varying volume percentages of SWCNT: (a) 1.84%, (b) 2.67% and (c) 3.49%.

Modulus of elasticity of CNT is much higher than the matrix material (Al) and as a result it is expected that significantly higher stresses are going to be generated in the nanotubes. Due to the difference in level of stresses between the CNTs and the matrix, a single contour plot is not sufficient to clearly depict the stress distribution in the system. So, two different contour plots are presented side by side, where, the figure marked (i) shows stress contour plot for the entire nanocomposite, while, the figure marked (ii) shows stress distribution in the Al matrix excluding the SWCNTs. These contour plots are presented for three different volume % (1.85%, 2.67% and 3.49%) as shown in Figs. 3.11(a) to 3.11(c). It is seen from the figures that there is considerable distortion in the shape of the CNTs near and directly below the contact zone, whereas, those nanotubes located further away, more or less, retain their shape. Consequently, higher stresses are found to be in these highly distorted nanotubes. As for the matrix material, high stress zones are located in the vicinity of the deformed CNTs located below the contact zone.

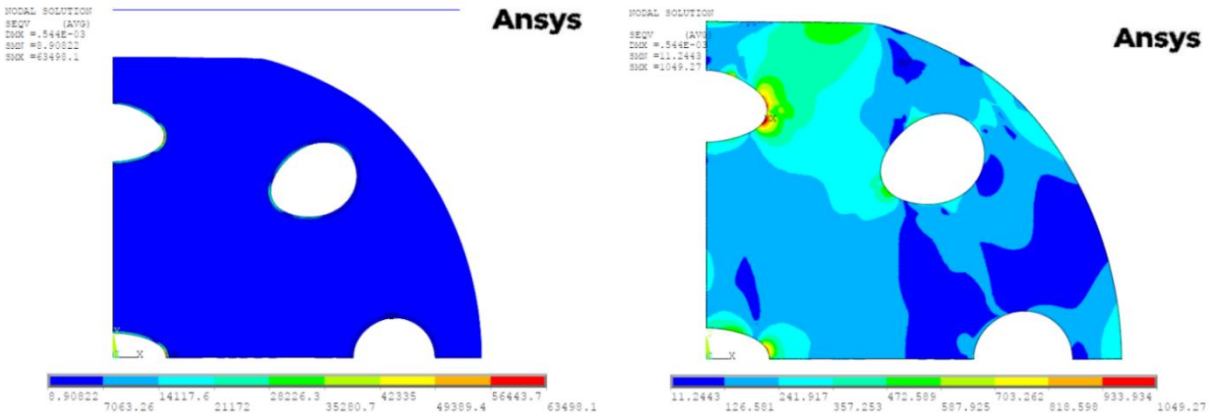

(i) (ii)

(a)

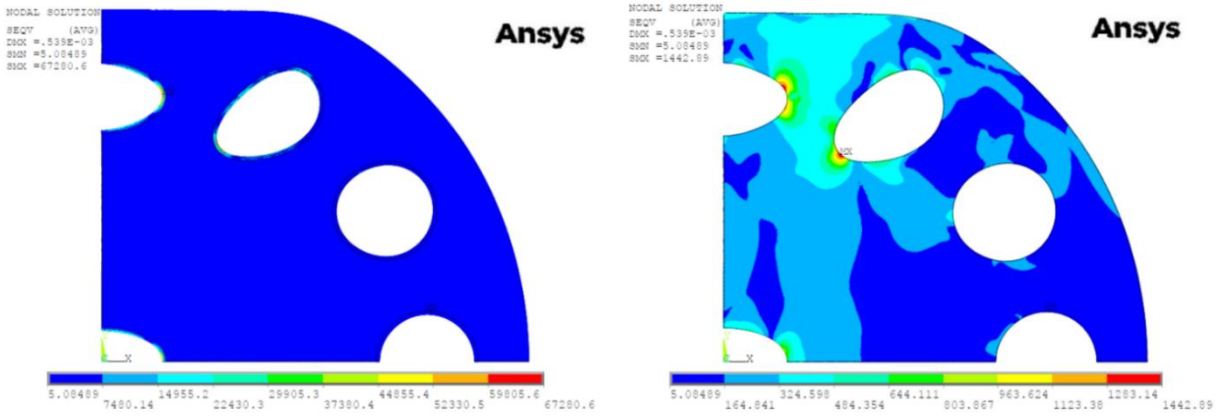

(i) (ii)

(b)

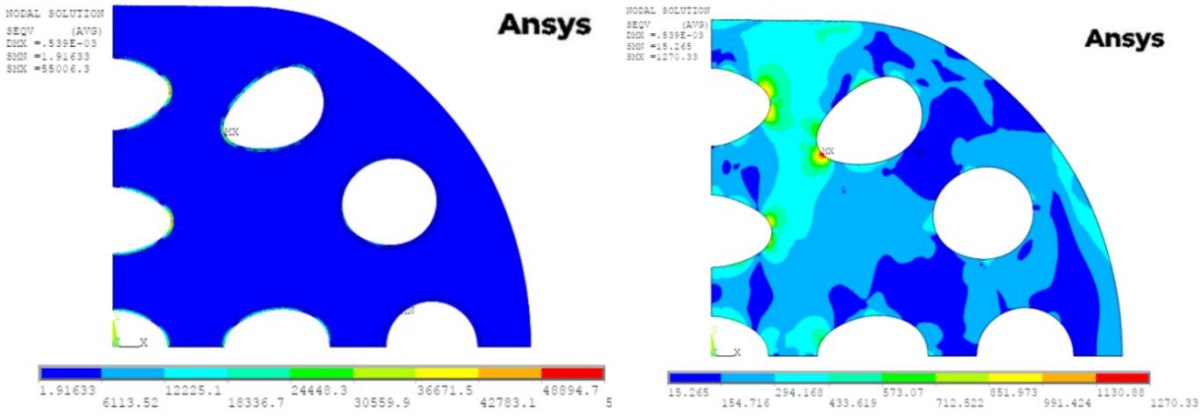

(i) (ii)

(c)

Figure 3.12: Contour plot of residual von-Mises stresses after unloading from interference of 0.6 nm with varying volume percentages of SWCNT: (a) 1.85%, (b) 2.67% and (c) 3.49%.

It is also important to observe the deformed geometry and residual stresses of the system once the rigid flat is completely unloaded. Figure 3.12 presents the contour plot of residual von Mises stress of Al-SWCNT nanocomposite with 0.034 nm nanotube wall thickness corresponding to variation in volume % of CNT. Here unloading is done from an interference of 0.6 nm. In this figure as well, for each volume % there are two stress distribution plots – one for the complete system including the CNTs and the other for the matrix material only. In all the scenarios, high residual stresses are found localized in the matrix near the distorted edge of the nanotube, i.e., these zones are directly below the contact region. However, the magnitude of the residual stresses in the matrix is found to be far smaller than the residual stresses in the CNTs.

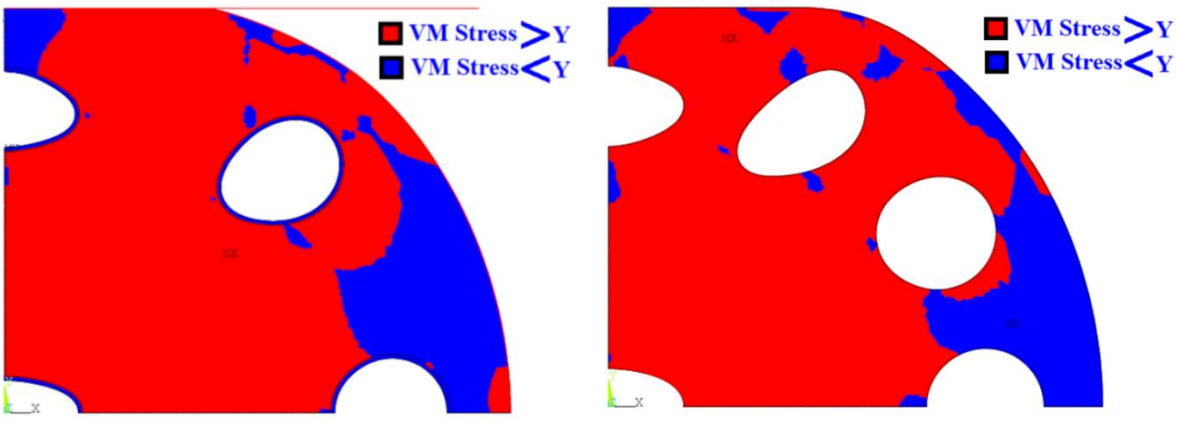

(a) (b)

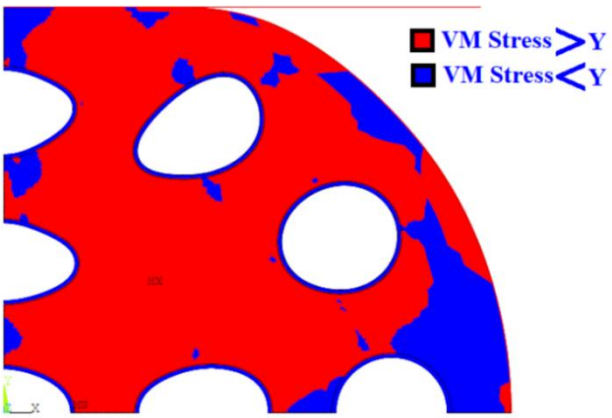

(c)

Figure 3.13: Stress state contour plot for the entire semi-cylinder with varying volume percentages of SWCNT: (a) 1.85%, (b) 2.67% and (c) 3.49%.

Stress state contour plots are generated by comparing the von Mises stress at each and every location within the system with the yield strength of the corresponding material. It provides visual indication of how much and which portions of the material has undergone yielding. In Figure 3.13 stress state contour plots of the flattening contact at an interference of 0.6 nm are provided for varying volume fraction of CNTs, whose wall thickness is 0.034 nm. The state of the material, whether it is in elastic or post-elastic regime at the end of loading phase, is clearly demonstrated through these plots. From the figures it is observed that with increase in volume % of SWCNTs, there is increase in the plastically deformed region. Interestingly, a few small elastic domains are also found directly below the contact zone. These elastic zones are found to be clustered around the location of the CNTs. The matrix material, in the plastically yielded region, undergoes plastic flow in the outward direction, i.e., away from the vertical axis. On the other hand, as the CNTs (with low wall thickness) gets deformed out of shape, some of the matrix material located in the vicinity of these CNTs get displaced towards the vertical axis, i.e., in an inward direction. As a result, stress relaxation takes place in certain small pockets of material causing partial unloading. Consequently, these small elastic zones are formed.

3.5.2 Analysis of Deformation

Important insights can be gained by analysing the deformation and nodal displacements at the end of loading and unloading phases of Al-SWCNT nanocomposite flattening. To maintain consistency with the previous section, the results presented in this section correspond to CNT wall-thickness of 0.034 nm. X and Y direction displacements of the nodes

situated on the cylinder surface are plotted for variation in volume % of CNTs in Figs. 3.14(a) and 3.14(b), respectively.

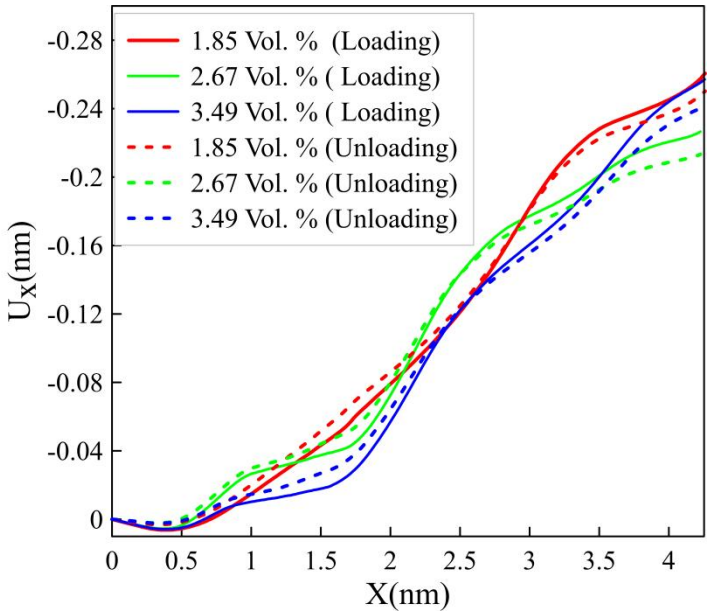

(a)

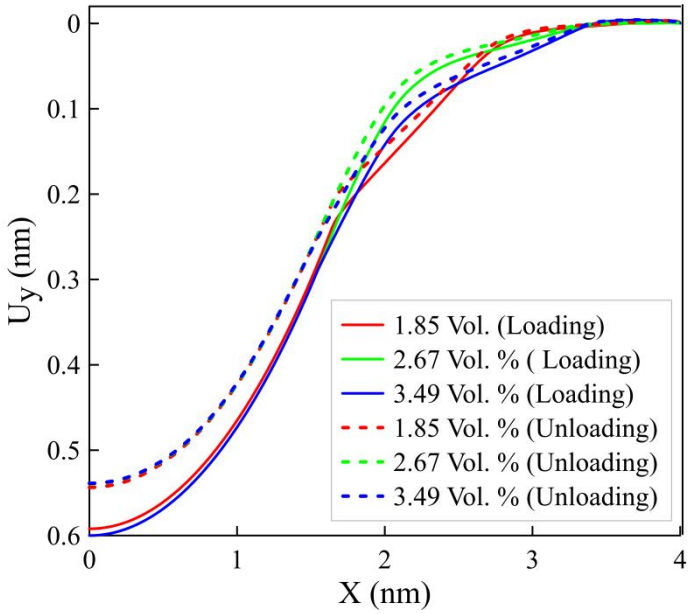

(b)

Figure 3.14: (a) X- and (b) Y-direction displacements of nodes located at the surface of the nanocomposite cylinder with variation of volume % of CNTs at the end loading to and unloading from interference of 0.6 nm.

In order to obtain these displacement curves, it is necessary to extract and keep track of the original position (coordinates) of the nodes, as well as the final deformed position after loading and unloading. Values of X and Y direction displacements are calculated by

subtracting the corresponding initial coordinate from the final coordinate. The set of curves represented in solid lines are indicative of displacements at the end of loading stage, which ends at an interference of 0.6 nm. On the other hand, dotted lines represent residual displacements at the end of unloading from the above-mentioned vertical displacement of the rigid flat.

From Figure 3.14(a) it is clear that at the locations of the SWCNTs there is some deviations in the X-displacement curves. Due to elastic compression close to the contact zone during loading, there is displacement in the negative X-direction. However, outward material flow, which results in outward plastic flow, is represented by positive X-direction displacement. In this scenario, it is understood that position of the CNTs also plays a significant role along with volume %.

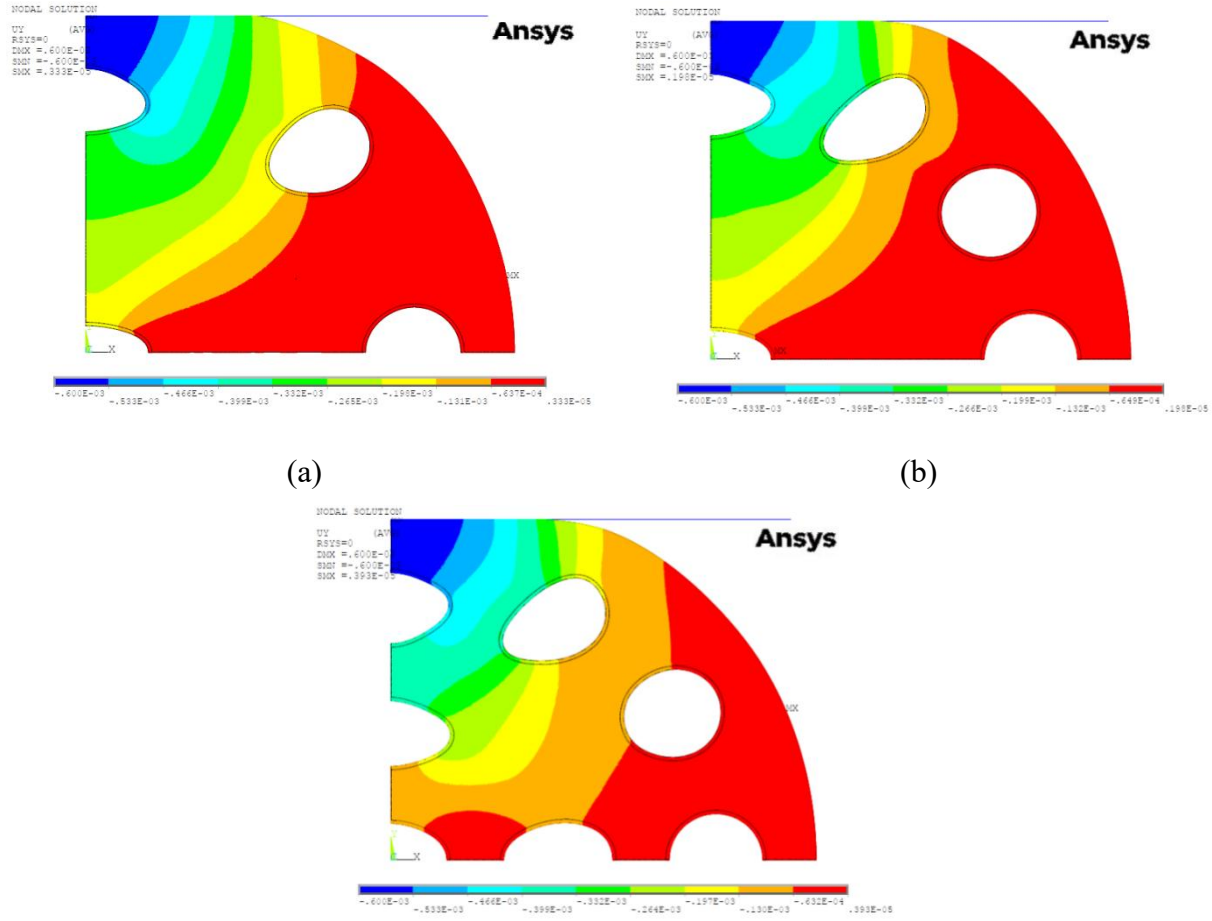

(a) (b)

(c)

Figure 3.15: Contour plot of Y-direction nodal displacement at the end of loading up to interference of 0.6 nm for varying volume percentages of SWCNT: (a) 1.84%, (b) 2.67% and (c) 3.49%.

Material on the cylinder surface flows in the Y-direction as indicated by Figure 3.14(b). As before, there are two sets of curves present in this plot representing Y-direction displacements at the end of loading and unloading phases. Within the contact zone Y-direction displacement is governed by the downward displacement of the rigid flat and hence for all three orientations of CNTs (Model I, II and III) the curve is almost identical. Beyond the contact region variation in the displacement curve is observed.

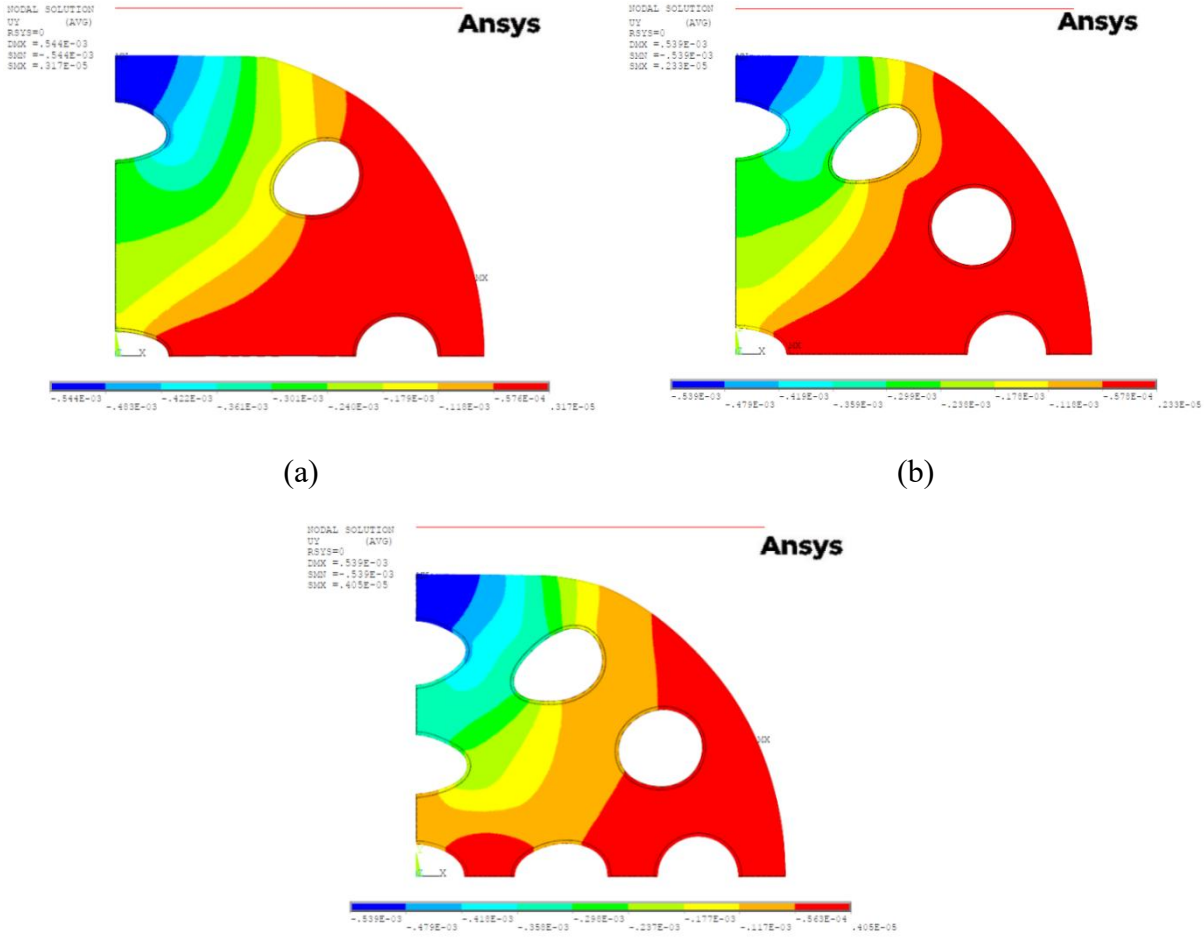

(a) (b)

(c)

Figure 3.16: Contour plot of Y-direction nodal displacement after unloading from 0.6 nm interference for varying volume percentages of SWCNT: (a) 1.85%, (b) 2.67% and (c) 3.49%.

At the end of the loading and unloading stages, the contour plot of the material displaced in the Y-direction is shown in Figs. 3.15 and 3.16, respectively. Figure 3.15 demonstrates that as SWCNT volume percentage grows, material displacement in the vertical direction becomes more dominant. It is observed that the material displacement is higher for the material above the SWCNTs close to the contact zone because there is more SWCNT deformation. The displacement is also higher for the material close to the vertical line of symmetry, but it

decreases as the distance increases from the axisymmetric line. After complete unloading, similar pattern of material displacement is observed in the system, as shown in Figure 3.16.

2.6 Summary

This chapter primarily investigates how varying SWCNT volume percentages affect contact parameters like contact force, contact area, and the stresses developed near the nanotubes. The analysis also explores deformation patterns to gain insights into the behavior of the contact interface.

Key observations include:

- Contact force and contact area generally increase with higher CNT volume percentages, except for CNTs with a 0.034 nm wall thickness.
- CNTs exhibit significantly higher stresses due to their high elastic modulus, with stress concentrations near the deformed nanotubes.
- The volume of plastically yielded material increases with higher CNT volume percentages, with small elastic zones beneath the contact area.
- The matrix material shows greater outward displacement near the contact zone, increasing with higher SWCNT volume percentages.

Chapter 4

3D Indentation Contact Analysis of FG-CNTRC Nanocomposite

4.1 Introduction

Carbon nanotubes (CNTs) are highly regarded as reinforcement materials for composites due to their exceptional mechanical, electrical, and thermal properties. CNTs possess a Young's modulus around 1 TPa, a tensile strength of 200 GPa, and high aspect ratios ranging from 30 to thousands (Shen and Zhang, 2010; Kirtania et al., 2014). They significantly enhance the strength, stiffness, and fracture toughness of composite materials, making CNT-reinforced nanocomposites highly attractive for various industries, including aerospace, automotive, electronics, and energy (Tang et al., 2013; Kirtania et al., 2014).

Research has demonstrated that the volume percentage of CNTs substantially impacts the mechanical, thermal, and electrical properties of nanocomposites (Tamayo-Vegas et al., 2022; Gorrasi et al., 2013; Gojny et al., 2006; Ürk et al., 2016; Zare et al., 2018). Multi-scale finite element method (FEM) simulations have been employed to investigate the mechanical behavior of CNT within nanocomposite matrices (Tzeng et al., 2008; Yang et al., 2013). Giannopoulos et al. conducted FEM analyses to understand the influence of single-walled CNTs on mechanical properties such as Young's modulus and stiffness (Giannopoulos et al., 2010). Aluminium and its alloys are favored matrix materials for CNT-based nanocomposites. Kwon et al. (2009) developed a novel method combining hot extrusion with spark plasma sintering to enhance the mechanical properties of CNT-reinforced aluminium matrix composites. Similarly, Zhan et al. (2003) and Ahmed et al. (2020) explored the mechanical properties and contact parameters of Al-CNT nanocomposites through experimental and FEM approaches. Functionally graded materials (FGMs) exhibit a gradual variation in properties across their volume, effectively mitigating stress concentration and improving mechanical performance under gradient thermal or structural loading (Miyamoto et al., 2013). FGMs are classified as compositionally or structurally graded materials. Compositionally graded materials transition element ratios throughout the material, while structurally graded materials vary in microstructure or phase distribution. Shen (2009) proposed that varying

CNT distribution patterns could substantially improve load-carrying capacity. Zhang et al. (2015) used a mesh-free model to analyze FG-CNT buckling, while Shen and Zhang (2009) studied post-buckling behavior and thermal effects. Phung-Van et al. (2014) developed a numerical approach using a novel cell-based smoothed plate element, and Abdelaziz et al. (2017) employed hyperbolic shear deformation theory for FGM sandwich plates. Numerous studies on FG-CNT materials have addressed buckling, vibration, bending, and mechanical properties (Civalek et al., 2020; Zhang et al., 2020; Soni et al., 2022; Liew et al., 2015; Adewunmi et al., 2016). Spherical indentation is a technique to characterize mechanical properties at small scales, inducing localized deformation to extract elastic properties, plasticity, fracture resistance, and surface interactions. Extensive research has been conducted on the contact mechanics of spherical indentation (Ghaednia et al., 2017). Notable studies on spherical indentation contact on FGMs include works by Giannakopoulos and Suresh (1997), Jorgensen et al. (1998), Wagih et al. (2019), Ziegler and Kraft (2014), and Liu and Wang (2008). These studies demonstrated the influence of material gradation on contact behavior and established empirical correlations between gradation indices and indentation parameters. Despite extensive research on FGMs, no studies have focused on indentation contact analysis for functionally graded carbon nanotube composites (FG-CNTRCs). This research gap highlights the need for comprehensive contact analysis of FG-CNTRC surfaces. This chapter presents a loading-unloading indentation contact analysis on an FG-CNTRC substrate, investigating the effect of gradation on contact parameters.

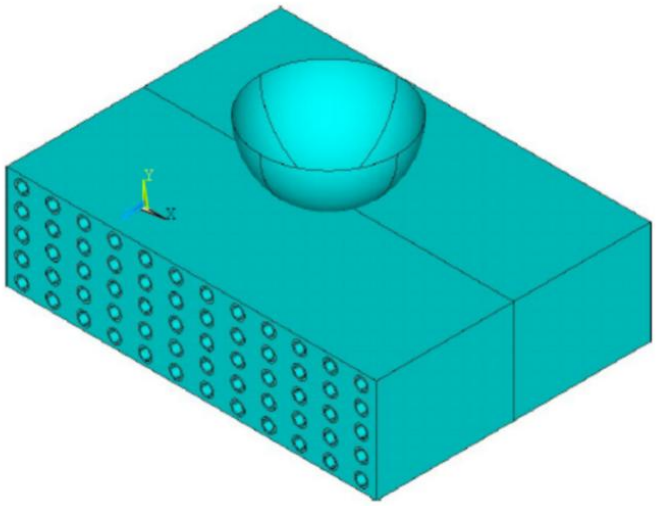

Figure 4.1: FG-CNTRC spherical contact system

Unlike previous studies, this work adopts three general CNT distribution types: positively graded distribution (PGD), negatively graded distribution (NGD), and uniform distribution

(UD). A 3D finite element model is created using APDL code in ANSYS, simulating loading and unloading phases of indentation. The model's validity is established by comparing results with published data for similar systems. The resulting contact parameters during loading and unloading stages are analyzed and discussed.

4.2 Finite Element Model

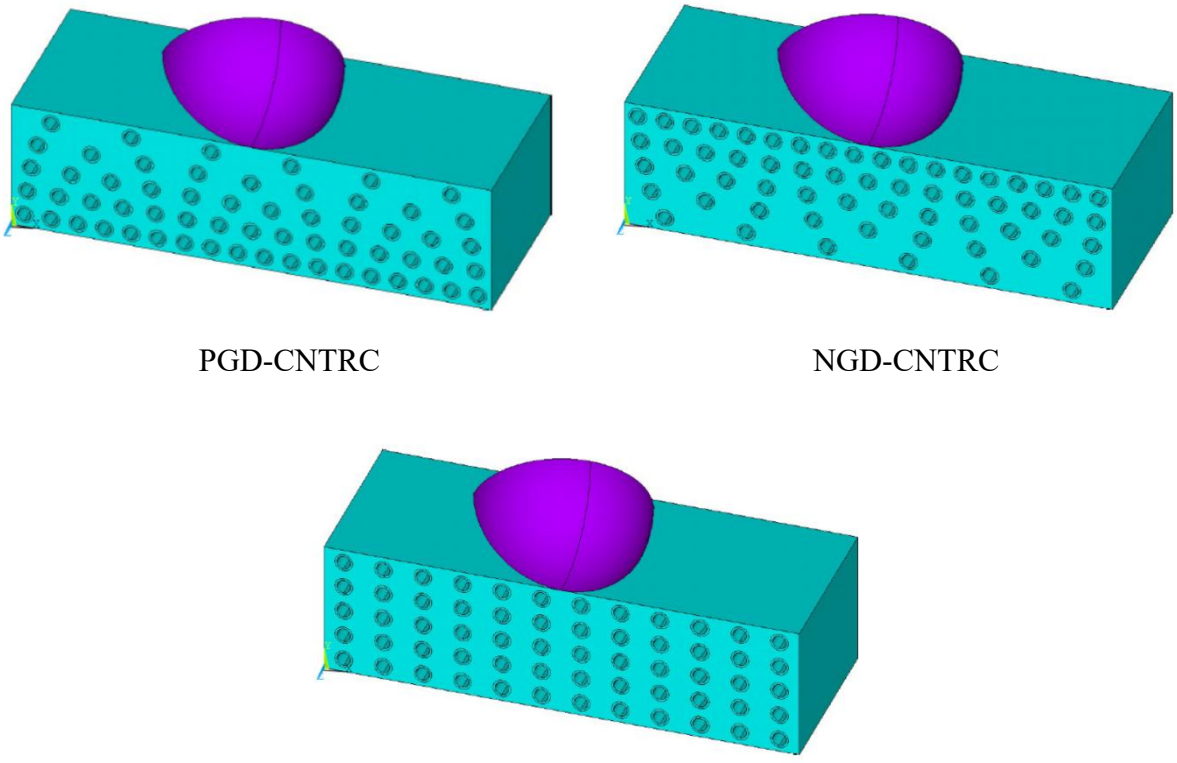

Figure 4.2: CNTs distribution pattern for three different FG-CNT nanocomposites

The present work deals with single asperity indentation contact analysis (with a rigid spherical indenter as shown in Fig. 4.1) of functionally graded (FG) substrate, where the gradation is achieved by CNT distribution along the thickness of the specimen. The model is compiled by APDL code using the finite element software package ANSYS. It consists of three core elements:

- Aluminium (Al) employed as the matrix material,
- Carbon nanotubes (CNTs) as the reinforcing material (whose distribution following a specific pattern introduces functional gradation characteristics)

- A rigid spherical indenter

So, the analysis involves a block of CNT-Al nanocomposite with a graded distribution of carbon nanotubes (CNTs). The material properties of Aluminium (Al) and CNTs include an elastic-plastic behaviour, with post-elastic properties exhibiting bilinear isotropic hardening with the stress-strain relationship as follows

$$\sigma = \begin{cases} E\varepsilon & \text{if } \sigma \le Y \\ kE\varepsilon & \text{otherwise} \end{cases} \tag{4.1}$$

Here, σ, ε, E and Y are stress, strain, Young's modulus and Yield strength, respectively. k is a constant with a value of 0.04. Yielding of the matrix material is identified by implementing the von Mises yield criterion as

$$\sigma_{vm} = \sqrt{\frac{3}{2} S_{ij} S_{ij}} \tag{4.2}$$

Here, σ_{vm} and S_{ij} are the equivalent von Mises stress and components of deviatoric stress tensor, respectively. As previously alluded to, three different gradation models characterized by three distinct patterns of CNT distribution along the depth/thickness of the block are examined in the current work. These distributions are namely as follows (Please refer to Fig. 2 for schematic representations of these distribution types):

1) Positive Graded Distribution (PGD) – gradual increase in CNT density with depth from the upper surface
2) Negative Graded Distribution (NGD) – gradual decreasing in CNT density with depth from the upper surface
3) Uniform Distribution (UD) – constant CNT density with depth

It is important to note that each of the distributions maintain a constant volume fraction in terms of the CNTs. Furthermore, all the CNTs are oriented in parallel alignment with each other. To perform the present simulations, certain assumptions have been made regarding the interaction of the embedded CNTs with the matrix material. It has been assumed that there is no interfacial slip between the two and it implies perfect bonding between the CNTs and the matrix material (Shen, 2009; Ahmed et al. 2020). At the nanoscale interface, effects of surface interactions (van der Waals forces) have been neglected. It should be mentioned here that an idealistic simulation should be capable of coupling both macroscopic and nanoscale effects, while taking into account influence of strain gradients on material behavior, size-dependent mechanical properties along with interface effects. But, simulations of such complexity require significant computational resources. The objective of the present study is

to develop a computational model that provides reliable and validated simulation results without the requirement of extensive computational capacity.

The nanocomposite has dimensions of 81 nm × 22.5 nm × 45 nm (length × height × width), with carbon nanotubes (CNTs) having an outer radius of 1.5 nm and a thickness of 0.34 nm. The material properties of both the carbon nanotubes (CNTs) and Aluminium (Al) are taken from the research works by Ahmed et al. (2020) and Nouri et al. (2012). It is also assumed that the nanocomposite is devoid of defects. The rigid indenter is modeled as a hemispherical volume of inflexible nature and it possesses a radius of 10 nm.

The model's coordinate system (Fig. 4.3) is such that the vertical axis along which the indentation takes place is considered the y-axis, while the x-z plane is considered as the base of the model. To expedite computation, an analysis of half the model has been conducted, with the x-y plane as the plane of bisection.

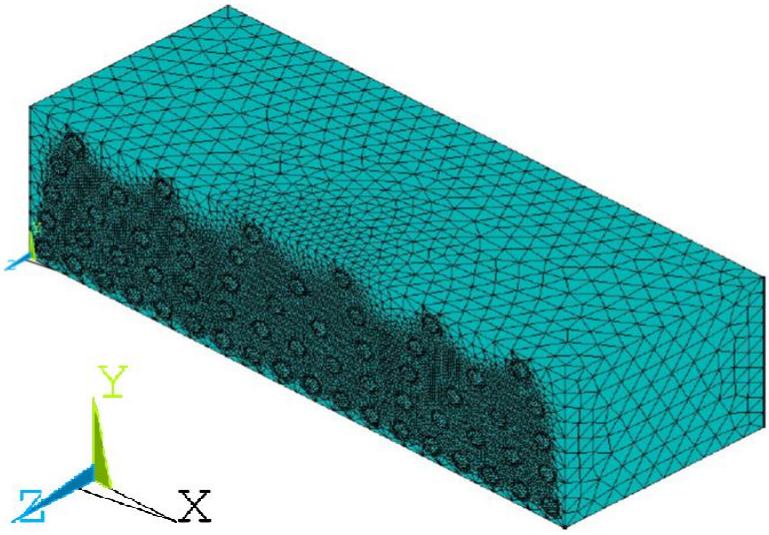

Figure 4.3 FE mesh of the model

For the purpose of conducting structural analysis, the model is meshed using a 3D structural element SOLID187. This element comprises 10 nodes, each possessing three degrees of freedom. The surface that interfaces with the rigid spherical indenter is meshed using a contact element, namely CONTA174. This contact element is paired with TARGE170 elements, which are employed to mesh the contact surface of the rigid spherical indenter. For enhanced mesh quality and to achieve accurate results while minimizing computational load, a strategic meshing approach is employed. This involves placing a fine mesh near the contact zone, where the indentation effect is significant, and a coarser mesh away from the contact zone, where the impact of indentation is less pronounced. It is essential to select a proper mesh configuration by performing a thorough convergence analysis. It is observed that refining the mesh beyond a certain point yields negligible changes in the outcomes, while,

increasing the computation time significantly. This step ensures a balance between accuracy and computational efficiency by identifying an optimum mesh configuration as shown in Fig. 3. In this study, a total of 285742 elements have been employed for all the analyses. For the contact interaction between the rigid spherical indenter and the nanocomposite, a frictionless contact condition is assumed, utilizing the Lagrange multiplier contact algorithm. The model's boundary conditions are meticulously defined to ensure that the analysis procedure accurately follows the intended course. The nodes situated at the base i.e. on the x-z plane, are constrained from movement in all directions. Moreover, the nodes located on the bisection plane (both on substrate and indenter) are constrained according to the following equations.

$$u_z = 0 \tag{4.3}$$

$$\omega_x = \omega_y = 0 \tag{4.4}$$

Here, u and ω denotes translation and rotation, respectively. The analysis commences with the rigid spherical indenter's contact surface making initial contact with the surface to be indented. Subsequently, the indenter is gradually moved downward until it reaches a displacement of 0.0015 μm. Following this, a controlled withdrawal process is executed, finally separating the indenter from the nanocomposite's contact surface. It should be mentioned here that the loading and unloading stages are considered as quasi-static in nature, i.e., they are carried out with extremely slow rate of deformation ensuring gradual alteration of the applied force without any sudden variations. It enables the material to deform uniformly at a rate which is deemed negligible.

4.3 Validation Study

Model validation constitutes a crucial and fundamental aspect of any numerical study. This validation procedure involves comparing the outcomes derived from the adopted model analysis with numerical or experimental results previously published in the literature. As per the comprehensive literature review, no existing research has been published on the analysis of spherical indentation contact involving functional gradation using CNT nanocomposites. In the current context, the validation of the present model is approached through two different avenues. Firstly, validation is carried out for the CNT-based Al nanocomposite model within a 2D domain, as previously presented by Ahmed et al. (2020). Secondly, to validate the spherical indentation model, the current 3D model's outcomes are compared with experimental results published by Suresh et al. (1997).

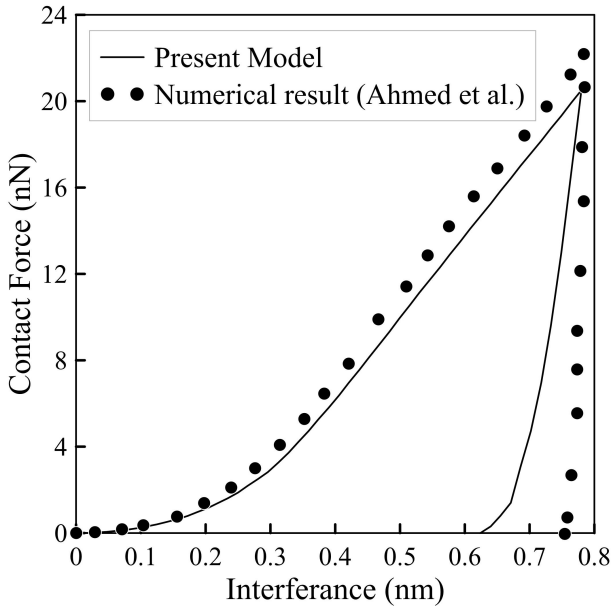

Figure 4.4: Validation of the present model with the results of Ahmed et al. (2020)

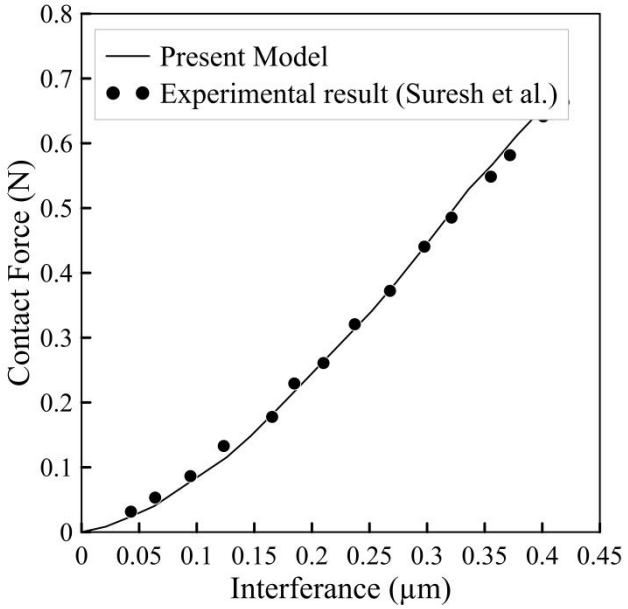

Figure 4.5: Validation of the present model with the results of Suresh et al. (1997)

The material model employed for the first validation study is derived from the framework outlined in the literature by Ahmed et al. (2020). The analysis is conducted for specific indentation processes, involving uniform distribution of carbon nanotubes (CNTs) within the nanocomposite. The nanocomposite possesses dimensions of 10 × 10 nm, with a CNT wall thickness of 0.168 nm. An indentation is performed using a Berkovic indenter, and the obtained results are examined under both loading and unloading conditions. The comparison between the published model and the current method is illustrated in Figure 4.4, displaying the relationship between contact force and indentation depth. Furthermore, Figure 4.5

exhibits the correspondence between the experimental findings presented by Suresh et al. (1997) and the 3D model using the present method. This comparison involves indentation analysis of a functionally graded material (FGM) utilizing a rigid spherical indenter, and both sets of results are graphically represented. Through these comparisons, a notable degree of agreement is observed, with the patterns aligning closely. The similarity between the two sets of results serves as a validation of the present model.

4.4 Results and Discussion

During the first phase of the analysis, the indenter is pressed to a predetermined indentation depth, which leads to deformation of the indented surface and the formation of a finite contact area. Subsequently, in the second phase, the indenter is withdrawn so that the contact area finally reduces to zero, but there remains certain amount of residual stresses and an indent on the surface. The analysis adopts a pure slip condition, ensuring that friction does not influence the creation of the contact area or the subsequent contact force during both loading and unloading phases. In the depicted model (Figure 4.1), the initial contact occurs between the Aluminium (Al) matrix and the rigid body of the indenter. Obviously, the material properties beneath the indented surface play a crucial role in shaping the analysis outcomes. Initially, it is expected that the matrix material would take up the entire load and there would be no deformation of the tubes. However, as the indentation depth increases, a noticeable effect of the distribution of carbon nanotubes (CNTs) should become prominent.

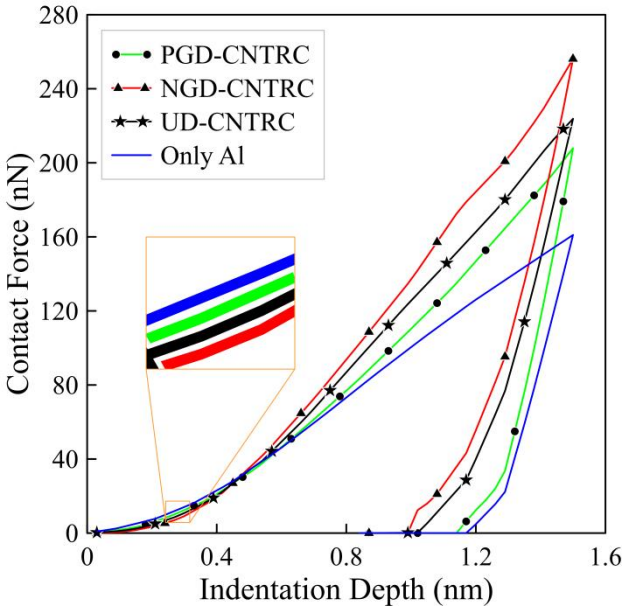

Figure 4.6: Indentation depth vs. Contact Force plots for different CNTs distribution pattern

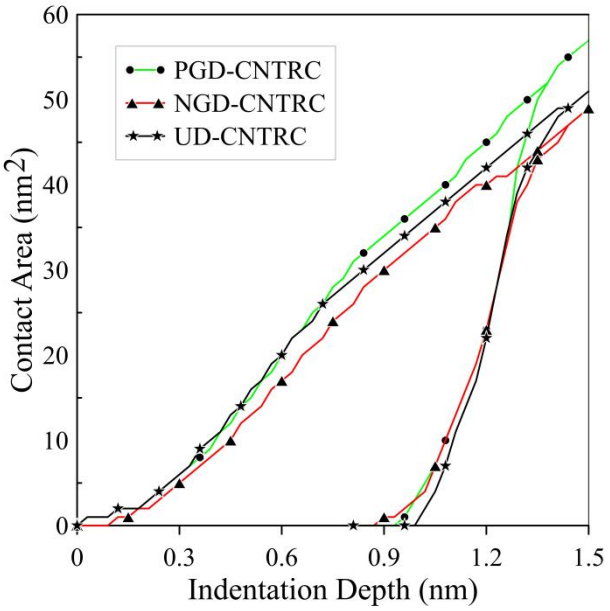

Figure 4.7: Indentation depth vs. Contact Area plots for different CNTs distribution pattern

Figure 4.6 illustrates the relationship between contact force and indentation depth for the three distinct CNT distributions (PGD-CNTRC, NGD-CNTRC, and UD-CNTRC, as shown in Figure 4.2). In the same figure contact force vs. indentation depth plot for a homogeneous Aluminium block is also provided as a reference and to gauge the effect of the distribution of CNTs on contact force behaviour.

At lower indentation depth, it is observed from the figure that at lower indentation depth the curves corresponding to the different distribution patterns are very close to each other. Moreover, in this phase, the PGD-CNTRC corresponds to highest contact force and NGD-CNTRC for the lowest. It is due to the fact that at this preliminary stage of indentation, the effect of the CNTs is negligible and the contact behaviour is primarily governed by the yielding of the matrix material located at the contact surface. This yielding of surface material, which leads to lower contact force, is found to be higher for NGD-CNTRC (demonstrated pictorially in a subsequent section). However, beyond a certain level of indentation (approximately until 0.45 nm), the trend is reversed where NGD-CNTRC distribution provides the highest contact force for a given indentation depth. In order to explain this behaviour, it is required to consider the variation of stiffness along the depth provided by the varying number of CNTs in the different distribution patterns. Closer to the surface, NGD-CNTRC has a large number of CNTs and the number progressively decreases with depth. Thus, there is a gradual decrease in stiffness with depth. However, near the contact zone (due to presence of large no. of CNTs), there exists a high stiffness zone and as the indentation depth enters this zone it contributes towards greater contact force. On the other hand, PGD-

CNTRC and UD-CNTRC have lower number of CNTs nearer to the surface and the number decreases or remains same (as per the distribution). For both these cases, the indenter encounters lower stiffness in the proximity of the indentation zone and as a result the contact force has a lower value compared to NGD-CNTRC. The lowest force-indentation curve is obtained for the homogeneous matrix material. The unloading stage follows a similar pattern as the later stages of the loading phase.

In Figure 4.7, the relationship between the indentation depth of the rigid spherical indenter and the contact area of the graded nanocomposite is depicted for various CNT distribution patterns. In the initial part of the indentation, due to the simultaneous opposing influences of matrix phase yielding and stiffening of the substrate due to CNTs, no clear trend emerges. However, as a significant amount of indentation takes place, the influence of the latter takes precedence. According to Hertzian spherical elastic contact theory, a higher substrate stiffness results in a lower contact area (Johnson et al., 1987). This explains the trend observed in the later and major part of the contact area curves, where a lower contact area is observed for NGD-CNTRC.

4.4.1 Analysis of Stress

Examination of stress distribution in case of any contact analysis is a sure way of gaining insights into the problem. The average von Mises stress distributions for the three different nanocomposites with varying patterns of CNTs at the end of loading and unloading stages are depicted in Figure 4.8 and 4.9, respectively. For a better understanding of the stress distributions existing in the CNTs and the matrix material, two different sets of plots are provided in these two figures. In the first column of both these figures (i.e., Figure 4.8(a)-(i) to 4.8(c)-(i) and Figure 4.9(a)-(i) to 4.9(c)-(i)), stress distribution across the entire block of nanocomposite including the CNTs is shown, while, the second column (i.e., Figure 4.8(a)-(ii) to 4.8(c)-(ii) and Figure 4.9(a)-(ii) to 4.9(c)-(ii)), exhibits the stress distribution in the matrix material only, without the presence of the CNTs. This separation allows for a clearer comprehension of stress patterns and their variations. It is evident upon careful examination of the figures that the peak von Mises stress induced for UD and NGD pattern is close to each other and significantly higher than the same in PGD-CNTRC.

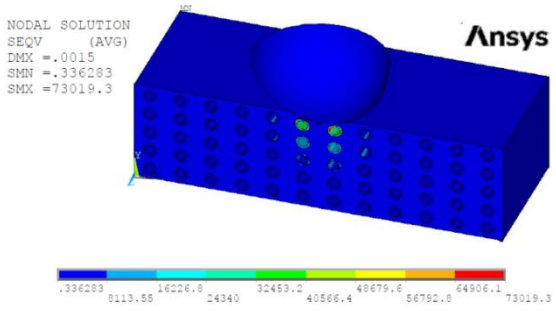

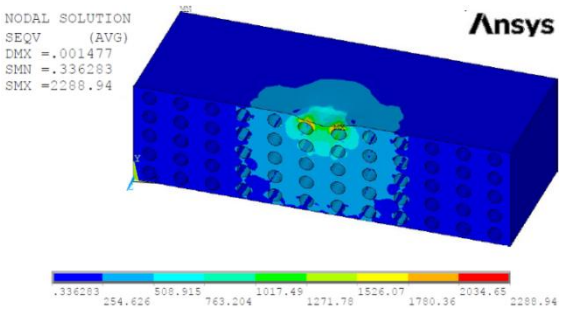

Entire Nanocomposite Only Al

(a) UD-CNTRC

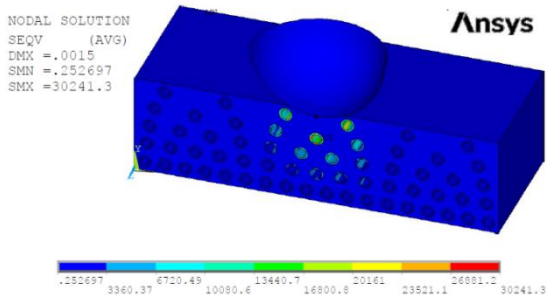

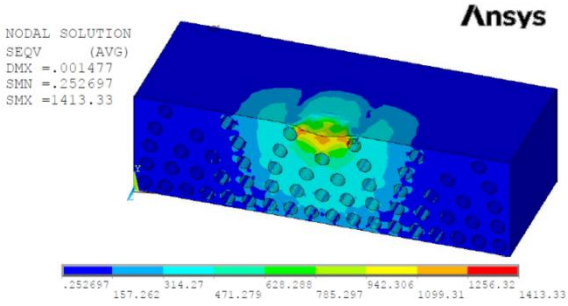

Entire Nanocomposite Only Al

(b) PGD-CNTRC

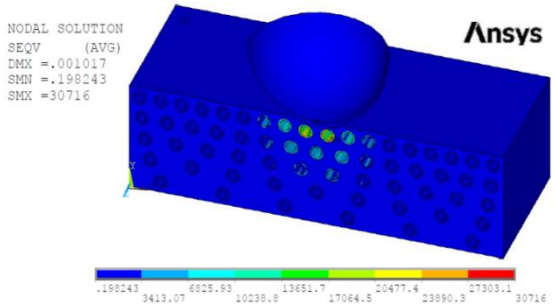

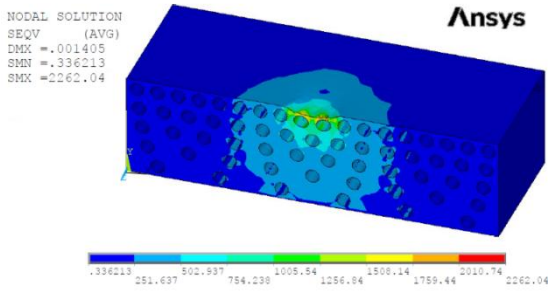

Entire Nanocomposite Only Al

(c) NGD-CNTRC

Figure 4.8: Contour plot of average von Mises stresses at the end loading for an indentation depth 1.5 nm for different FG-CNTRC (PGD, NGD and UD).

As expected, these maximum stresses occur in the nanotubes situated close to and just below the contact zone. Overall, the maximum stresses are generated in the CNTs as the Elasstic Modulus of the nanotubes is much higher compared to the matrix material. The level of stresses in the matrix is restricted to quite a low value. Nevertheless, a similar trend as the overall nanocomposite is observed in terms of the peak stresses within the matrix material

solely. From the figures, it is clearly evident that fewer number of CNTs are effected in case of both UD- and NGD-CNTRC, though these distribution patterns have larger number of tubes in the proximity of the indentation zone. It is also observed that the generated stresses are dispersed over a smaller volume of the system in these two cases of distribution patterns as compared to the PGD-CNTRC. In case of PGD, the high stress zones in the Al matrix material, although quantitatively lower (in terms of peak stress), are distributed over a larger volume – extending to a greater depth as well as higher surface area.

In Figure 4.9, a series of contour plots representing residual von Mises stress for three distinct FG-CNTRCs are shown. These plots are generated at the completion of unloading from an indentation depth of 1.5 nm. The average residual von Mises stress upon completing the unloading stage is found to be closely similar to the trend exhibited by stress distribution observed at the end of loading. Peak stress points are obviously situated in the region where the material experiences the maximum displacement. It is clear that the highly stressed locations are situated in the immediate neighbourhood of the CNTs close to the contact zone and are caused by the plastic deformation of the material. The nanotubes in the contact zone are deformed/distorted the highest, thus resulting in higher material displacement from their original positions. Figure 4.9(a)-4.9(c) also show that the average residual von Mises stress zone is spread over a larger volume in the case of PGD-CNTRC, even though the actual values of the stresses are lower in comparison to UD- and NGD-CNTRC. From the above findings, it could be inferred that, for any CNTRC that undergoes normal indentation loading, tailoring the CNT distribution in the form of positive gradation would reduce the chance of failure or damage inside the material significantly. This reduction is achieved by bringing down the peak stress and delocalizing the distribution of stress within the material, potentially mitigating localized damage.

Greater clarity into how the nanocomposite behaves under indentation can be obtained through a visual depiction of the portion of the material that has yielded under loading. Figure 4.10 displays stress-state contour plots of the three different FG-CNT nanocomposites corresponding to an indentation depth of 1.5 μm (at the end of the loading phase). These visual representations are compiled by a point-by-point comparison of the generated stresses and the Yield strength of the associated material and exhibit exactly the regions that have gone into the post-elastic regime.

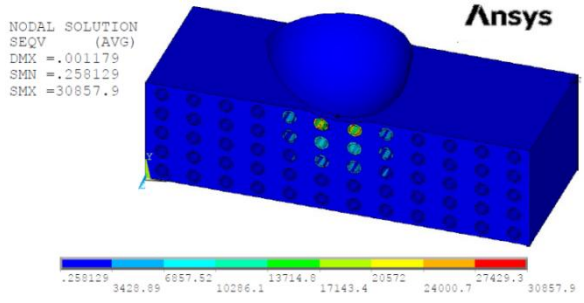

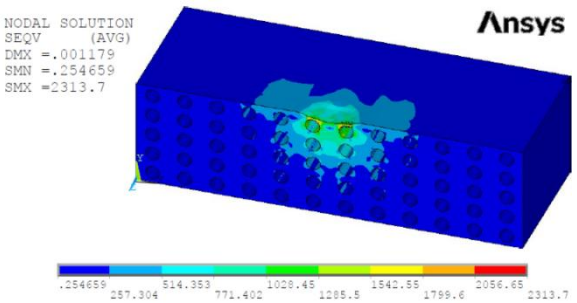

Entire Nanocomposite Only Al

(a) UD-CNTRC

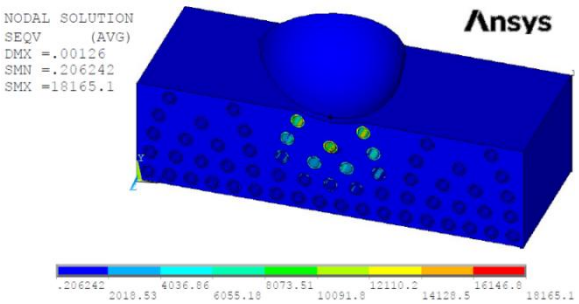

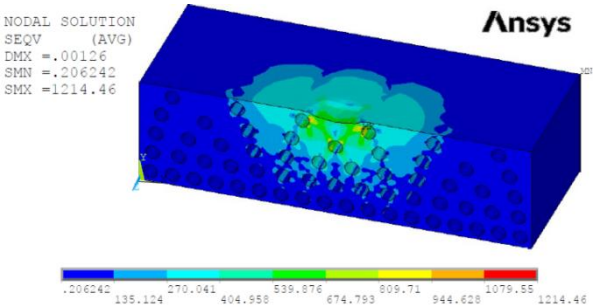

Entire Nanocomposite Only Al

(b) PGD-CNTRC

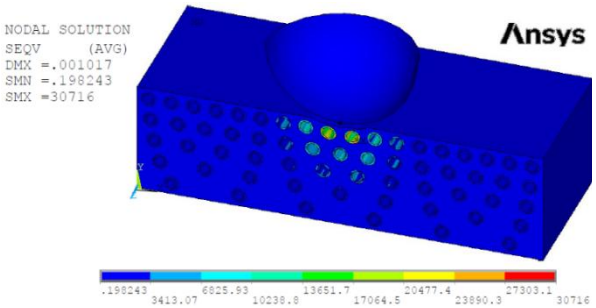

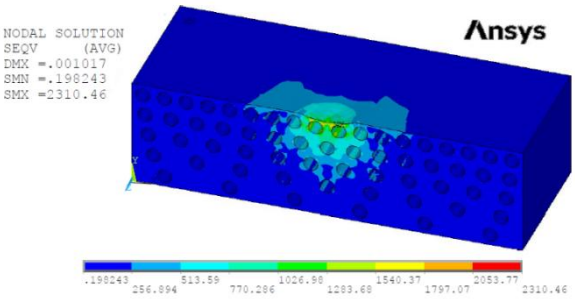

Entire Nanocomposite Only Al

(c) NGD-CNTRC

Figure 4.9: Contour plot of residual von Mises stresses after complete unloading from an indentation depth 1.5 nm for different FG-CNTRC (UD, NGD, and PGD).

It is clearly shown that the highest volume of the material is yielded for NGD-CNTRC and the lowest for PGD-CNTRC. As far as the yielding of the top contact surface is concerned, the same trend is observed, i.e. more contact surface gets yielded for NGD-CNTRC. This clearly explains the initial trend in the contact force plot provided in Figure 4.6. The increased yielding in NGD-CNTRC is a consequence of its higher concentration of CNTs positioned close to the contact zone. This concentration contributes to enhanced strength of the CNT phase compared to the matrix material, effectively granting it a quasi-rigid

characteristic. Consequently, its interaction with the surrounding softer matrix material leads to a more pronounced yielding of the latter.

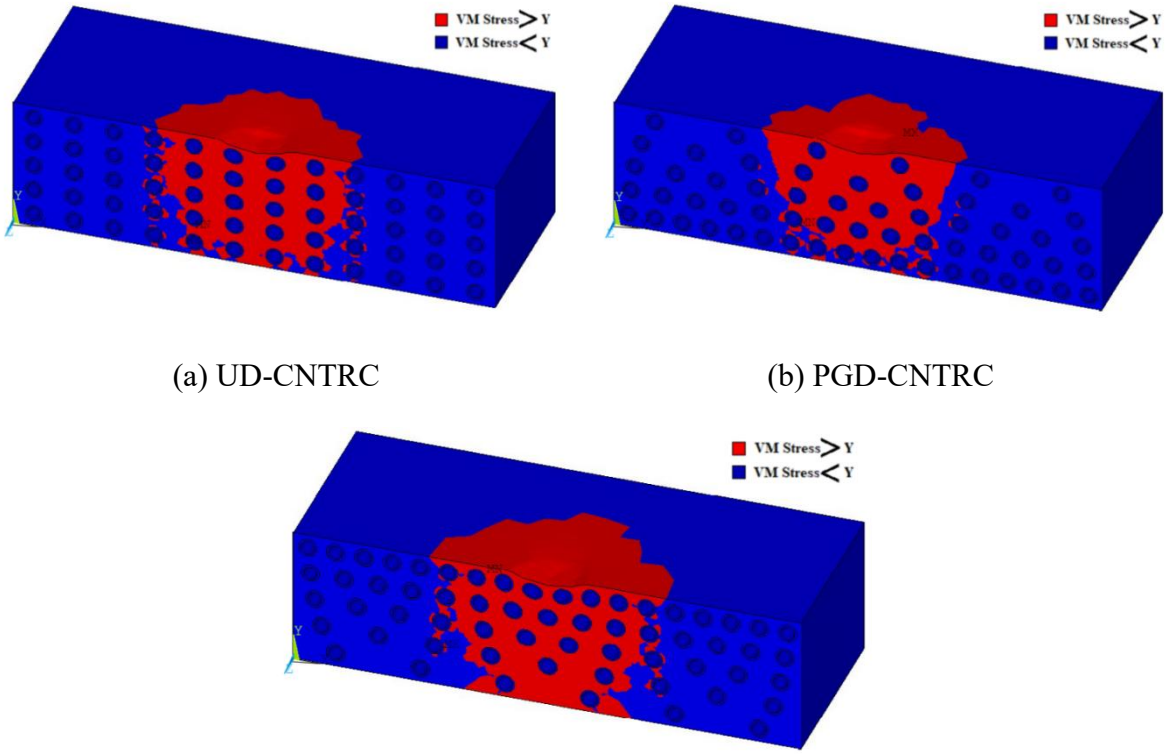

(a) UD-CNTRC (b) PGD-CNTRC

(c) NGD-CNTRC

Figure 4.10: Stress state contour plot for the entire nanocomposite block with varying CNTs distribution pattern corresponding to the indentation depth of 1.5 μm

The state of stress inside the nanocomposite is directly associated with the deformation taking place inside the substrate, especially, for a substrate that undergoes significant plastic deformation. Therefore, quantifying and analysing the loss of energy due to plastic deformation is extremely critical. In order to do so, a non-dimensional parameter named Energy Loss Index (ELI) that measures the dissipated energy due to plasticity is extracted from the force-displacement loading-unloading data (Etsion et al., 2005; Jana et al., 2020). It is defined as follows.

$$ELI = \frac{\int_0^{\omega max} \mathrm{F}_{loading} d\omega - \int_{\omega_{res}}^{\omega max} \mathrm{F}_{unloading} d\omega}{\int_0^{\omega max} F_{loading} d\omega} \tag{4.5}$$

Here, F and ω represent contact force and indentation depth, respectively. The subscripts 'max' and 'res' correspond to maximum and residual indentation depths, respectively. The values of ELI for the three CNT gradation models are furnished in Table 4.1. From the ELI

data, it could be inferred that the maximum dissipation of energy due to plasticity takes place for PGD-CNTRC substrate and the minimum for NGD-CNTRC.

Table 4.1: Energy Loss Index for the three CNT gradation models

Gradation	PGD-CNTRC	NGD-CNTRC	UD-CNTRC
Energy loss Index (ELI)	0.7803	0.61587	0.7011

4.4.2 Analysis of Deformation

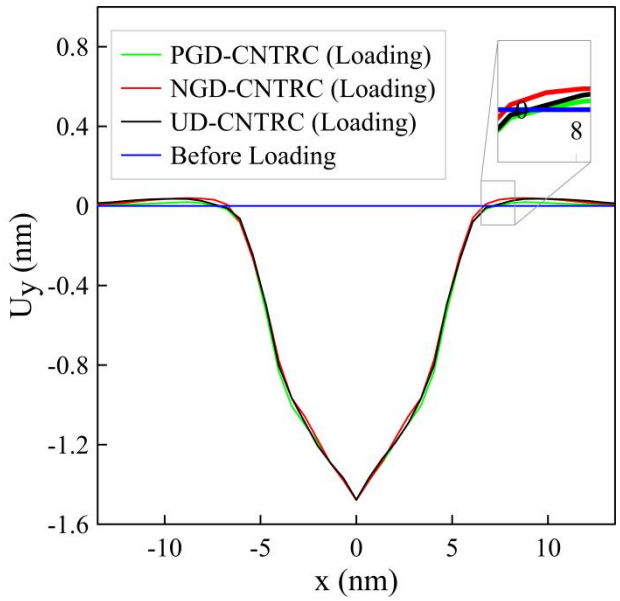

(a) Loading

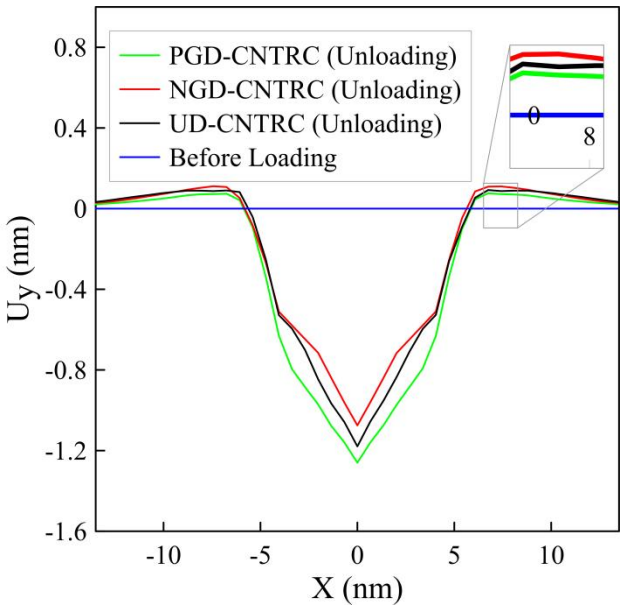

(b) Unloading

4.11: Nodal displacement in the y-direction at the line of contact on the bisectional plane and plane of contact at an indentation depth of 1.5 nm at the end of the loading and unloading stage with varied FG-CNTRC

Investigation of the deformation taking place under indentation is expected to reveal certain insights into the behaviour of CNT reinforced nanocomposites. Figure 4.11(a) and 4.11(b) display the y-directional or vertical displacement of the nodes located on the line that results from the intersection of the plane of bisection and the contacting surface, also known as the surface profile. These figures correspond to the three graded nanocomposites at the completion of both loading and unloading stages. The effect of the CNT distribution pattern is to be observed on the vertical displacement of the contact surface i.e., variation in node positions at the end of loading (up to 1.5 nm) and unloading (from 1.5 nm till detachment). A small pile-up is visible at the edge of the contact zone for all the variants of the nanocomposite where material accumulates at the edge of the indenter. This observation aligns with prior experimental observations that demonstrate the pile-up phenomenon during the indentation of pure aluminium (Moharrami et al., 2014). Additionally, the magnified view reveals that the pile-up height is highest for the NGD-CNTRC substrate and lowest for the PGD-CNTRC substrate. This observation can be explained by the higher concentration of CNTs in the NGD-CNTRC substrate, which increases the effective Young's modulus near the surface. It has been demonstrated by Taljat and Pharr (2004) that a higher ratio between Young's modulus and yield strength (E/Y) leads to a more pronounced pile-up. This trend of pile-up in the loaded condition remains consistent even after unloading, as evidenced by Figure 4.11(b), which presents the residual vertical displacement of the surface profile after the indenter has been detached at the end of the unloading stage. As an interesting observation, the unloaded state exhibits a greater degree of pile-up compared to the loaded state. Additionally, a significant outcome from the residual deformation plot is that the profile corresponding to positively graded distribution exhibits the maximum permanent deformation, whereas the one corresponding to the negative, shows the least. This result aligns perfectly with the energy dissipation results presented in Table 4.1, where the substrate with the maximum dissipation corresponds to the lowest deformation recovery. In the residual displacement plot (Figure 4.11(b)), the curves corresponding to the negative and uniformly graded distribution have local curved patterns, which is a result of the existence of two CNTs on both sides. They regain their original shape and size after elastic unloading unlike the plastically yielded matrix material and hence influence the unloaded surface profile.

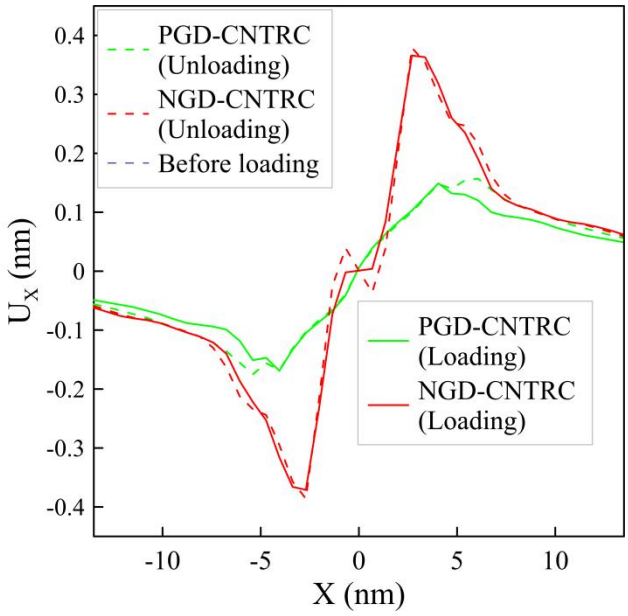

Figure 4.12: Horizontal displacement at the line of contact on the bisectional plane and plane of contact at an indentation depth of 1.5 nm at the end of the loading and unloading stage for positive and negatively graded CNT distributions.

Displacement in the horizontal or x-direction of the surface profile is shown in Figure 4.12 corresponding to NGD and PGD CNTRC. It could be noted from the figure, that the substrate is predominantly displaced in the outward direction under the influence of the indentation. This displacement is primarily because of the plastic flow, taking place in the matrix material. This is the reason that NGD-CNTRC undergoes maximum displacement as it corresponds to higher plastic yielding compared to the positively graded distribution. The same trend is maintained for the unloaded profile as well.

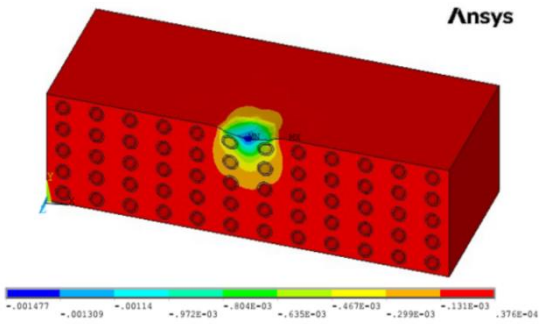

UD-CNTRC

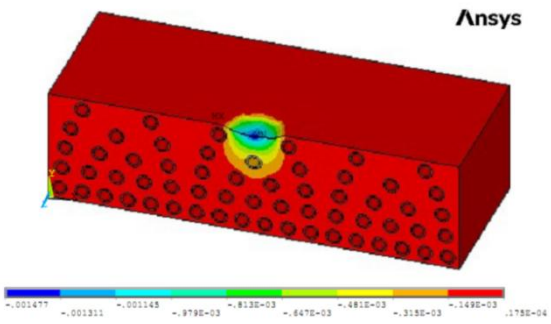

PGD-CNTRC

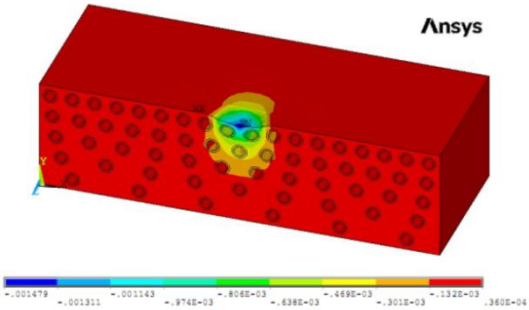

NGD-CNTRC

Figure 4.13: Contour for the displacement in the y-direction at an indentation depth of 1.5 nm at the end of the loading stage with three different FG-CNTRCs.

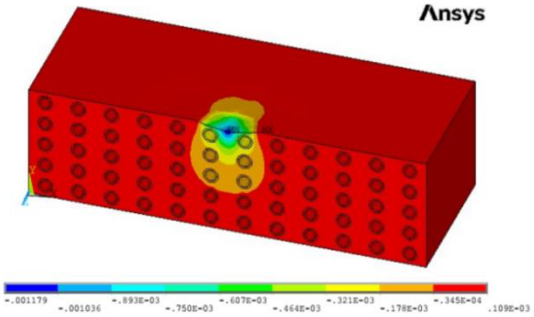

UD-CNTRC

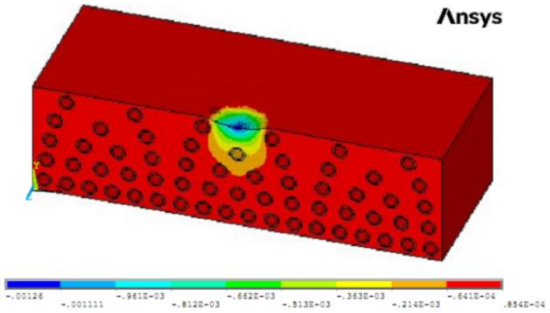

PGD-CNTRC

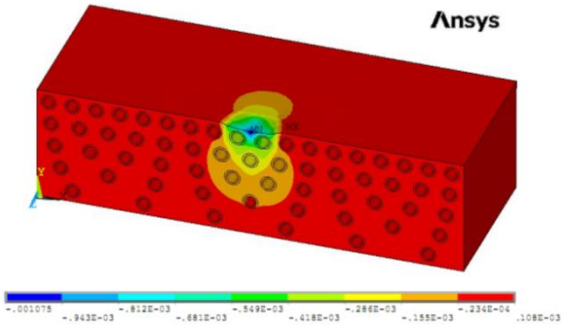

NGD-CNTRC

Figure 4.14: Contour plot for the displacement in the y-direction at an indentation depth of 1.5 nm at the end of the unloading stage with varied FG-CNTRC.

The contour plots of the vertical nodal displacement at the end of the loading and unloading stages are shown in Figure 4.13 and 4.14, respectively. The plots corresponding to the end of the loading phase (Figure 4.13) indicate that the transmission of the displacement into deeper substrate corresponding to UD and NGD-CNTRC are in close range. However, for PGD-CNTRC, it is considerably reduced. Examining the contour plot of the residual displacement in Figure 4.14, an interesting observation emerges. The PGD-CNTRC substrate, which exhibits the maximum residual displacement value at the centre of the contact zone, tends to

experience more localized deformation. Conversely, the NGD-CNTRC, with the least residual displacement, has its deformation transmitted more towards the base. This trend could be directly linked to the pattern observed in the stress state contour plot (Figure 4.10) where the yielding of the aluminium matrix penetrates deeper for NGD-CNTRC, since residual deformation is directly associated with yielding of material.

4.5 Summary

This study employs the Finite Element Technique (ANSYS platform) to simulate indentation contact between FG-CNTRC nanocomposites and a rigid spherical indenter. The contact behavior during loading and unloading phases is analyzed with varying distributions of CNTs in the nanocomposite, creating functional gradation. Multiple element types are used to model the contact interface, and a convergence study determines the number of elements. The model is validated against relevant published literature. The primary goal is to understand the impact of various FG distributions of CNTs on contact parameters.

Key observations include:

- Different contact properties such as contact force, contact area, average von Mises stresses, residual von Mises stresses, and deformation behavior are presented.
- Contact force increases for NGD-CNTRC and decreases for PGD-CNTRC due to CNT density at the contact surface.
- Contact area is higher for PGD-CNTRC during significant loading phases.
- Uniformly distributed and negatively graded composites exhibit higher peak stress compared to positively graded CNTRC.
- Pile-up phenomenon at the indentation edge is higher for NGD-CNTRC.
- NGD-CNTRC shows deeper substrate displacement and higher deformation recovery after unloading.
- Negatively graded substrates undergo more horizontal displacement due to plastic flow compared to positively graded distributions.

This page is left blank intentionally

Chapter 5

3D Indentation Contact Analysis of CNT-reinforced Functionally Graded Material Matrix Composite (CNTR-FGMMC)

5.1 Introduction

As discussed earlier in the introduction chapter, the resilience of the interacting solid surfaces in any mechanical system is significantly influenced by the induced stress dynamics during its contact loading-unloading cycles (normal or tangential). In order to understand and analyze the contact phenomena taking place at surface interfaces, flattening and indentation-based fundamental contact models are often relied upon. Especially, the indentation contact analysis has its own importance in material property assessment, particularly in instrumented tests.

In the rapidly evolving technological landscape and emergence of novel materials, analysing the contact behavior for such materials become imperative for ensuring optimal performance and durability. With increasing demands for materials tailored to specific applications, functionally graded materials (FGMs) reinforced with carbon nanotubes (CNTs) are emerging as promising candidates. FGMs, introduced by Japan in the 1980s, represent a novel class of composites with graded properties tailored for specific applications (Boggarapu et al., 2021). CNTs represent significant technological advancements, offering high strength, stiffness, toughness, and excellent thermal and electrical conductivity.

Designing, fabricating, and characterizing these composites are complex tasks. Advanced manufacturing methods like chemical vapor deposition and powder metallurgy enable the production of CNT reinforced-functionally graded material matrix composites (CNTR-FGMMC). These materials are may be useful in various fields, including aerospace, biomedical devices, and high-temperature environments, where they surpass traditional FGMs in performance.

The foundation of contact mechanics was laid by Johnson (1985) with analytical models for unloading contact behavior involving a spherical indenter. Tabor (1948) validated Johnson's models, showing that unloading followed a perfectly elastic path despite significant plastic deformation. Hardy et al. (1971) used the Finite Element Method (FEM) to model indentation, focusing on elastic-plastic deformation. Recent studies have focused on the mechanical, thermal, and electrical properties of CNT-based nanocomposites. For instance, El Moumen et al. (2017) used a numerical model to study CNT-reinforced polymer composites, while similar studies has been used to explored CNT-Al nanocomposites, analysing the influence of CNT wall thickness-to-radius ratio (Ahmed et al., 2020) and using 3D models for mechanical properties (Nuri et al., 2012). Rodríguez-Tembleque et al. (2018) examined the contact behavior of CNT-based nanocomposites under frictionless and frictional conditions. In the domain of contact mechanics, coated materials are significant. Hou et al. (2019) employed a 3D numerical model to investigate indentation with a conical indenter, revealing the impact of yield stress mismatch between coated and substrate materials. Suresh et al. (1997) developed a FEM-based numerical model for indentation contact analysis in FGMs. Chen et al. (2020) formulated a nonlinear contact force law for analysing FGM-coated elastic materials. Given the necessity for advanced materials, CNTs are a rational choice due to their unique properties and high aspect ratio.

In this chapter, the study explores embedding CNTs in FGMs instead of isotropic materials, emphasizing the gradation parameter and the impact of CNTs during indentation contact. A finite element method (FEM) model is developed, featuring a uniform CNT distribution and exponentially varying matrix properties, and is validated with published results with similar analysis. The study thoroughly analyzes deformation and stress distribution, providing significant findings and insights for future research.

5.2 Finite Element Model

In this current investigation, the primary focus is on conducting a FE based contact analysis through spherical indentation on a CNTR-FGMMC substrate. The contact occurs between the nanocomposite substrate and a spherical, rigid indenter. The present finite element model consists of a CNTR-FGMMC substrate with a dimension of 81 x 60 x 22.5 nm, and a spherical indenter with a radius of 15 nm, as depicted in Figure 5.1(a). In order to ensure accurate results, the detailed FE model of the nanocomposite substrate, which comprises a matrix and CNTs, requires a sufficiently refined mesh. However, a highly refined mesh results in significantly high computational time. To reduce the computational load, only

half of the model has been adopted with dimension of 81 x 30 x 22.5 nm for the analysis instead of the entire model as shown in Figure 5.1(b). To simplify the model, the following assumptions are considered:

- The CNTs are defect-free and perfectly bonded to the matrix material i.e. there is no slippage or detachment from the matrix material,
- All CNTs are parallel to each other's, and uniformly distributed in the matrix.
- Frictionless contact condition is assumed between the indenter and the nanocomposite.

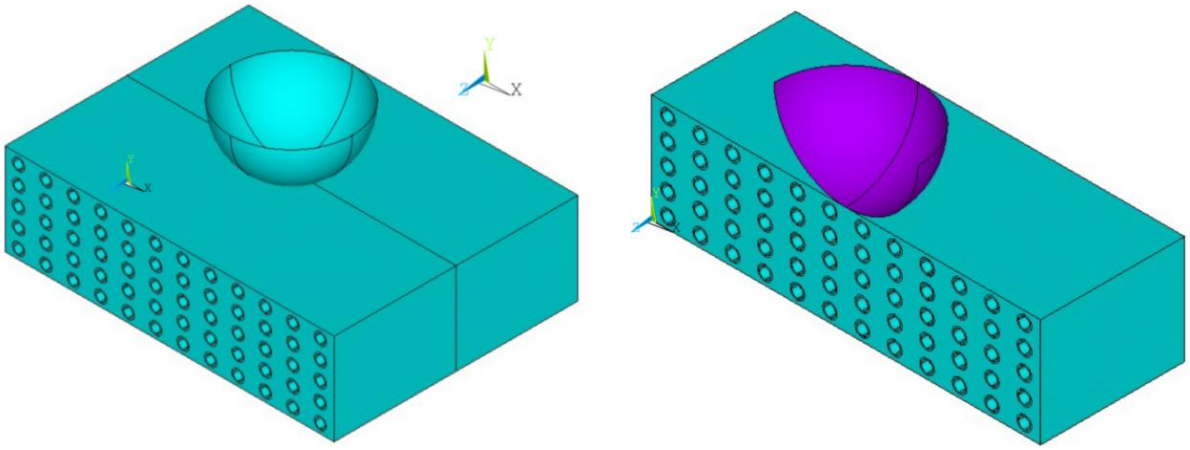

(a) Full Model (b) Half Model for the analysis

Figure 5.1: 3D indentation Model

The elastic graded material (EGM) is used as matrix material. The elastic property varies continuously (exponentially) from the contacting surface to the base of the model. Figure 5.2 illustrates the stress-strain behavior of the EGM. In the substrate, for a positive gradation parameter, the material's modulus of elasticity increases from the surface toward the base of the model, whereas for a negative gradation parameter, it decreases. When the gradation parameter is zero, the material behaves as a homogeneous isotropic material, with its properties remaining constant throughout the asperity.

During modelling, the base of the model is aligned with the *XZ*-plane, whereas thickness is along the Y-axis, as shown in Figure 5.1. The rigid indenter is modeled by a hemispherical surface, interacting with the top surface of the substrate. The von Mises yield criterion is adopted to identify the onset of yielding of the matrix material and the post-elastic behavior is modeled with bilinear isotropic hardening model. The Young's modulus and tangent modulus of the functionally graded matrix material vary spatially along the thickness i.e. Y-direction.

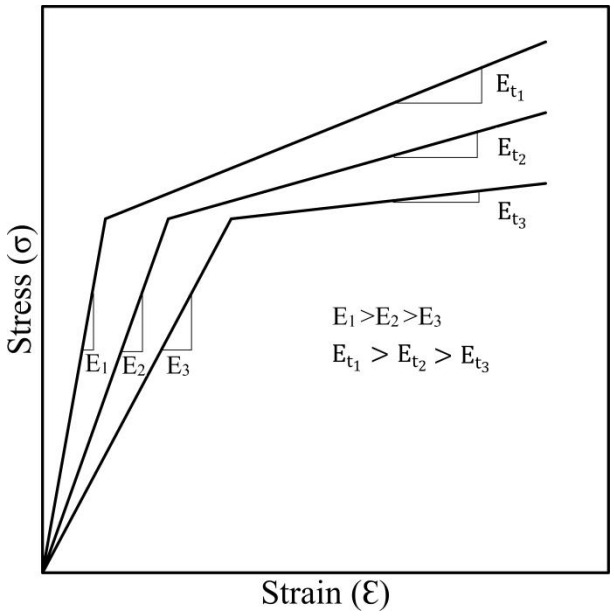

Figure 5.2: Stress-strain curve for EGM

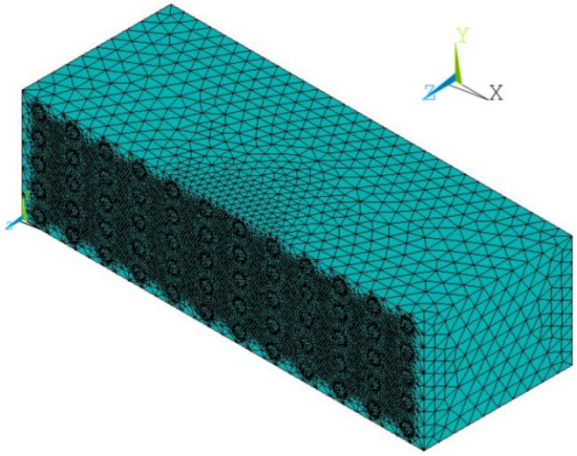

Figure 5.3: Mesh of the model

The material modelling of the functionally graded matrix material is accomplished in two steps. First, a preliminary thermal analysis is carried out to assign temperature distribution according to the required gradation. Subsequently, the temperature distribution is utilized to assign the graded material property by incorporating temperature dependent material properties.

The ten-node tetrahedral thermal solid elements (SOLID87) are used to mesh the model for the thermal analysis. The meshing strategy is designed to ensure a fine mesh near the contact zone, where higher stress gradients are expected, while comparatively coarser mesh is used in the regions farther from the contact zone, as illustrated in Figure 5.3. Fine mesh is used during meshing the matrix in the vicinity of the CNTs. During the thermal analysis, both

thermal conductivity and thermal expansion coefficient are treated as zero, ensuring no change in dimensions. The gradation equation adopted for Young's Modulus and Tangent Modulus of the material is as follows (Giannakopoulos and Suresh, 1997 a, Giannakopoulos and Suresh , 1997 b):

$$E = E_0 e^{\gamma_e (1-\frac{y}{Y})} \tag{5.1a}$$

$$E_t = E_{t_0} e^{\gamma_e (1-\frac{y}{Y})} \tag{5.1b}$$

Where E_0 is the Young modulus and E_{t_0} is the Tangent Modulus at the top surface or surface of contact, E_t is the Tangent Modulus at any point of the material, Y is the full thickness of the substrate, y is the distance of any point in the matrix material from the base of the substrate, and γ_e is the elastic gradation parameter or inhomogeneity parameter. From the equation, it could be inferred that with different values of γ_e, the gradation in the elastic properties in the matrix material is altered. When the gradation parameter γ_e is positive, both the Young's modulus and tangent modulus increase with depth, whereas they decrease when γ_e is negative. Zero value γ_e implies the matrix material is homogeneous.

After assigning the material properties of the FGM matrix and CNTs, structural analysis is conducted. The thermal solid element SOLID87 is transformed into its equivalent 3D structural element, SOLID187. The contact surface of the nanocomposite is meshed using CONTA174 elements, forming a contact pair with the TARGE170 element employed for meshing the rigid indenter surface in contact. The contact algorithm utilized in this context is based on the pure Lagrange multiplier contact algorithm. The structural boundary conditions are set such that the nodes on the *x*-*z* plane at the base are constrained from moving in all directions. Additionally, nodes located in the bisection plane (XY plane), are restricted to move along the Z-axis and rotate about the *x* and *y*-axes.

In this analysis, the FGM's Young's modulus is set to 150 GPa at the contact surface, with the tangent modulus defined as 5% of the Young's modulus at any point. Yield strength of 750 MPa and Poisson's ratio of 0.3 are considered. For the reinforced material CNTs, Young's modulus is taken as 1000 GPa and Poisson's ratio of 0.3 (Ahmed et al., 2020; Nouri et al., 2012). The analysis involved studying the variation of the gradation parameter across values of +1, 0, and -1 while keeping the CNTs wall thickness constant. Additionally, the study considered cases where the wall thickness of the CNTs is varied at values of 0.26, 0.30, 0.34, and 0.38 nm with a constant radius of 1.5 nm for each of the gradation parameters. The final

mesh configuration of the finite element model is determined through a mesh convergence analysis. This analysis ensures that the optimal number of elements is selected, achieving a balance between solution accuracy and computational efficiency. It has been determined that increasing the number of elements beyond 923,198 SOLID87 elements, 54 TARGE170 elements, and 933 CONTA174 elements resulted in negligible change to the outcomes.

The indentation process starts with the initial contact between the indenter and the surface of the nanocomposite. Starting from its initial position, the indenter is driven downward (in the negative Y direction) until it reaches a pre-set depth of 2 nm. Once the indentation depth achieved, the indenter is gradually withdrawn until it just detaches from the surface of contact. As the indentation of the rigid sphere takes place, the material beneath the indenter gets deformed and the resulting contact parameters e.g. contact force, contact area, contact stresses etc. are recorded.

5.3 Validation Study

After developing the model, validation is required. Since indentation analysis of CNTR-FGMMC is not available in the literature, two similar analyses with different materials are considered for validation. These analyses are selected with regard to indentation on FGM, and CNT-based nanocomposite substrates, which are relevant to the present model.

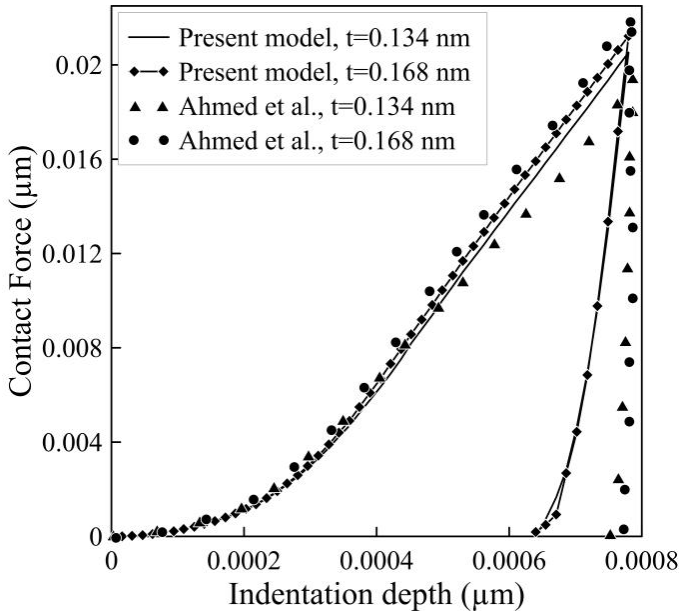

(a)

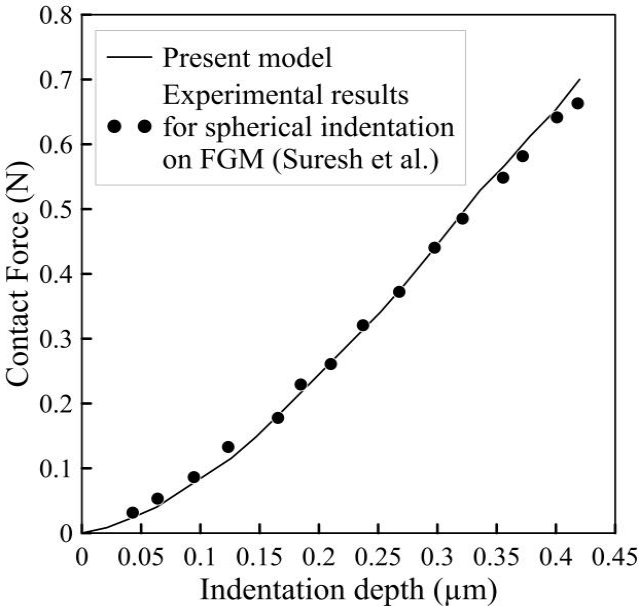

(b)

Figure 5.4: Illustrates a comparison of results, showcasing (a) Numerical results reported by Ahmed et al. (2020) and (b) Experimental results presented by Suresh et al. (1997)

Figure 5.4(a) illustrates a comparison between two result sets: one from the numerical results published by Ahmed et al. (2020), and the other from the model created through the present methodology. A 2D model (10x10 nm) for CNT-Al nanocomposite undergoing indentation depth of 780 nm by a Berkovich indenter is developed. The two sets of contact force results are extracted based on variations in CNT wall thicknesses of 0.134 nm and 0.168 nm. Remarkably, the results from the present model closely align with those from the two sets of results published by Ahmed et al. (2020), confirming the coherence and concurrence between the models (validated the CNT base nanocomposite model).

Figure 5.4 (b) provides a visual comparison between the experimental findings presented by Suresh et al. (1997) and the results obtained from the present FGM indentation model employing a spherical indenter. In this comparison, the equation utilized in material model has been replaced with the one adopted by Suresh et al. (1997) in their material model. Remarkably, it is observed that the outcomes of present model closely coincide with those published by Suresh et al. (1997), thus validating both the FGM material model and the spherical indentation model.

5.4 FE Analysis Results

The current study, initially focuses on analysing the influence of CNT wall thickness on the contact behavior. Subsequently, the analysis explores effect of the gradation parameter of the matrix material while keeping constant CNTs wall thickness.

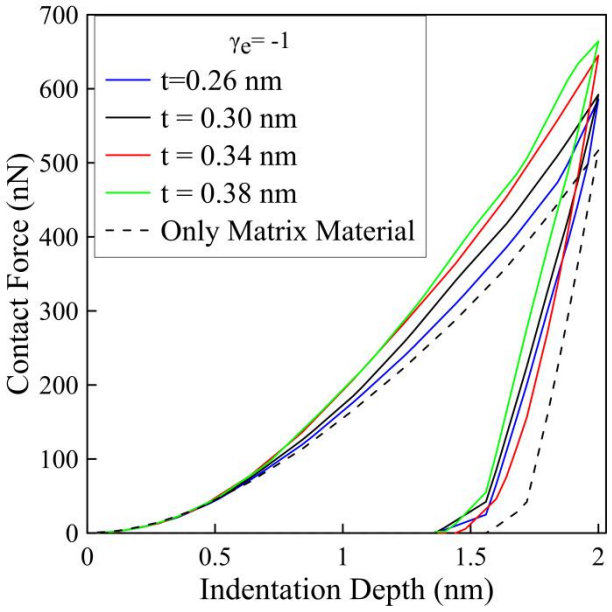

(a)

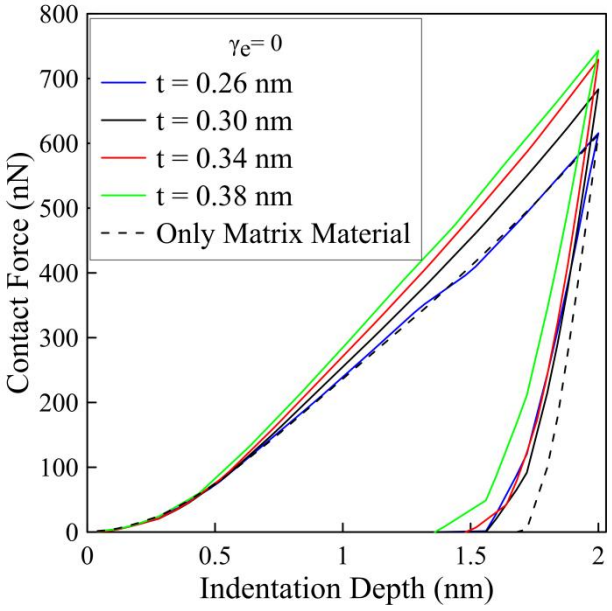

(b)

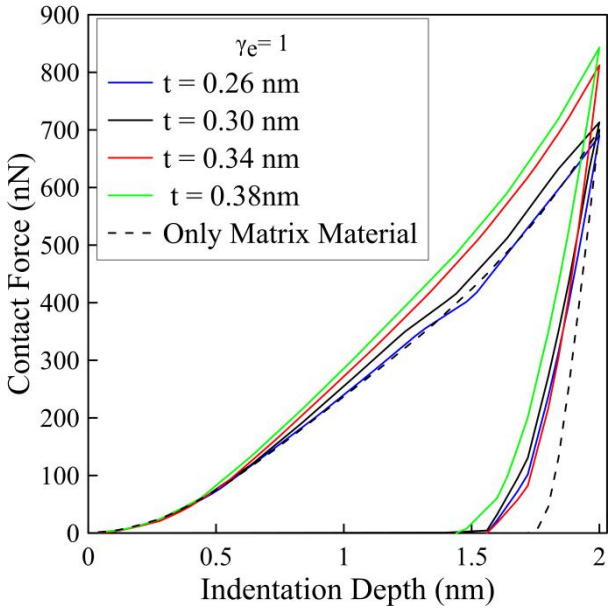

(c)

Figure 5.5: Contact force vs Indentation depth graph for constant gradation value with the variation in CNTs wall thickness (t), (a) γ_e = -1 (b) γ_e = 0 and (c) γ_e = +1

Figure 5.5 illustrates the correlation between contact force and indentation depth or contact interference considering variations in CNT wall thickness during loading and unloading phases. In this analysis, CNT wall thickness values of 0.26 nm, 0.30 nm, 0.34 nm, and 0.38 nm are considered. From the plots clearly show that with increases of CNTs wall thickness increases in the contact force. The reason of such behavior is that with higher thickness-to-radius ratio, the stiffness of the individual CNTs increases, hence resulting in higher stiffness of the overall nanocomposite substrate (Ahmed et al. 2020). Furthermore, the plots reveal that the initial increase in the contact force with the increase of the wall thickness is significant. However, beyond a certain thickness (0.34 nm), this increase becomes much lower. The reason of such trend is that once the stiffness difference between the CNTs and the matrix material reaches a certain threshold, the CNTs behave as rigid bodies due to their significantly higher stiffness compared to the matrix material. Consequently, further increases in CNT stiffness have a negligible effect on the overall response as the contact surface area between the CNTs and the matrix remains unchanged across all cases. As the thickness increases, the change in deformation gradually decreases and becomes negligible beyond a certain point.

In particular, plots 5.5(a),(b), and (c) depict the results for consistent gradation parameters of -1, 0, and +1, respectively. The variation of contact force with the variation in CNTs wall thickness observation aligns with findings from Ahmed et al. (2020) and Nouri et al. (2012),

who reported similar results in their analysis. It is noteworthy that in all plots, the peak contact force increases with the gradation parameter for the FGM matrix. For positive gradation values and CNT wall thicknesses of 0.20 nm and 0.30 nm, a deflection in the load-indentation curve is observed at an indentation depth of 1.5 nm, attributed to the onset of the deformation in CNTs with lower wall thickness. However, for a gradation value of zero, this phenomenon occurs only in CNTs with a thickness of 0.20 nm, as thicker CNTs exhibit significantly higher stiffness compared to the matrix, thereby preventing the deformation. The 'matrix only' curve nearly coincides for gradations 0 and +1 but is distinct for γ_e = -1. Due to the lower gradation at -1, the CNT wall thickness of 0.26 exhibits higher stiffness than the matrix. In contrast, for gradations 0 and +1, the stiffness is close to that of the matrix, resulting in no significant improvement in the overall stiffness of the composite.

Therefore, to clarify the influence of the gradation parameter on the contact behavior of the nanocomposite, further analysis is conducted with a fixed CNT wall thickness of 0.34 nm, while varying the gradation parameter.

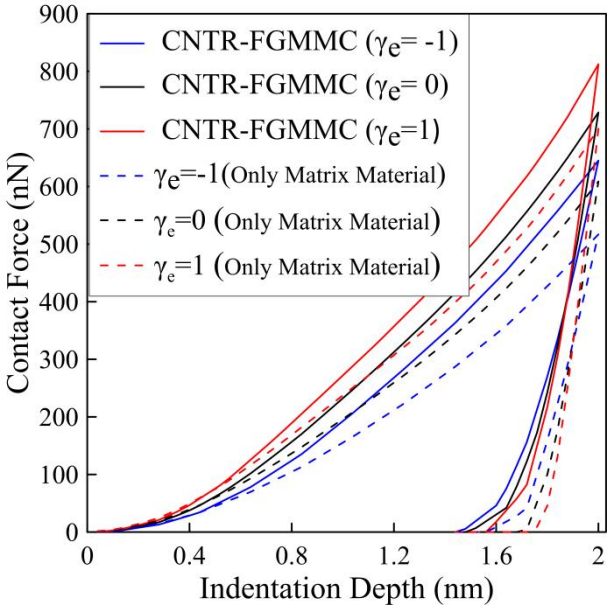

Figure 5.6: Contact force Vs indentation depth for the variation in gradation parameter

Figure 5.6 shows the influence of gradation parameter on contact force for two distinct scenarios: CNT reinforced-FGM (constant wall thickness and radius) and pure matrix material substrate. Significantly, the CNT-based nanocomposite consistently exhibits higher contact force levels compared to the only matrix material substrate throughout the indentation procedure. This heightened contact force can be attributed to the presence of CNTs, whose elastic modulus is much higher than that of the matrix material. The inclusion of CNTs in the FGM enhances its overall stiffness, leading to an increase in the contact force. The figure also

shows that both the CNT-based nanocomposites and matrix material exhibit higher contact forces as the gradation parameter increases.

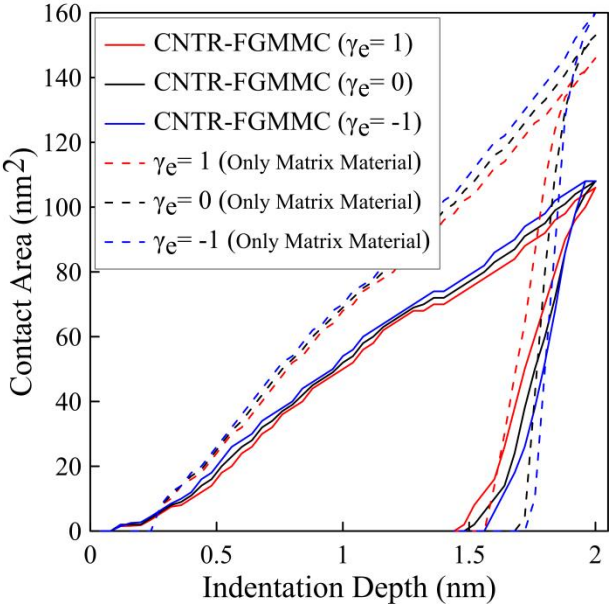

Figure 5.7: Contact area vs indentation depth with the variation in gradation parameter.

For the same gradation parameter, the curves for the CNTR-FGMMC and the pure matrix material almost coincides, since, at low indentation depth, the deformation is restricted to the matrix material at the surface i.e. the CNTs are not affected. Figure 5.7 illustrates the variation in contact area for both the nanocomposite and the only FGM with the gradation parameter changes. The trend is observed to be opposite to that of contact force, i.e. higher gradation parameter results in lower contact area. Moreover, compared to CNTR-FGMMC substrates, pure matrix material substrates exhibit higher contact area. This variation can be attributed to the plastic deformation occurring on the contact surface during indentation, which is briefly discussed in the proceeding sections.

5.4.1 Analysis of Stresses

In contact analysis, a thorough investigation and understanding of stress distribution are essential. The Figure 5.8 & 5.9 present contour plots that illustrate the von Mises stress and residual von Mises stress distributions on the CNTR-FGMM nanocomposite following at the end of loading and unloading stages. This distributions are examined to understand the effect of gradation parameters (-1, 0, and +1) on the contact behaviour of the nanocomposite. Two types of contour plots are presented from different viewpoints. The first plots (i) display illustrating the stress distribution across the entire nanocomposite, including the CNTs. In

contrast, the second plots (ii) offers a more focused view, highlighting the stress distribution for the matrix material alone.

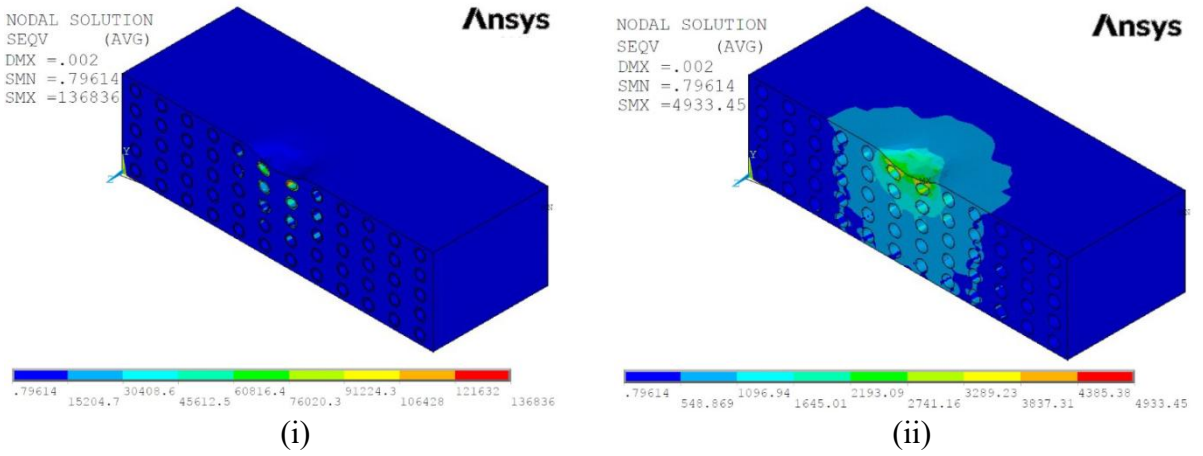

(i) (ii)

(a) γ_e =-1

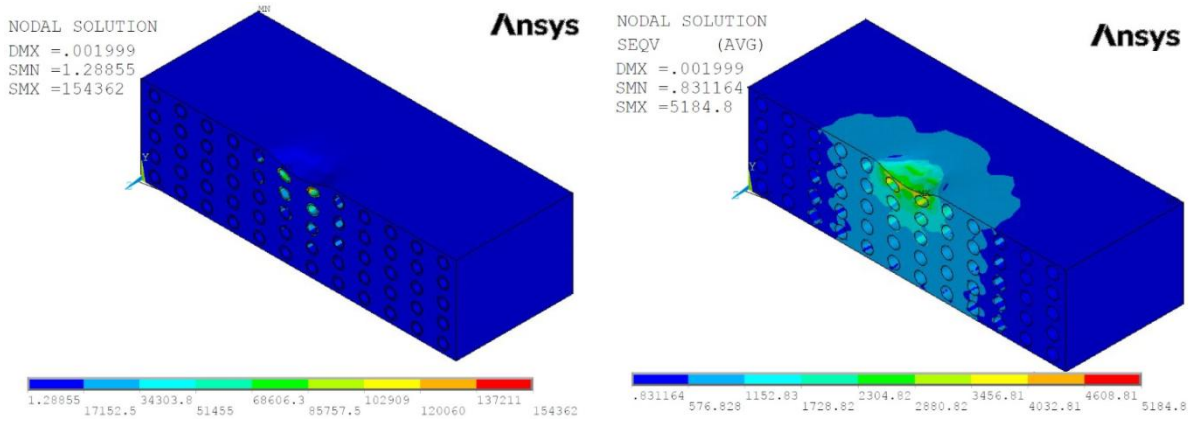

(i) (ii)

(b) γ_e =0

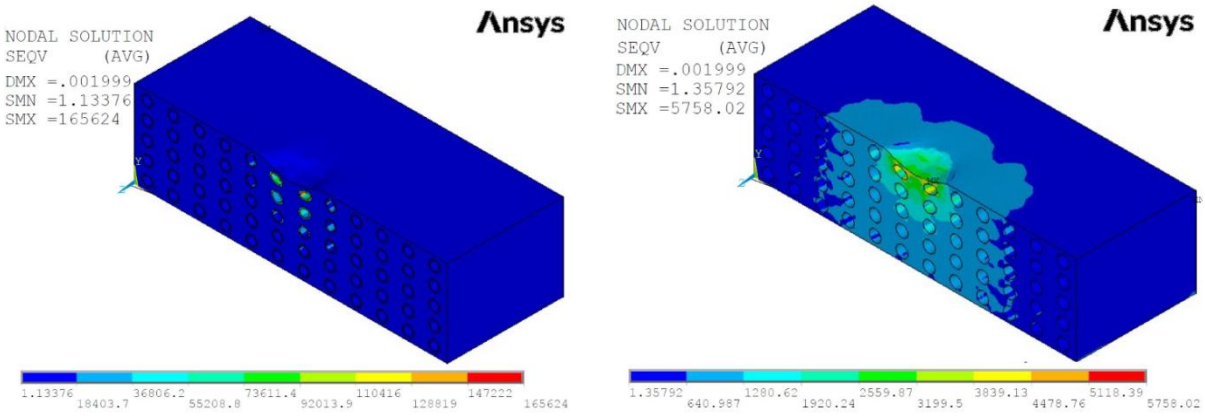

(i) (ii)

(c) γ_e =+1

Figure 5.8: Average von Mises stress distribution over the nanocomposite at the indentation depth of 2 nm with the variation of gradation parameter (γ_e = -1, 0 & +1)

Figure 5.8 shows the von Mises stresses distribution for varying the gradation parameter (-1,0 and 1) of the matrix material in the nanocomposites at the end of loading. The peak stresses developed in the negative-graded composites are lower compared to those in the positive-graded composites. The plots clearly demonstrate that the peak von Mises stress at the end of the loading stage increases with increases in the gradation parameter. This occurs because of higher gradation parameter results in greater resistive force, consequently leading to the development of higher stress. Analysis of the von Mises stress distribution reveals a similar pattern in the matrix material as observed in the entire nanocomposite. However, the peak stress developed in the nanocomposite is significantly higher than in the matrix material alone, as the maximum stress occurs in the CNTs near the contact zone due to the much higher elastic modulus of the CNTs compared to the matrix. Another observation is that in nanocomposites with higher gradation value, larger volume of the material is affected. The composites with lower gradation, corresponding to a reduced elastic modulus, exhibit localized deformation primarily in the vicinity of the contact zone within the matrix material, thereby limiting the affected material volume.

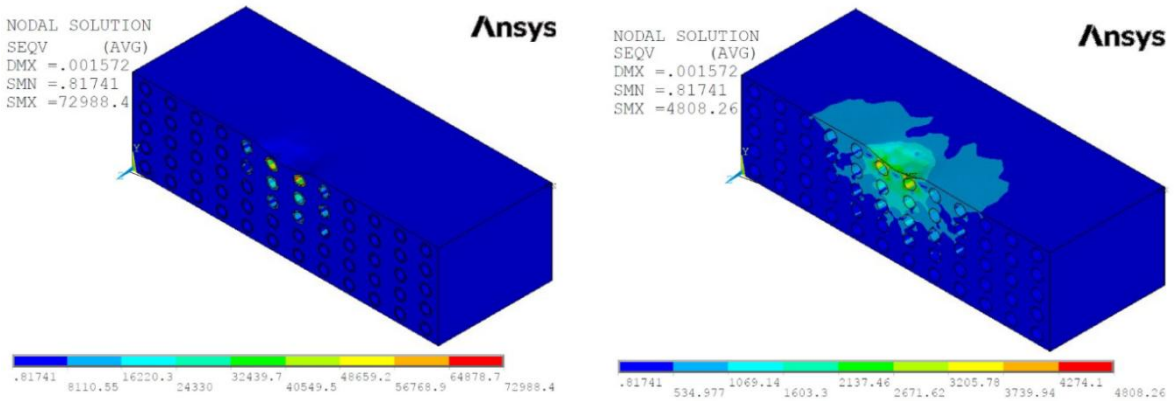

(i) (ii)

(a) γ_e =-1

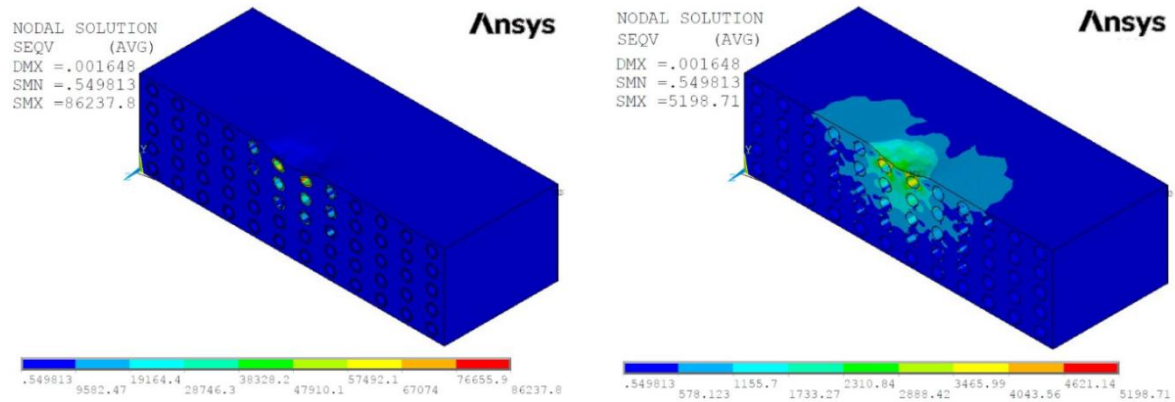

(i) (ii)

(b) γ_e =0

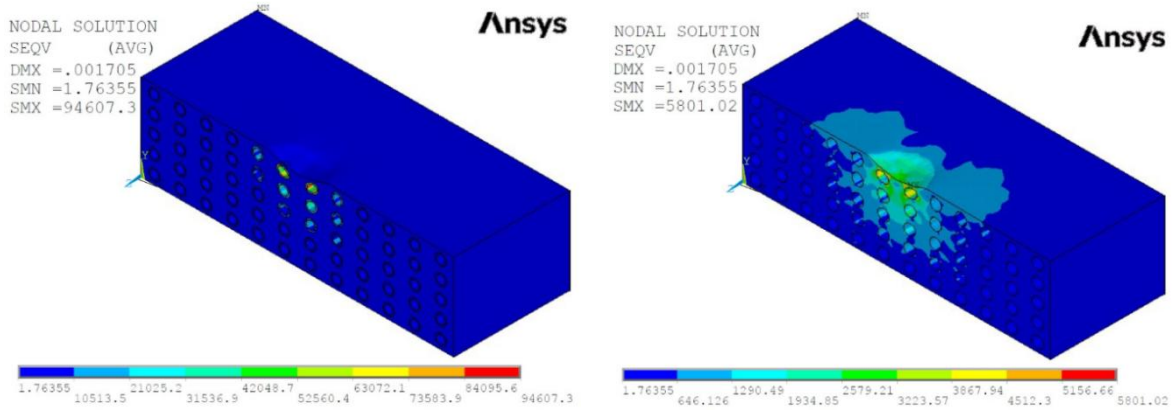

(i) (ii)

(c) γ_e =+1

Figure 5.9: Average residual von Mises stress distribution over the nanocomposite after withdrawn the indenter from an indentation depth of 2 nm with the variation of gradation parameter (γ_e = -1, 0 & +1)

The residual von Mises stresses play a pivotal role in understanding the deformation behavior of the material. In this study, the indentation process serves as a means to explore the contact behavior of the CNTR-FGMMC. A critical aspect of this analysis involves investigating the material's deformation response upon unloading. By examining contour plots illustrating the distribution of the average residual von Mises stresses, valuable insights into the deformation characteristics are gained. Figure 5.10 depicts contour plots showcasing the average residual von Mises stresses distribution at the end of unloading. The observation reveals that the peak residual stress is higher for higher-elastic-grade material and comparatively lower for lower-grade material. This behavior reflects the similar patterns discussed earlier regarding stress development at the end of the loading stage.

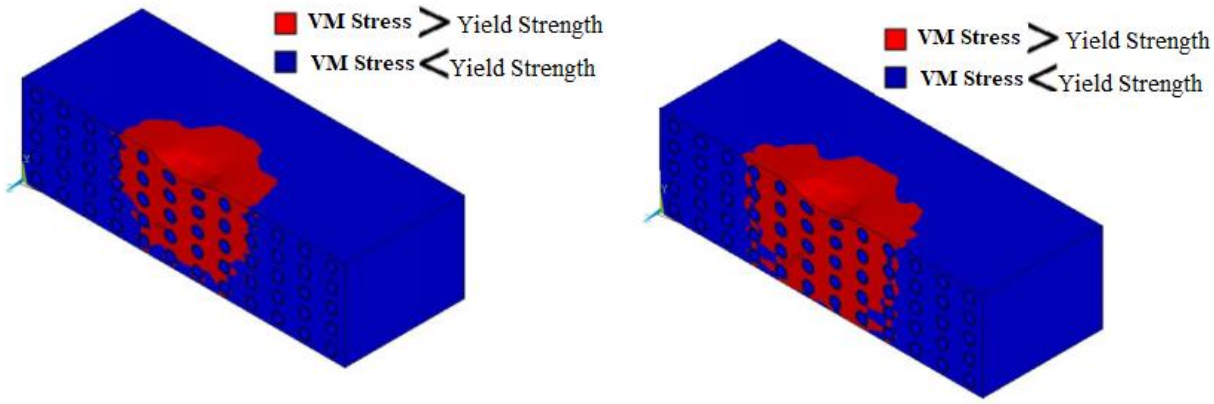

(a) γ_e =-1 (b) γ_e =0

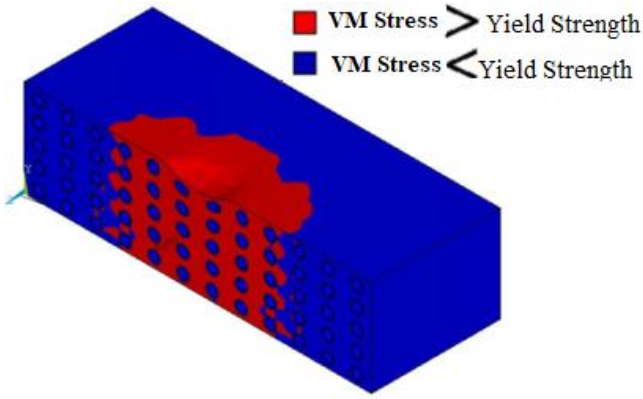

(c) γ_e =+1

Figure 5.10: Stress state contour plot comparing von Mises stress (a) γ_e=-1, (b) γ_e = 0 and (c) γ_e=+1. Indented up to indentation depth of 2 nm.

Figure 5.10 illustrates the contour plot depicting the stress state of the CNTR-FGMMC, at the end of loading stage. These plots are generated by evaluating the von Mises stress distribution at each point and comparing it with the corresponding Yield Strength of the material. This visualization effectively highlights the regions where the material has transitioned into the post-elastic regime.

Table. 5.1: Volume of material yielded

At the end of loading stage			
	Vol. of matrix material (FGM) (μm^3)	**Vol. of Yielded material FGM (μm^3)**	**% of Material Yielded**
$\gamma_e = -1$	4.19E-05	5.42E-06	12.935
$\gamma_e = 0$	4.19E-05	7.16E-06	17.088
$\gamma_e = 1$	4.19E-05	9.17E-06	21.885

The contour plots illustrate that a lower volume of material is yielded when the matrix material exhibits a negative gradation in the nanocomposite. This observation aligns with the stress distribution contour plot depicted in Figure 5.8, where lower stress propagation correlates with a lower volume of material being yielded. Conversely, a higher volume of material is yielded for the positive gradation parameter, as quantified in Table 5.2. This increased volume of material yield implies a greater amount of energy required during the process, as depicted in the force-displacement diagram.

5.4.2 Analysis of Deformation

The research emphasizes the analysis of nodal displacement for nodes situated at the intersection line between the contacting surface and the plane of bi-section in both the *x* and *y* directions. Following this, the subsequent section elaborate on the nodal displacements of the contacting surface of the substrate at the end of loading and unloading stages. These discussions offer valuable observations into the material's deformation response, contributing to comprehensive understanding of the CNTR-FGMMCs contact behavior.

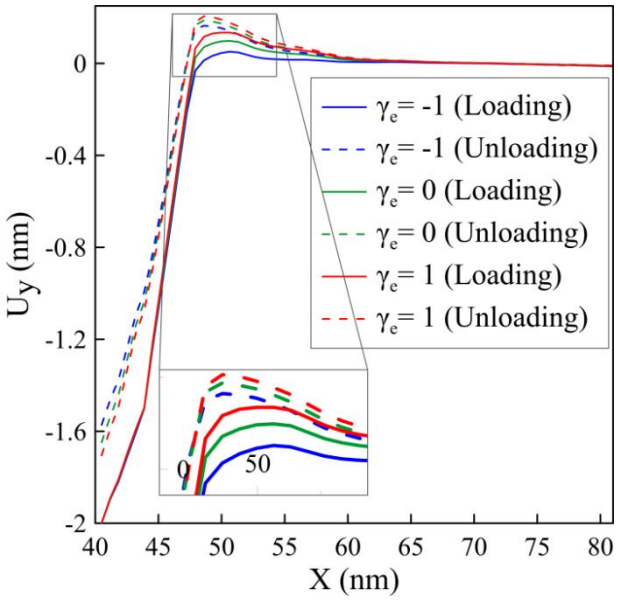

(a)

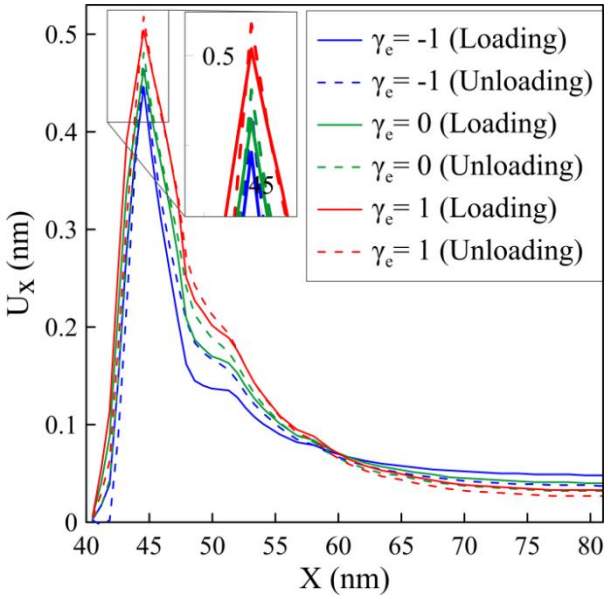

(b)

Figure 5.11: Nodal displacement of the contact surface (a) in y-direction and (b) in x-direction with the variation of gradation parameter at the end of loading and unloading.

The nodal displacements in the Y-direction (vertical displacements) are shown in Figure 5.11(a), aligning with the direction of indentation at the end of the loading and unloading stages. In Figure 5.12(b), the nodal displacements along the X-direction (horizontal displacements) at the end of loading and unloading stages are displayed. In Figure 5.11(a), it is evident that the nodal displacement in the Y direction is positive at the edge of the contact zone. The positive displacement indicates the pile-up behavior of the material. Even after the unloading, this pile up persists at the edge of the contact zone. Upon closer examination, it is noted that the pile-up behavior is more pronounced in positively-graded matrix material and less prominent in negatively-graded matrix material. In Figure 5.11(b), it is noted that the nodal displacement in the *x*-direction is zero at the central point of indentation. As the distance from the indentation point increases within the contact zone, the *x*-direction displacement gradually rises as the material is displaced sidewise by the indenter. It reaches its peak at the end of the contact zone, just beneath the contact surface, where the CNT is located. This phenomenon occurs because the CNT possesses a higher elastic modulus compared to the FGM. As a result, the FGM material is compressed and shifts in the direction of the CNT movement. As the distance from the indenter increases away from the contact zone, there is a decrease in the displacement observed. The depiction also reveals that a lower gradation parameter corresponds to a higher likelihood of recovery, whereas a higher gradation parameter is associated with an decrease probability of recovering from deformation**.** The blue curve has higher recovery than the red one. Since, more plastic deformation for higher gradation, it would result in lower recovery. The gradation parameter of the matrix material increases, it causes increases in the elastic module, which is the reason for the higher recovery of the deformed body that is also exhibited in the figures. These phenomena may be correlated with the contour plot of residual von Mises stress depicted in Figure 5.9.

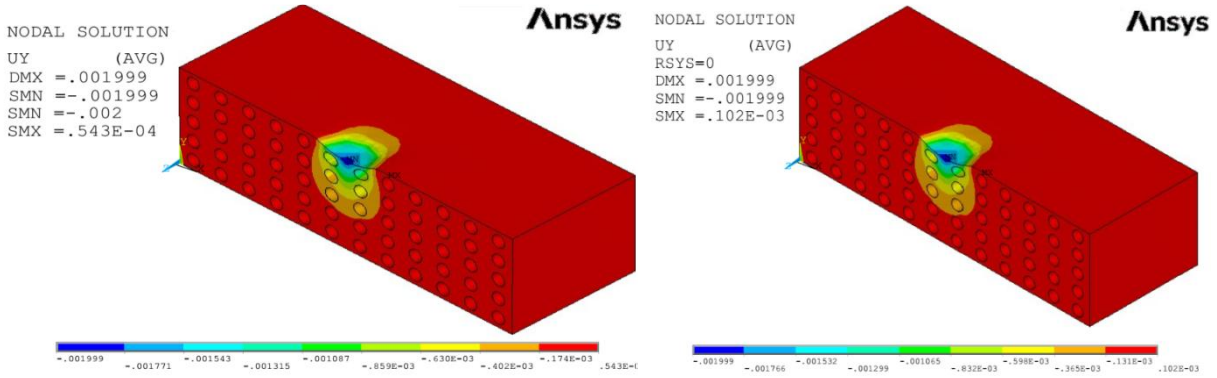

(a) γe =-1 (b) γe =0

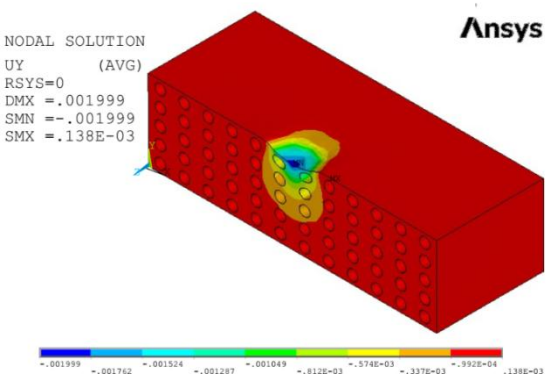

(c) γe =+1

Figure 5.12: Contour plots depict the nodal displacement in the y-direction when subjected to indentation depth of 2 nm at the end of the loading (γ_e = -1, 0 & +1)

In Figure 5.12, the deformation contour along the y-axis at the end of the predefined depth of indentation. This plot specifically highlights the influence of the elastic gradation index of the matrix material in the CNTR-FGMMC. The contour plot reveals that the greatest displacement occurs at and around the indentation point, and this displacement is observed to propagate. As the distance from the indentation point increases, the impact of contact diminishes. The greater volume of material displacement observed at the end of the loading stage is clearly linked to the positive gradation parameter as compared to others. In contrast, a lower volume of material deformed when the gradation parameter is set to a negative value as compared to higher graded matrix material. This exhibited deformation is predominantly contributed by plastic deformation of the matrix material. As indicated by Figure 5.10 and Table 5.1, more matrix material undergoes plastic deformation for higher gradation parameter, hence resulting in higher vertical deformation.

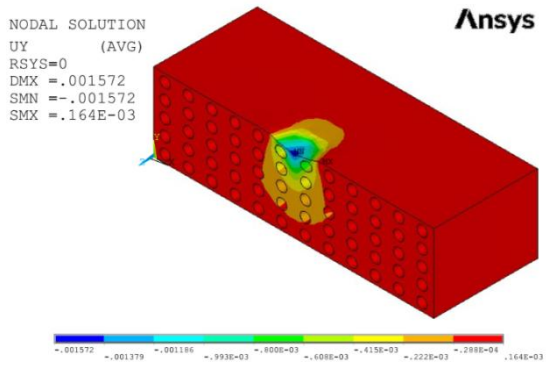

(a) γ_e =-1

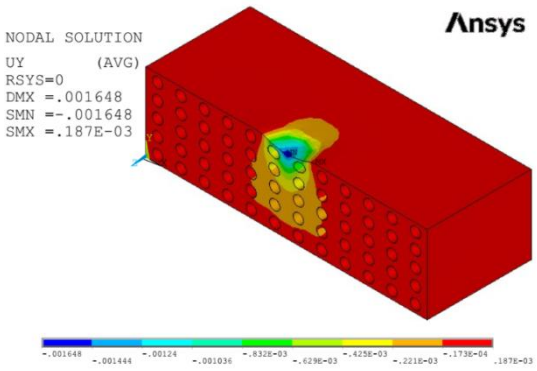

(b) γ_e =0

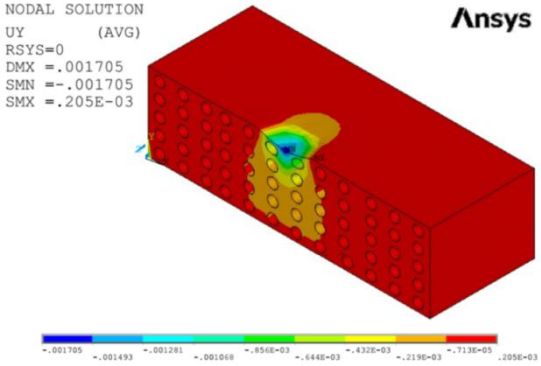

(c) γ_e =+1

Figure 5.13: Contour plots depict the nodal displacement in the y-direction when subjected to indentation depth of 2 nm at the end of the unloading (γ_e = -1, 0 & +1)

Following the completion of the indentation process, when the indenter is withdrawn and fully detached from the nanocomposite, contour plots of permanent deformation in the Y-direction are presented in Figure 5.13. The pattern of the residual deformation is observed to be similar to that observed at the end of the loading stage. The deformation recovery can also be correlated with the energy dissipated due to plasticity, which is represented in terms of the parameter Energy Loss Index (ELI). The ELI is defined in Equation 5.2. The integrals in the equation are obtained from the loading-unloading force-displacement data. Table 5.2 furnishes the ELI corresponding to three values of gradation parameters. It could be noted that $\gamma_e = +1$ corresponds to the highest ELI which corroborates the trend observed in the stress-state contour plot (Figure 5.10) and the residual deformation plot (Figure 5.13).

$$ELI = \frac{\int_0^{\omega max} P_{loading} d\omega - \int_{\omega_{res}}^{\omega max} P_{unloading} d\omega}{\int_0^{\omega max} P_{loading} d\omega} \quad (5.2)$$

Here, ω represents the indentation depth value, and P corresponds to the contact force.

Table 5.2: Energy Loss Index (ELI)

FGM-CNT Nanocomposite	**Loading (Ld)**	**Unloading (Uld)**	**Energy Loss Index (ELI) [(Ld-Uld)/Ld]**
$\gamma_e = -1$	4.65E-04	1.22E-04	0.738201
$\gamma_e = 0$	5.87E-04	1.18E-04	0.799416
$\gamma_e = 1$	6.09E-04	1.16E-04	0.810381

5.5 Summary

The present analysis focuses on exploring the impact of the "gradation parameter" on the contact behavior of CNTR-FGMM nanocomposite. This study uses a contact model that has been created on the ANSYS platform using FEM with code written in the APDL. Based on the interaction of nanocomposite blocks indented by a spherical indenter, the contact model has been created.

Key findings derived from the analysis are as follows:

- The elastic gradation parameter significantly influences the contact behavior of CNT-reinforced FGM nanocomposites under indentation loading and unloading.
- An increase in the CNT thickness-to-radius ratio improves the contact properties of the nanocomposite, but beyond a threshold thickness (~0.34 nm), the improvement in contact force becomes negligible.
- CNTR-FGMM nanocomposites demonstrate superior contact performance compared to FGMs without CNT reinforcement.
- During unloading, higher gradation parameters initially show higher contact forces, but beyond a certain point, this trend reverses due to enhanced plasticity and reduced deformation recovery.
- The maximum deformation is observed at the indentation point and spreads outward, becoming more significant with increasing gradation due to changes in elasticity and yield stress.
- The trends observed in stress distribution (via von Mises stress analysis) and energy loss index support the mechanical response variations with gradation.

Chapter 6

Flattening Contact Analysis of CNTR-FGMMC Nanocomposite

6.1 Introduction

The interaction between contact surfaces during loading and unloading is an important aspect in determining the longevity of contact-engaged components. Rapid stress increases during loading, followed by sudden decrease during unloading, can lead to microcrack formation, which poses challenges for interconnected machine components. In the context of modern micro- and nanotechnology advancements, such as MEMS microswitches (Majumder et al., 2001 & 2003), AFM systems (Chung et al., 2003) and magnetic storage devices (Suh et al., 2005; Li et al., 2009), in-depth comprehension of contact phenomena is essential. A flattening-based single asperity contact analysis is a first step towards comprehensive understanding of such a complex contact phenomena.

Contact analysis has a history of more than a century of pioneering research work and a steady stream of work has been ongoing throughout pushing the boundaries of the domain. In the late 19th century, Hertz (1881) correlated force, contact area, and deformation in contact models, proposing an elliptical nature for the contact surface. Johnson (1985) expanded this by presenting equations for contact radius and deformation in circular contacts. Ghaednia et al. (2016) integrated yield strength ratio into elastic-plastic contact modelling, highlighting the transition from flattening to indentation. Wei et al. (2020) developed a formula for maximum contact stress in cylindrical gears, considering various factors. Researchers like Olsson et al. (2016) and Kogut and Etsion (2002) have conducted numerous contact analyses focusing on flattening, emphasizing both numerical and experimental approaches.

With contemporary material development, functionally graded (FG) materials and carbon nanotubes (CNTs) have gained attention for their unique properties. The present research aims to explore the contact behavior of CNTR-FGMMC hybrid nanocomposites through flattening-based contact analysis and involves assessing deformation, stress distribution, and other characteristics during contact. Prior studies (Nahas and Alzahrani, 2012; Zuberi and

Esat, 2015) have investigated the role of CNTs in nanocomposites, but no existing literature addresses the flattening-based contact analysis of CNTR-FGMMC composites. This study introduces a novel material with CNTs in the FGM, exploring the impact of CNT wall thickness and gradation parameters on contact behavior, using a finite element model validated against published results. The validity of the model has been established against results published in literature (for similar problem with lesser complexity).

6.2 Finite Element Modelling

The physical contact interface is considered to be a cylindrical asperity is made of CNT reinforced FGM matrix nanocomposite, whose material properties vary along the radius. A schematic representation of the 3-D physical system shown in Figure 6.1. In order to conducted to analyze the loading and unloading of cylindrical flattening contact between the cylindrical asperity and a rigid flat, a finite element model has been constituted. To minimize computational time, instead of a 3D cylinder model, 2D semi-circular model with a plane stress condition [Sharma & Jackson, 2017] is considered, as shown in Figure 6.2. The radius of the cylindrical asperity is 9.5 nm, while the CNTs have a radius of 1 nm. The CNTs are uniformly distributed within the matrix and they are assumed to be perfectly bonded with the functionally graded matrix material.

In the finite element model configuration (as shown in Figure 6.2), the X-axis is attached to the base of half-cylinder and this base is considered to be anchored to the bulk element. It is reasonable to assume that this base is fixed and hence, all nodes along the previously maintained X-axis (which is coincident on the base) are constrained w.r.t. any movement, ensuring immobility in all directions. The rigid flat is represented by straight line tangent to the semicircle (half cylinder) apex. Loading process is initiated by downward displacement of the flat, while its up-word displacement constitutes unloading. The interface between the cylindrical surface and rigid flat is treated as frictionless contact.

The semicircular model representing asperity tip is discretized using quadrilateral PLANE223 elements which are capable of performing coupled thermo-structural analysis. The contact surface of the semicircular asperity is meshed using CONTA172 elements, while the rigid surface in contact is meshed using TARGE169 elements. The mesh density is refined near the contact zone and in vicinity of the embedded CNTs with coarser mesh used in regions away from these zones. This is done to optimized computational efficiency without compromising result accuracy.

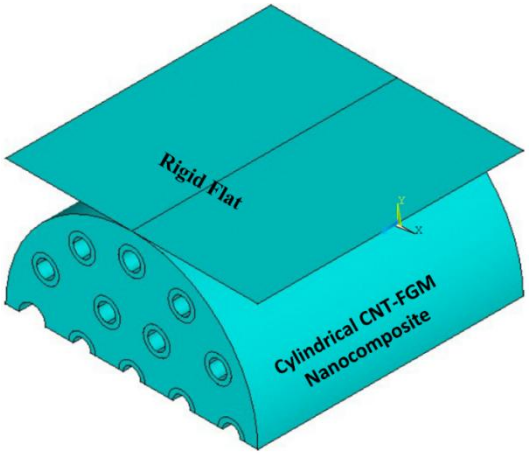

Figure 6.1: 3D model

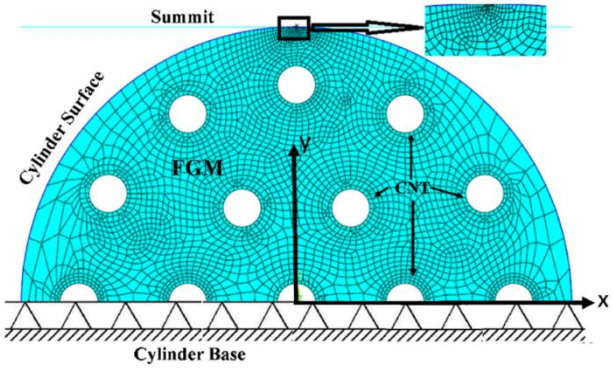

Figure 6.2: 2D mesh model

The material of the asperity comprises of two components viz. the reinforced carbon nanotubes (CNTs) and the matrix functionally graded material (FGM). Here, FGM is elastic graded material (EGM), which is used as matrix material. EGM is a special type of FGM whose elastic properties vary continuously with in the material (yield strength remains constant and elastic modulus varies).

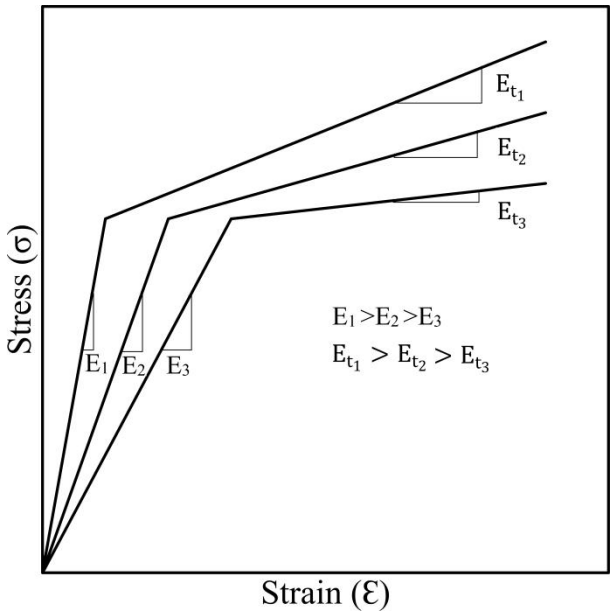

Figure 6.3: Stress-strain curve for EGM

Figure 6.3 presents a schematic representation of the stress-strain behavior for the EGM. In the cylindrical substrate, for positive value of γ_e the modulus of electricity of the material increases towered the central line of the cylinder from the surface and decreases for negative value of the γ_e. Zero value of gradation parameter, material behaves as an homogeneous isotropic material, with material properties remaining constant over the entire asperity. The

gradation that is introduced in the matrix material is in the form of elastic gradation, in which the Young's modulus (E) and tangent modulus (E_t) are varied radially, while maintaining the yield strength (Y) and the E_t/E ratio constant. Bilinear isotropic hardening model is employed to characterize the post-elastic behavior of the matrix material, with the von Mises yield criterion to determine the onset of yielding.

For the EGM matrix, the Young's modulus is graded according to the following exponential function.

$$E = E_0 e^{\gamma_e(1-\frac{r}{R})} \tag{6.1a}$$

$$E_t = E_{t_0} e^{\gamma_e(1-\frac{r}{R})} \tag{6.1b}$$

Where γ_e is the inhomogeneity parameter (gradation parameter) for an elastically graded cylindrical asperity. R is the radius of the cylinder, and r is the radial distance from the central line of the cylinder. E_0 and E_{t_0} represents the modulus of elasticity and is the Tangent Modulus of the material at the contact surface. Equation 6.1 for the gradation function indicates that the modulus of elasticity at the surface of the cylindrical asperity remains unaffected by the inhomogeneity parameter. However, variations in the inhomogeneity parameter influence the material properties beneath the contact surface.

The variation of the material properties in the graded material is achieved by attaching the material properties as a function of temperature. To achieve this variation, a thermal analysis is setup, allowing temperature to serve as a controlling factor for the material properties across the model. In this thermal analysis, the thermal expansion coefficient and the thermal conductivity of the material are set to zero. It ensuring that there is no geometrical distortion of the model. Time-dependent variation of temperature is also ignored as thermal loads are applied are applied to the nodes based on appropriately chosen gradation parameter. After developing the geometry of the model and incorporating material properties, the boundary condition are prescribed. All the nodes on the base, which are considered fixed or have no movement in any direction. The rigid flat in the negative y-direction to interference values of 0.25 nm, 0.5 nm, 0.75 nm, and 1 nm is displaced gradually. Once the rigid flat reaches the specified interference level, it is then slowly withdrawn until it detaches from the cylinder's surface. It constitutes the loading process to a specific interference and the unloading from that level of interference is done by slowly withdrawing the flat until there is detachment.

In the present analysis, the material property is considered to be that the modulus of elasticity (E_0) at the surface of the cylinder is 150 GPa, Poisson's ratio is 0.3, the tangent modulus is 4% of the modulus of elasticity, the yield strength is 750 MPa for the entire cylinder, and the

elastic gradation parameter (γ_e) varies from -2,0, and 2, when considering the EGM with gradation parameter of 0, and the property of the CNTs is taken from published literature (Ahmed et al., 2020).

6.3 Mesh Convergence Analysis

Convergence analysis is an important part of any FE model before extracting the results for analysis. The goal of convergence analysis is to find a mesh size that is fine enough to produce accurate results but not so fine that the running time or load becomes excessive.

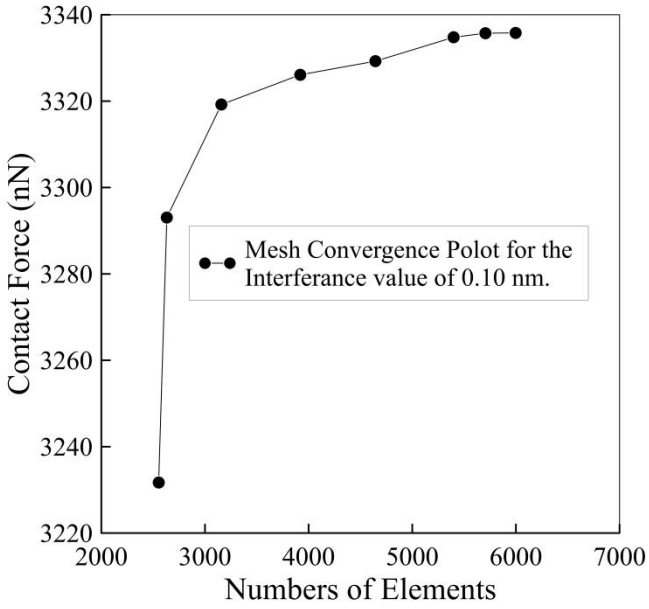

Figure 6.4: Contact force versus numbers of elements during meshing plot at the interference value of 0.10 nm.

In the present study also mesh convergence analysis was performed to determine the optimal mesh density for accurately calculating the contact force with the optimum computational time. The present convergence analysis is conducted for the contact force generated with an interference value of 0.10 nm. The material properties of the model is assumed to be the same as the material properties considered in the present analysis. But the gradation parameter is zero. A fine mesh is used near the contact zone, and the mesh density decreased as the distance from the contact zone increases. The analysis begins with a low number of elements, and the contact force is extracted at the end of the loading stage. This process is repeated with increasing numbers of elements. The contact force was recorded for each stage, and it is observed that after 5705 elements, there is a negligible change in the contact force with further increases in the number of elements. The convergence analysis plot is shown in Figure

6.4. Therefore, the corresponding mesh configuration elements were used in the subsequent analysis.

6.4 Validation Study

Model validation is another important part of any numerical analysis. As per the author's knowledge, there are no theoretical, numerical, or experimental flattening contact analysis results for CNTR-FGMMC nanocomposite in the published literature. In the above scenario, the model is validated with similar results published in the literature.

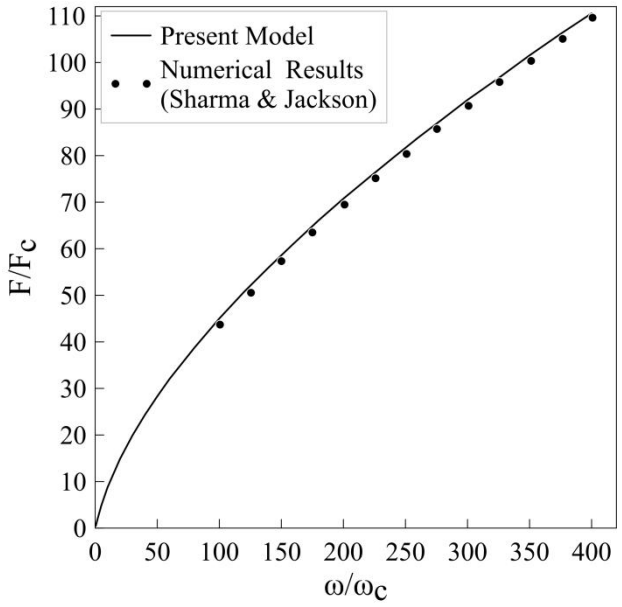

Figure 6.5: Comparison of the results from the present model versus those published in the literature by Sharma and Jackson (2017) .

The validation process is conducted against the findings published by Sharma and Jackson (2017). In this model, an elastoplastic material has been used to form a cylinder that is subsequently flattened by a rigid flat surface. To accomplish this, the present model replaces the matrix material of the functionally graded material (FGM) with elastoplastic material, and instead of CNTs, a solid cylinder with elastoplastic properties is utilized. The results obtained are then compared with the published results, as depicted in Figure 6.5, where 'F' represents contact force, 'ω' corresponds to interference, 'F_c' denotes critical contact force, and 'ω_c' represents critical interference. Notably, the comparison demonstrated a close alignment between the two sets of results, confirming the validation of the flattening model.

6.5 Results and Discussion

6.5.1 Findings from Finite Element (FE) Analysis

Variation in contact force during the flattening process (both loading and unloading) of cylindrical CNT-reinforced functionally graded (FG) material matrix nanocomposites is an important parameter to understand the overall contact behavior. The impact of variation in CNT wall thickness on contact force for three scenarios: positive gradation (γ_e =+2), negative gradation (γ_e =-2), and no gradation (γ_e =0) in the matrix material are presented as results.

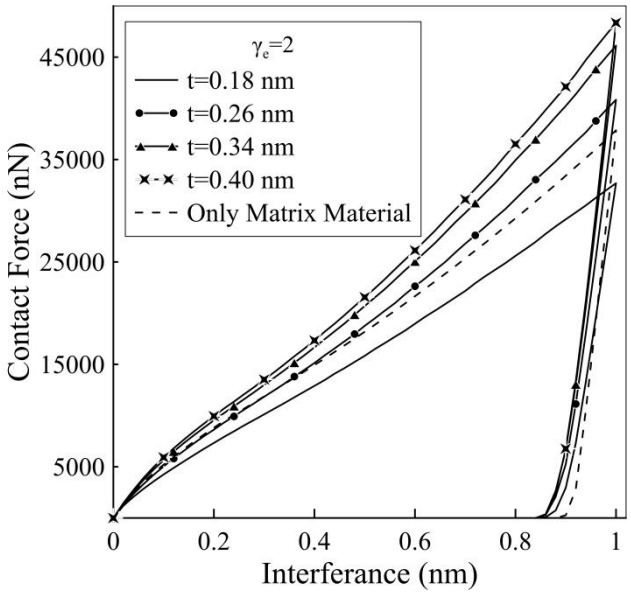

(a) γ_e =+2

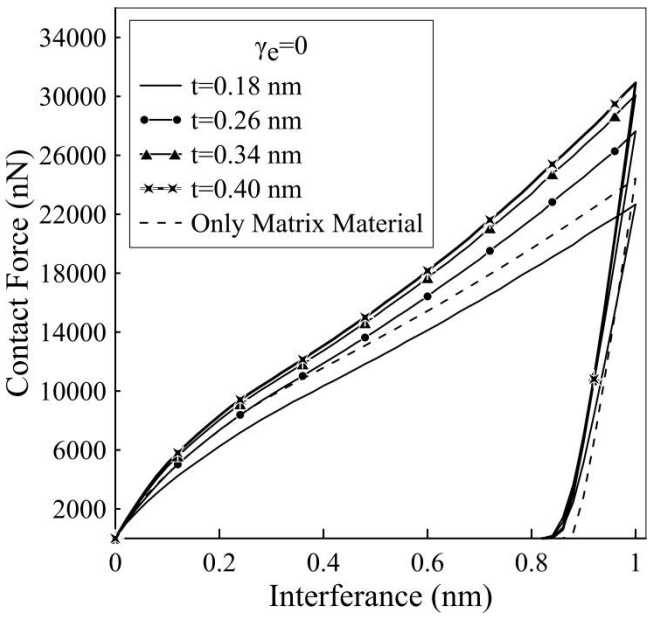

(b) γ_e =0

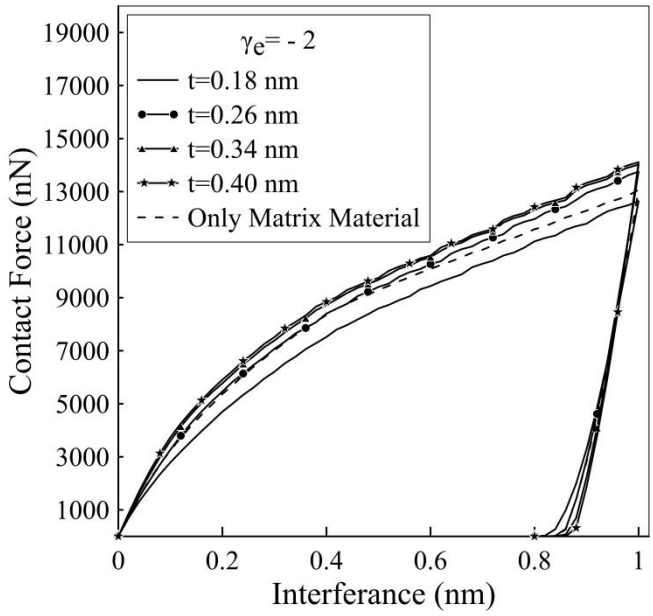

(c) γ_e =-2

Figure 6.6: Contact force vs interference for constant gradation value with the variation in CNTs wall thickness (a) γ_e =+2, (b) γ_e =0 and (c) γ_e =-2

Figure 6.6 illiterates the contact force behaviour through the entire loading and unloading cycle of the flattening of cylindrical nanocomposite. Results corresponding to the three different gradation parameters of elastically graded matrix materials (γ_e =+2, 0, -2) are shown in Figures 6.6.(a), 6.6(b) and 6.6(c), respectively. It could be pointed out that γ_e =0 represents a curve where the matrix material is homogeneous in nature (without any gradation). The wall thickness of the CNT varies between 0.18 nm, 0.26 nm, 0.34 nm, and 0.40 nm with an interference value of 1 nm. Across all three figures, it is evident that the contact force increases as the wall thickness of the CNT increases. In all three figures, contact force data for cylindrical flattening without CNT reinforced is also included as a reference. Notably, CNT wall thickness of 0.18 nm results in a lower contact force compared to the unreinforced half-cylinder (without any CNT embedded in the matrix). This reduced contact force likely results from the comparatively lower stiffness of CNTs due to lower wall thickness.

Furthermore, it is observed that a positive gradation value of +2 yields the highest contact force, while a negative gradation value of -2 results in a lower contact force. Initially, as the CNT wall thickness increases, the increment in contact force is more pronounced. However, as the CNT wall thickness continues to increase, the change in contact force increment decreases. This effect is prominently observed for positive gradation (γ_e =+2) and homogeneous (γ_e =0) matrix material. Interestingly, after reaching a CNT wall thickness of

0.34 nm, the increment in contact force becomes minimal, and it can even be considered negligible, for negatively graded matrix materials (γ_e =-2). Consequently, further analysis is the contact force data performed by comparing corresponding to different levels of interference and subsequent unloading from that level. For different interference depths are taken into account (0.25 nm, 0.5 nm, 0.75 nm and 1.00 nm) and loading is done till there values before initiating the unloading phase. In all the cases CNT wall thickness is kept fixed at 0.34 nm. There results are presented in Figure 6.7(a) and the figure contains three sets of curves pertaining to the different gradation parameters.

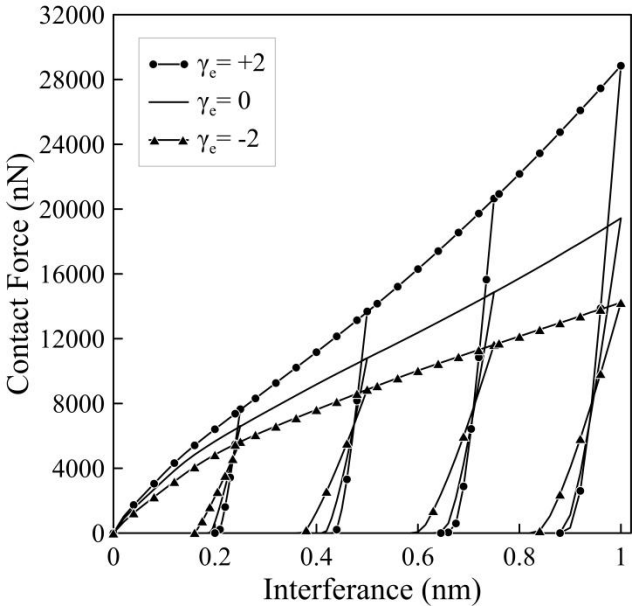

(a)

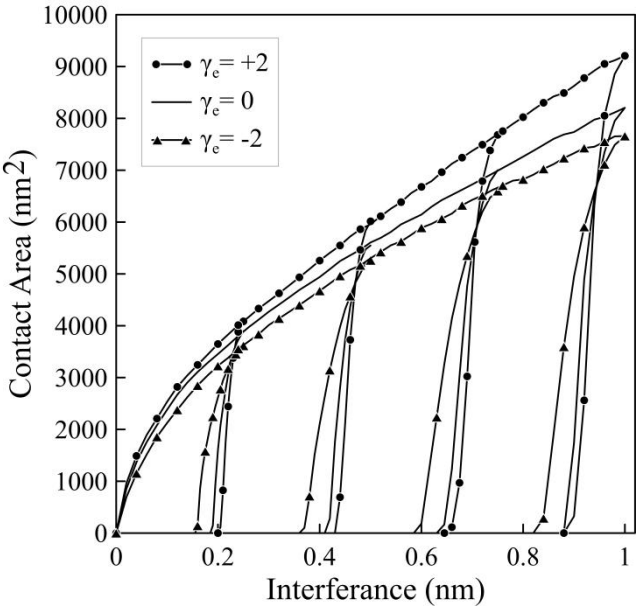

(b)

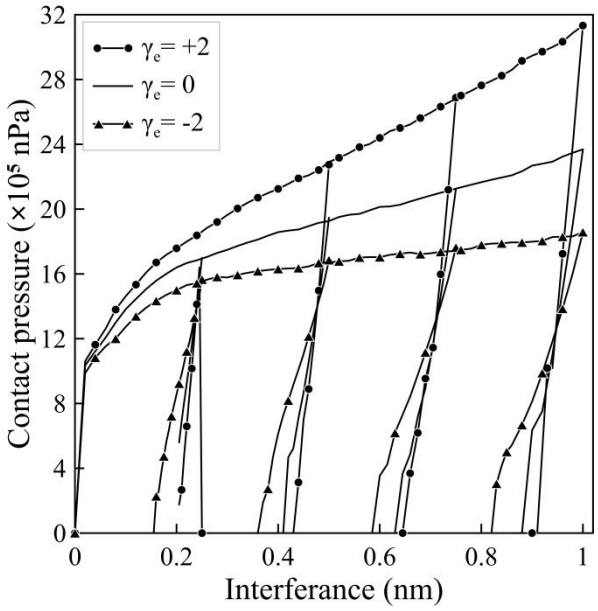

(c)

Figure 6.7: (a)The rigid flat interference vs. contact force plots for loading and unloading (b) interference vs. contact area plots (loading-unloading) and (c) interference vs. contact pressure plots (loading-unloading) of elastically graded cylinder CNTR-FGMMC with a constant wall thickness of 0.34 nm.

Similarly, Figures 6.7(b) and 6.7(c) provide insights into the relationship between the contact area and interference, and the contact pressure and interference, respectively for CNT reinforced elastically graded material (EGM) for different values of the gradation parameter (γ_e =+2, 0 and -2). It is evident from the results that a higher contact force value is observed when the gradation parameter is higher. This indicates that there is a greater yield stress and modulus of elasticity at the cylindrical substrate, which makes it more resistant to deformation when in contact with the rigid flat. As a result, a higher elastic gradation parameter leads to a stronger resisting force against the flattening of the cylindrical block. Additionally, it's worth noting that a higher value of the elastic inhomogeneity parameter (γ_e) corresponds to a lesser recovery of the deformation behavior, as seen from the unloading curve. During unloading, higher contact force is observed as a higher value of the inhomogeneity parameter up to a certain limit, but after this point, the opposite nature is observed as a higher value of the inhomogeneity parameter and a lower value of contact force. Contact area vs interference and contact pressure vs interference behaviour during the loading-unloading cycle exhibit similar trends as compared to the contact force behaviour (as evident from Figures 6.7 (a) and 6.7 (b)).

6.5.2 Analysis of Stresses

Studying the distribution of stresses across the deformable cylindrical asperity under flattening is an important aspect of contact analysis. The results presented in this section are contour plots illustrating the von Mises stress distribution of the cylindrical nanocomposite (CNTR-FGMMC) following the loading phase (with an interference value of 0.25 nm). These distributions are obtained for three different gradation parameters (positively graded, γ_e =+2, negatively graded, γ_e =-2 and homogeneous γ_e = 0) with the CNT wall thickness held constant at 0.34 nm. It should be mentioned here that the stress distribution in its entirely can not be captured in a single contour plot as the CNTs have much higher stresses in comparison to the matrix. The first contour plot (denoted by (i) in Figure 6.8) provides the distribution for the entire nanocomposite and as expected it is shows the highest stress in the CNT. However the stress distribution in the matrix is not clear at all. Hence, a second contour plot (denoted by (ii) in Figure 6.8) is presented excessively for the matrix , highlighting the stress distribution within it.

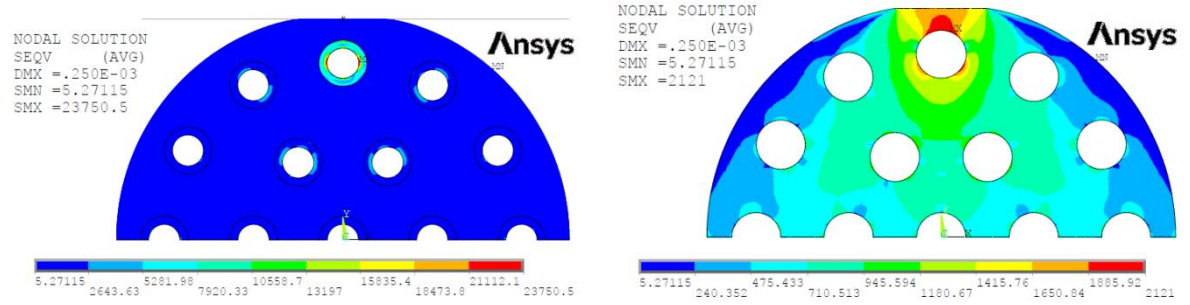

(i) (ii)

(a) γ_e =+2

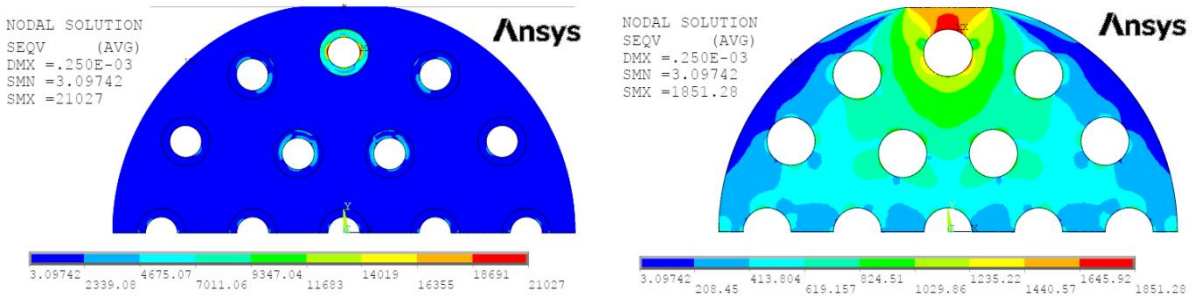

(i) (ii)

(b) γ_e =0

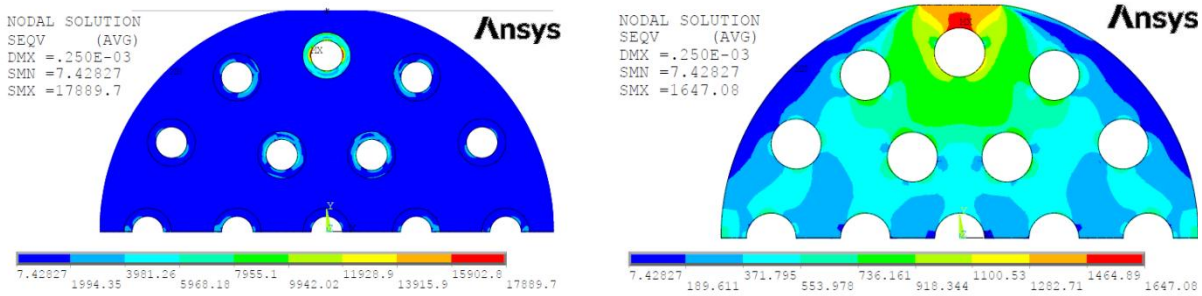

(i) (ii)

(c) γ_e =-2

Figure 6.8: Average von Mises stress distribution over the nanocomposite at the interference of 0.25 nm with the variation of gradation parameter (γ_e = +2, 0 & -2)

According to the contour plots as shown in Figure 6.8, it is evident that the peak stress is elevated when using higher gradation parameters in comparison to a non-graded metal matrix CNT-reinforced nanocomposite. Conversely, a negatively graded composite exhibits a lower peak stress compared to a material without gradation in the matrix. Figure 6.8(ii) illustrates the von Mises stresses distribution exclusively within the matrix material of the nanocomposite. The distribution pattern is similar to that discussed earlier for the entire nanocomposite. It is evident that the peak stress developed in the matrix material is lower compared to the peak stress in the CNTs, as the CNTs possess a much higher Young's modulus than the matrix material. From the comparison of the stress contours of the nanocomposites with varying gradation parameters, the maximum stress is observed to develop in the CNTs located in the vicinity of the contact zone.

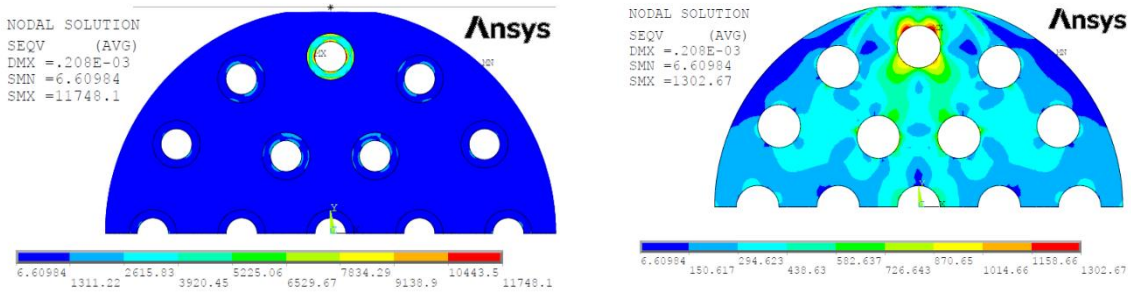

(i) (ii)

(a) γ_e =+2

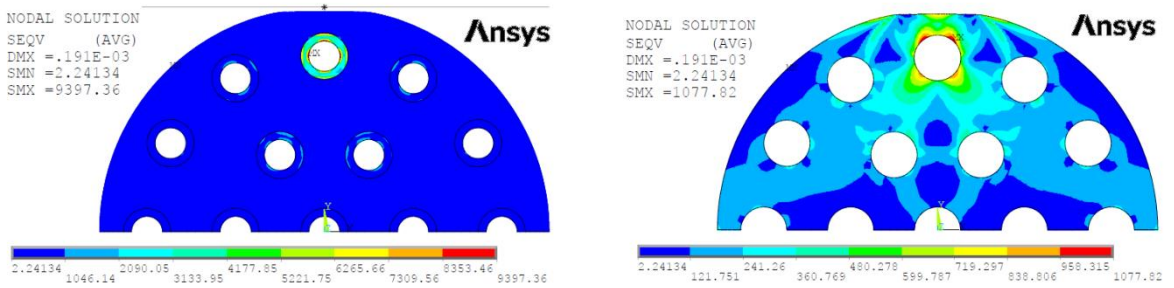

(i) (ii)

(b) γ_e =0

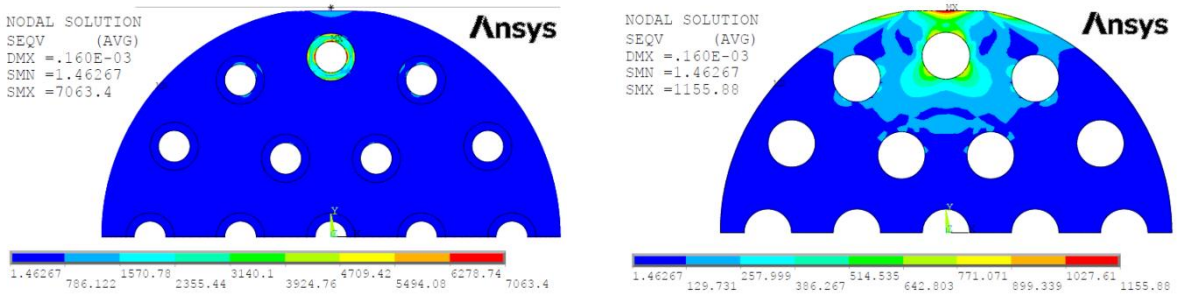

(i) (ii)

(c) γ_e =-2

Figure 6.9: Average residual von Mises stress distribution over the nanocomposite at the end of the unloading stage from an interference of 0.25 nm with the variation of gradation parameter (γ_e = +2, 0 & -2)

Figure 6.9 presents contour plots of the average residual von Mises stress distribution, exhibiting a pattern consistent with the von Mises stress distribution associated with variations in elastic gradation (as shown in Figure 6.8). In all the cases, high residual stress zones are found below the contact zone and surrounding the CNT immediately below the contact zone. In this figure (as with the previous stress distribution figures), there are two sets of contour plots- one showcasing the stress state in the entire system (including the CNTs) and the other only highlighting the stresses present in the matrix.

The observations from these contour plots can be linked to Figure 6.7(a), which illustrates contact force behavior in relation to interference values. The residual von Mises stress is indicative of permanent deformation taking place in the matrix and consequently gives an idea of deformation recovery. Energy loss index (ELI), derived from force-displacement curve during loading and unloading phases, indicates the deformation recovery potential and discussed in detail later (section 6.5.4). Higher energy loss index indicates lower chances of deformation recovery and it agrees with the residual stress behaviour as demonstrated in the contour plots of Figure 6.9.

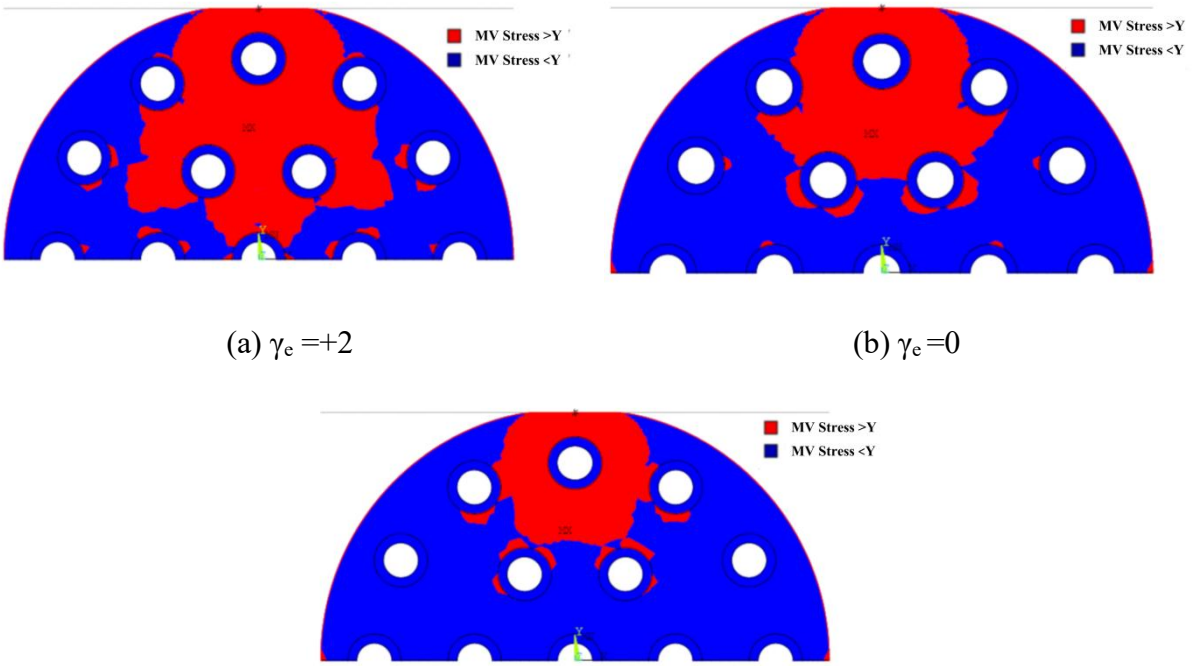

(a) γ_e =+2 (b) γ_e =0

(c) γ_e =-2

Figure 6.10: Stress state contour plot comparing von Mises stress (a) γ_e=+2, (b) γ_e = 0 and (c) γ_e=-2. Loaded up to interference of 0.025 nm of the CNTR-FGMMC cylindrical block with CNT wall thickness of 0.34 nm.

Figure 6.10 displays stress state contour plots for the elastic-graded cylindrical nanocomposite. These plots are generated at end loading to an interference of 0.25 nm. Maintaining continuity with the previous stress plots, constant CNT wall thickness of 0.34 nm is considered, while, the gradation parameter (γ_e) has three different values, +2 (Figure 6.10(a)), 0 (Figure 6.10(b) and -2 (Figure 6.10(c)). These figures are created by comparison between von Mises stress values and yield strength at any given point within the nanocomposite and offer a visual perspective on how much of the matrix has gone into past-elastic domain. The plots also depict the distinction between the elastic and post-elastic phases at various points within the material. It is evident that a higher value of the elastic gradation parameter in the matrix material results in a greater volume of plastic yield. This yielding behavior correlates with the findings in Figure 6.7, where a larger contact area is associated with a greater amount of material yielding at the contact surface. Additionally, the higher energy requirement during loading is another factor contributing to the increased volume of material yield. The energy aspect of the contributing factors is discussed later in the chapter.

6.5.3 Analysis of Deformation

The effect of the elastic gradation parameter on deformation behavior is examined at the end of the loading and unloading stages for interference of 0.25 nm in Figures 6.11, 6.12, and 6.13. The elastic gradation indexed varies as -2, 0, and +2, whereas CNT wall thickness is considered constant at 0.34 and is distributed uniformly over the matrix material FG.

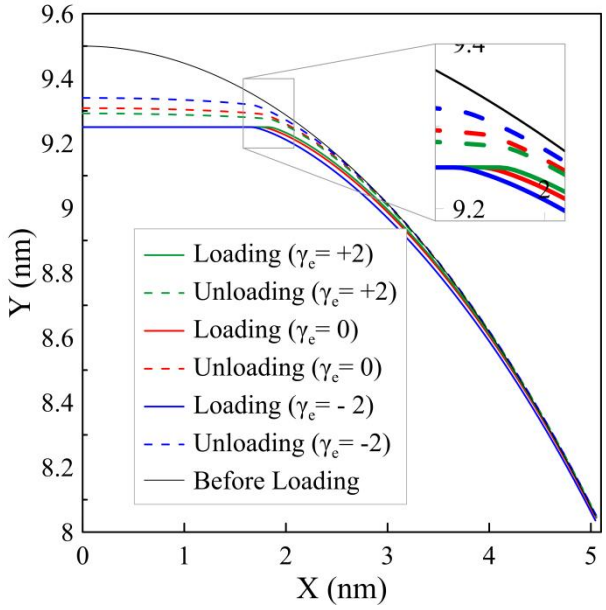

(a)

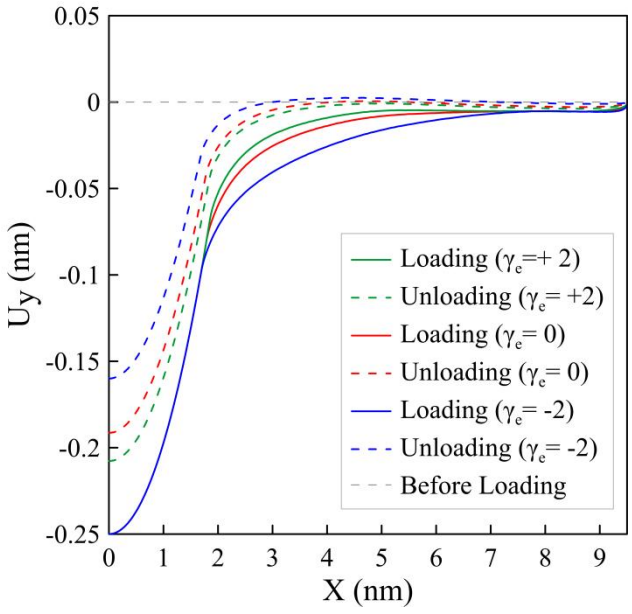

(b)

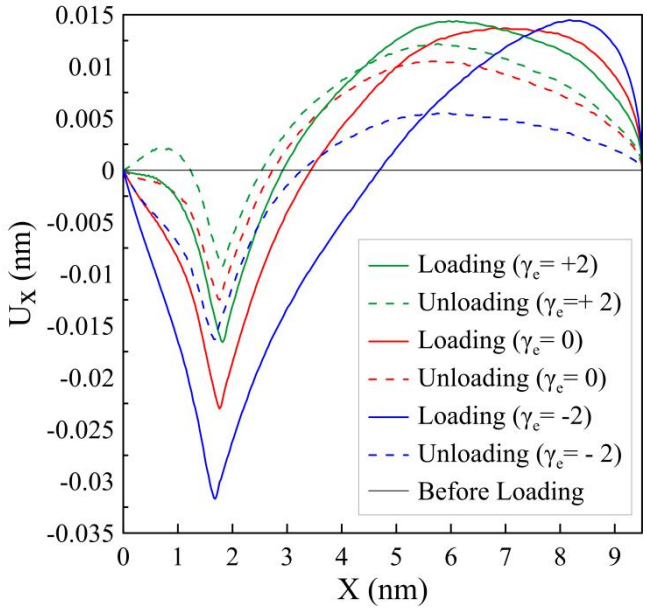

(c)

Figure 6.11: (a) Deformed and undeformed geometry (b) Nodal displacement in the Y-direction (c) Nodal displacement in the x-direction of the nodes located at the top surface of the cylinder at an indentation depth of 0.25 nm with the variation of elastic gradation index (+2, 0 and -2) at the end of loading and unloading

Figure 6.11 (a) shows the contact surface of the cylindrical substrate at the end of loading and unloading for the previously mentioned interference value. For case of comparison, the undeformed surface of the cylinder is also shown. From the unloading curve, it is evident that higher elastic gradation parameter is associated with reduced recovery at the end of unloading. Figures 6.11(b) and 6.11(c) demonstrate the displacements of the nodes situated on the surface along Y and X axis respectively. As before results are plotted corresponding to the different γ_e values (+2, 0 and -2) at the completion of loading and unloading stages. During loading, nodes exhibit displacement in the negative Y-direction (Ref. Figure 6.11(b)), with displacement amplitude diminishing as the distance from the Y-axis increases. By the end of unloading recovery is notable grater for higher gradation parameters. In Figure 6.11(c), initially there is negative X-direction displacement. Beyond a certain point, nodes begin to shift in the positive X-direction. This phenomenon likely arises due to the compression of material beneath the contact zone.

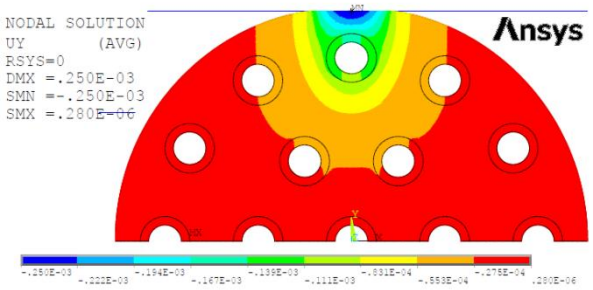

(a) γ_e =+2

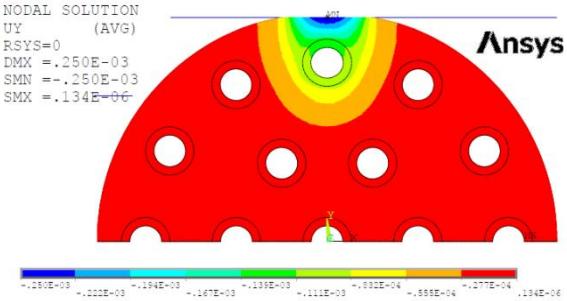

(b) γ_e =0

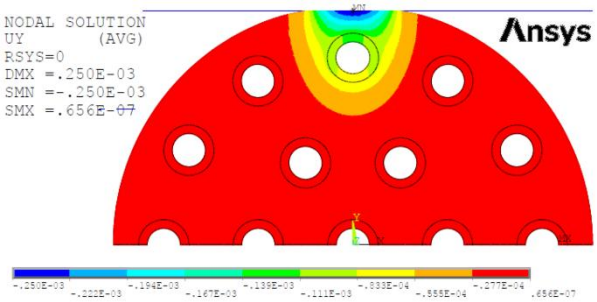

(c) γ_e =-2

Figure 6.12: Contour plots depict the nodal displacement in the y-direction when subjected to interference of 0.25 nm at the end of the loading (γ_e = +2, 0 & -2)

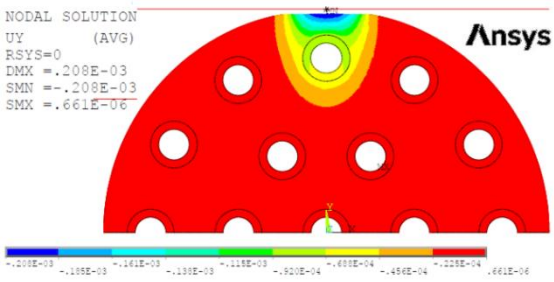

(a) γ_e = +2

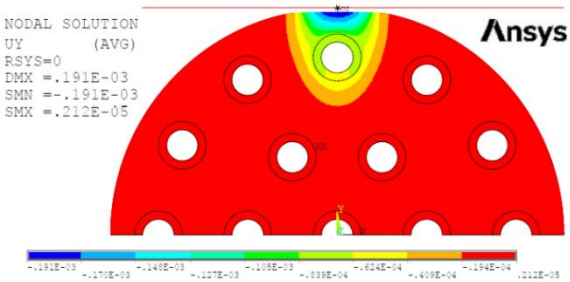

(b) γ_e =0

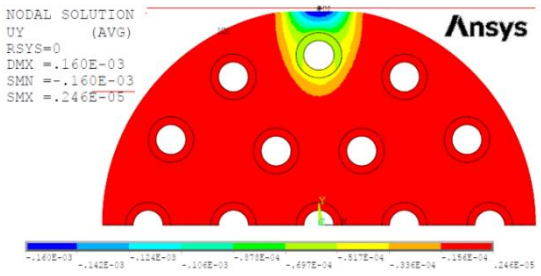

(c) γ_e =-2

Figure 6.13: Contour plots depict the nodal displacement in the y-direction when subjected to the interference of 0.25 nm at the end of the unloading (γ_e =+ 2, 0 & -2)

In Figure 6.12, a contour plot is presented, illustrating the displacement of nodes in the Y direction within a cylindrical matrix composed of CNTR-FGMMC nanocomposite. These contour plots are observed at the end of the loading stage, with an interference value of 0.25 nm. It is also seen from the plots that the volume of material displaced is higher in cases of higher elastic gradation parameters. As the elastic modulus increases, a higher resistive force is developed, so a higher amount of material is affected.

Figure 6.13 illustrates the nodal displacements in the Y direction following complete unloading. It is apparent that the increase in the positive gradation of the nanocomposite corresponds to increases in the amount of permanent deformation. The relation between lower gradation index and the extend of recovery in displacement is evident in Figure 6.11 and 6.12. This recovery can be also linked to the residual von Mises stress observed at the end of unloading (as illustrated in Figure 6.9). Notably, lower gradation values correspond to reduction in residual von Mises stress, resulting in decreased permanent deformation of the material upon unloading.

6.5.4 Energy Loss Index

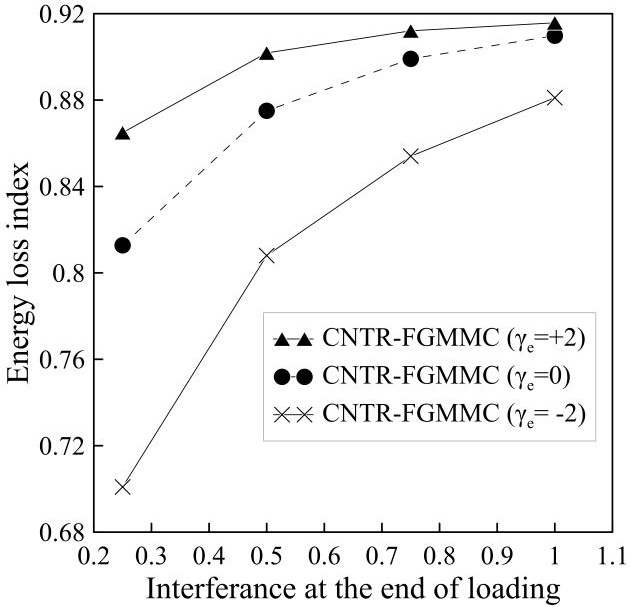

Figure 6.14: Interference at the end of loading vs. energy loss index (ELI) plot for different values of elastic gradation parameter.

The previous sections discussed how the volume of plastic yielding occurs and how the development of residual stress causes permanent deformation of the cylindrical substrate. This permanent deformation can be correlated with energy loss during the process. As Jana et al. (2020) discussed, the volume of material yield is directly proportional to the interference

value. The present study determines the energy loss index (ELI) using the force-displacement curve.

$$ELI = \frac{\int_0^{\omega max} P_{loading} d\omega - \int_{\omega_{res}}^{\omega max} P_{unloading} d\omega}{\int_0^{\omega max} P_{loading} d\omega} \quad (2)$$

Here, ω represents the interference value, and P corresponds to the contact force.

Figure 6.14 presents the maximum interference vs. energy loss index for the variation of the elastic gradation parameter. It is clearly observed that the energy loss index increases as the gradation parameter increases, and the outcome of the energy loss index validates the results as discussed before.

6.6 Summary

The study employs the Finite Element Technique (FET) on the ANSYS platform to simulate the contact between a CNTR-FGMMC cylindrical asperity and a rigid flat surface, examining both loading and unloading phases with variations in the gradation inhomogeneity parameter. It analyzes contact properties such as contact force, area, average von Mises stresses, residual stresses, deformation behavior, and energy loss index (ELI).

Key findings are:

- Contact force increases with CNT wall thickness up to a certain point, beyond which the increase is minimal. Lower CNT wall thickness results in lower contact force than the matrix material alone due to lower stiffness.
- Elastic gradation inhomogeneity parameters significantly impact contact force, area, and pressure, with these properties increasing proportionally to the parameter.
- The von Mises stresses and residual von Mises stresses rise with higher gradation parameters, particularly in the contact zone and at the matrix-CNT interface.
- Higher gradation parameters lead to increased plastic zone volume, deformation, and energy loss index, correlating with stress distribution and plastic yielding patterns.

This page is left blank intentionally

Chapter 7

Conclusions and Future Scope

7.1 Introduction

This thesis provides an in-depth examination on the contact analysis of CNT-based nanocomposites, with a particular emphasis on their behavior under single-asperity contact scenarios. The analysis is comprehensive, covering both indentation contacts, where a rigid indenter interacts with the nanocomposite material, and flattening contact, which occurs between a rigid flat and a cylindrical substrate. The research delves into the contact properties of various CNT-based nanocomposites, including CNT-Al nanocomposites, CNTR-FGMMC, and CNTs functionally distributed within aluminum metal matrix. In this study, variation in CNT thickness, distribution patterns, and elastic gradation parameter of the matrix material FGM is meticulously explored to understand their impact on the material's contact performance. The investigation thoroughly examines the critical contact parameters, such as contact force, contact area, stress distribution and deformation pattern etc. taking into account these variations of CNT thickness, gradation parameter (in case of FGM matrix) and CNT distribution pattern. All analyses are carefully conducted with a particular focus on the contact behavior of the material in the specific domains of both indentation and flattening contacts. The study utilizes the APDL code within the commercial ANSYS finite element software package, ensuring accurate and detailed modelling of the contact phenomena being investigated and validated with the similar published results.

7.2 Conclusions

The present thesis investigates the influence of CNTs and the matrix material on the contact behavior within CNT-based nanocomposites. The analysis is conducted in the domain of single asperity contact, focusing on both indentation and flattening-based contact models. The analysis leads to the establishment of several key findings.

- Effect of CNT Wall Thickness:
  - Lower wall thickness of CNTs in the nanocomposites exhibits lower contact force and higher contact area as compared to high wall thickness CNT rainforced composites during indentation/flattening contact analysis.

- Sink-in behavior is observed at the end of loading for all cases, with pile-up occurring at lower CNT wall thickness compared to others during indentation of CNT-Al nanocomposite.
- For high wall thickness CNTs, unloading causes outward displacement of material in the vicinity of contact occurs due to secondary plastic flow during the unloading process during flattening analysis of CNT-Al nanocomposite.

- Effect of CNT Volume Percentage:
  - Contact force increases and contact area decreases with higher CNT volume percentages, except for CNTs with lower wall thickness causes lower stiffness as compared to matrix material during indentation contact anlysis.
  - High stress developed in the CNTs due to their high elastic modulus, with stress concentrations at the vicinity of contact zone for both of the single asperity contact analysis.
  - The volume of yielded material increases with higher CNT volume percentages, with small elastic zones beneath the contact area observed in the flattening contact analysis.
  - The matrix material shows greater outward displacement near the contact zone, increasing with higher CNT volume percentages during indentation contact analysis.

- Effect of CNT Distribution Pattern in Functionally Graded Nanocomposites (FG-CNTRC) During Spherical Indentation Contact Analysis:
  - Contact force increases for negatively graded FG-CNTRC and decreases for positively graded FG-CNTRC.
  - Contact area is higher for positively graded FG-CNTRC during loading phases.
  - Uniformly distributed and negatively graded composites exhibit higher peak stress compared to positively graded CNTRC.
  - Pile-up phenomenon at the indentation edge is higher for negatively graded FG-CNTRC.
  - Negatively graded substrates undergo more horizontal displacement due to plastic flow compared to others.

- Effect of Gradation Index in CNTR-FGMMC Nanocomposites During Indentation and Flattening Contact Analysis:
  - Increasing the thickness-to-radius ratio of CNTs enhances contact properties up to a threshold.

- Higher gradation parameters lead to higher contact forces and lower gradation parameters result in reduced forces.
- CNTR-FGMMC exhibits superior contact behavior compared to matrix alone.
- Higher gradation parameters lead to more pronounced deformation.

7.3 Contributions of the Thesis

The novelty of this thesis lies primarily in the modelling and analysis of CNT-based nanocomposite single-asperity contact interfaces during indentation and flattening. The study considers rectangular and cylindrical asperities composed of CNT-elastoplastic matrix composite with uniform distribution patterns and graded distribution patterns. This approach is particularly appropriate for investigating the behavior of a single asperity among the countless ones in a physical CNT-based composite, a method not previously attempted by any researcher. The work provides detailed insights into the static contact behavior of the material in single-asperity contact interfaces. Additionally, it contributes to understanding the contact behavior of CNTs uniformly distributed within the FGM matrix (CNTR-FGMMC), with a key focus on the influence of elastic gradation on the contact system. A major contribution of the thesis is that it provides a robust computational model (based on a finite element tool) that assures reliable and accurate simulation results without the requirement of extensive computational capacity.

Major contributions of the thesis can be listed as below.

i. The influence of CNT wall thickness on contact parameters such as contact force, contact area, and contact pressure are investigated in the context of both indentation and flattening contact scenarios with a rigid indenter and a rigid flat surface.
ii. The impact of CNT volume percentage on contact parameters, including deformation behavior and stress distribution, is analyzed to understand how varying CNT content affects these factors.
iii. The contact behavior of FG-CNTRC is examined through single-asperity contact models, including both indentation and flattening contact scenarios, to assess how different CNT distributions influence contact performance.
iv. A novel hybrid composite material that is a functionally graded with properties varying as per an exponential function) matrix reinforced with CNTs is proposed in the last part of the thesis (Chapter 5 & 6). These chapter put forward the first and thorough investigation of indentation and flattening contact behaviour for

CNT reinforced FGM matrix composite. The results provided in the thesis are capable of providing insight into stress distribution and deformation behaviour and will serve as benchmark for further reference of such nanocomposites.

v. The effects of gradation index of CNT reinforced FGM matrix composite (CNTR-FGMMC) on contact behavior are explored using 2D and 3D single-asperity contact models, employing both rigid indentation and rigid flat surfaces to provide a comprehensive analysis of these factors.

7.4 Future Scope of Work

In the realm of scientific inquiry, each breakthrough often sparks a cascade of new questions and approach for exploration. The present thesis, while providing valuable insights into the contact behavior of single-asperity CNT-based nanocomposite surfaces, also opens up the way for several promising research directions. Potential future research directions could take into the following areas:

Dynamic Contact Analysis:

i. Extend the analysis to include multi-asperity contact scenarios.
ii. Incorporate adhesive forces and interfacial friction to enhance the realism of the model.
iii. Consider the size effect to improve the accuracy of the analysis, particularly in the context of nanoscale materials.
iv. Explore the impact of transient temperature environments on the contact behavior.

Tangential and Normal-Tangential Loading: Analyze the contact behavior under tangential or simultaneous normal-tangential loading conditions.

Wear Modelling: Investigate the wear mechanisms and their impact on the contact properties of the surfaces.

Electrical and Thermal Resistance: Analyze the electrical and thermal resistance between the contacting surfaces.

Contact Vibration Control: Explore methods to control contact vibration, considering the influence of surface complexities.

References

Abdelaziz, H. H., Meziane, M. A. A., Bousahla, A. A., Tounsi, A., Mahmoud, S. R., & Alwabli, A. S. (2017). An efficient hyperbolic shear deformation theory for bending, buckling and free vibration of FGM sandwich plates with various boundary conditions. *Steel and Composite Structures*, *25*(6), 693-704.

Abdullahi, U., Maleque, M. A., & Ali, M. Y. (2021). Hardness behaviour of carbon nanotube-aluminium nano-composite using nanoindentation technique. *Materials Today: Proceedings*, *46*, 6097-6101.

Abdullahi, U., Maleque, M. A., & Nirmal, U. (2013). Wear mechanisms map of CNT-Al nano-composite. *Procedia Engineering*, *68*, 736-742.

Adewunmi, A. A., Ismail, S., & Sultan, A. S. (2016). Carbon nanotubes (CNTs) nanocomposite hydrogels developed for various applications: a critical review. *Journal of Inorganic and Organometallic Polymers and Materials*, *26*, 717-737.

Ahmadi, M., Ansari, R., & Hassanzadeh-Aghdam, M. K. (2019). Micromechanical analysis of elastic modulus of carbon nanotube-aluminum nanocomposites with random microstructures. *Journal of Alloys and Compounds*, *779*, 433-439.

Ahmed, K. S., Ibrahim, I., & Keng, A. K. (2020). Advanced nanoindentation simulations for carbon nanotube reinforced nanocomposites. *Heliyon*, *6*(8), 1-15.

Alaboodi, A. S., & Hussain, Z. (2019). Finite element modeling of nano-indentation technique to characterize thin film coatings. *Journal of King Saud University-Engineering Sciences*, *31*(1), 61-69.

Al-Saleh, M. H., & Sundararaj, U. (2009). A review of vapor grown carbon nanofiber/polymer conductive composites. *Carbon*, *47*(1), 2-22.

Asgari, M. (2015). Material distribution optimization of 2D heterogeneous cylinder under thermo-mechanical loading. *Structural Engineering and Mechanics, 53*(4), 703-723.

Bartier, O., Hernot, X., & Mauvoisin, G. (2010). Theoretical and experimental analysis of contact radius for spherical indentation. *Mechanics of Materials*, *42*(6), 640-656.

Big-Alabo, A., Harrison, P., & Cartmell, M. P. (2015). Contact model for elastoplastic analysis of half-space indentation by a spherical impactor. *Computers & Structures*, *151*, 20-29.

Biwa, S., & Storåkers, B. (1995). An analysis of fully plastic Brinell indentation. *Journal of the Mechanics and Physics of Solids*, *43*(8), 1303-1333.

Boggarapu, V., Gujjala, R., Ojha, S., Acharya, S., Chowdary, S., & Kumar Gara, D. (2021). State of the art in functionally graded materials. *Composite Structures*, *262*, 113596, 1-29.

Borodich, F. M. (2014). The Hertz-type and adhesive contact problems for depth-sensing indentation. *Advances in Applied Mechanics*, *47*, 225-366.

Borodich, F. M., & Keer, L. M. (2004). Contact problems and depth-sensing nano-indentation for frictionless and frictional boundary conditions. *International Journal of Solids and Structures*, *41*(9-10), 2479-2499.

Bourago, N. G., & Kukudzhanov, V. N. (2005). A review of contact algorithms, *Mechanics of Solids, 40(1)*, 35–71.

Brake, M. R. (2012). An analytical elastic-perfectly plastic contact model. *International Journal of Solids and Structures*, *49*(22), 3129-3141.

Brizmer, V., Kligerman, Y., & Etsion, I. (2006). The effect of contact conditions and material properties on the elasticity terminus of a spherical contact. *International Journal of Solids and Structures*, *43*(18-19), 5736-5749.

Brizmer, V., Zait, Y., Kligerman, Y., & Etsion, I. (2006). The effect of contact conditions and material properties on elastic-plastic spherical contact. *Journal of Mechanics of Materials and Structures*, *1*(5), 865-879.

Buczkowski, R., Kleiber, M., & Starzynski, G. (2014). Normal contact stiffness of fractal rough surfaces. *Archives of Mechanics*, *66*(6), 411-428.

Carlsson, S., & Larsson, P. L. (2001). On the determination of residual stress and strain fields by sharp indentation testing. Part I: theoretical and numerical analysis. *Acta materialia*, *49*(12), 2179-2191.

Carneiro, Í., & Simões, S. (2020). Effect of morphology and structure of MWCNTs on metal matrix nanocomposites. *Materials*, *13*(23), 5557, 1-16.

Carpenter, N. J., Taylor, R. L., & Katona, M. G. (1991). Lagrange constraints for transient finite element surface contact. *International journal for numerical methods in engineering*, *32*(1), 103-128.

Carvalho, O., Buciumeanu, M., Madeira, S., Soares, D., Silva, F. S., & Miranda, G. (2015). Optimization of AlSi–CNTs functionally graded material composites for engine piston rings. *Materials & Design*, *80*, 163-173.

Celentano, D. J., Guelorget, B., François, M., Cruchaga, M. A., & Slimane, A. (2012). Numerical simulation and experimental validation of the microindentation test applied to bulk elastoplastic materials. *Modelling and Simulation in Materials Science and Engineering*, *20*(4), 045007, 1-32.

Chatterjee, B., & Sahoo, P. (2012). Effect of strain hardening on elastic-plastic contact of a deformable sphere against a rigid flat under full stick contact condition. *Advances in Tribology*, *2012*(1), 472794, 1-8.

Chatterjee, B., & Sahoo, P. (2014). Finite element based contact analysis of fractal surfaces–effect of varying elastic modulus. *Procedia Engineering*, *90*, 116-122.

Chen, X. W., & Yue, Z. Q. (2020). Nonlinear contact force law for spherical indentation of FGM coated elastic substrate: An extension of Hertz's solution. *International Journal of Solids and Structures*, *191*, 550-565.

Choi, Y., Lee, H. S., & Kwon, D. (2004). Analysis of sharp-tip-indentation load–depth curve for contact area determination taking into account pile-up and sink-in effects. *Journal of Materials Research*, *19*(11), 3307-3315.

Chudoba, T., & Jennett, N. M. (2008). Higher accuracy analysis of instrumented indentation data obtained with pointed indenters. *Journal of Physics D: Applied Physics*, *41*(21), 215407.

Chung, K. H., & Kim, D. E. (2003). Fundamental investigation of micro wear rate using an atomic force microscope. *Tribology Letters*, *15*, 135-144.

Civalek, O., & Jalaei, M. H. (2020). Buckling of carbon nanotube (CNT)-reinforced composite skew plates by the discrete singular convolution method. *Acta Mechanica*, *231*, 2565-2587.

Daeinabi, K., & Korayem, M. H. (2011). Indentation analysis of nano-particle using nano-contact mechanics models during nano-manipulation based on atomic force microscopy. *Journal of Nanoparticle Research*, *13*, 1075-1091.

Durst, K., Göken, M., & Pharr, G. M. (2022). Finite element simulation of spherical indentation in the elastic–plastic transition. *International Journal of Materials Research*, *93*(9), 857-861.

El Moumen, A., Tarfaoui, M., & Lafdi, K. (2017). Mechanical characterization of carbon nanotubes based polymer composites using indentation tests. *Composites Part B: Engineering*, *114*, 1-7.

Erdogan, F. (1995). Fracture mechanics of functionally graded materials. *Composites Engineering*, *5*(7), 753-770.

Esawi, A. M., Morsi, K., Sayed, A., Taher, M., & Lanka, S. J. C. S. (2010). Effect of carbon nanotube (CNT) content on the mechanical properties of CNT-reinforced aluminium composites. *Composites Science and Technology*, *70*(16), 2237-2241.

Etemadi, E., Khatibi, A. A., & Takaffoli, M. (2009). 3D finite element simulation of sandwich panels with a functionally graded core subjected to low velocity impact. *Composite Structures*, *89*(1), 28-34.

Etsion, I., Kligerman, Y., & Kadin, Y., 2005. Unloading of an elastic–plastic loaded spherical contact. *International Journal of Solids and Structures, 42*(13), pp.3716-3729.

Fallah, M., Daneshmehr, A., Zarei, H., Bisadi, H., & Minak, G. (2018). Low velocity impact modeling of functionally graded carbon nanotube reinforced composite (FG-CNTRC) plates with arbitrary geometry and general boundary conditions. *Composite Structures*, *187*, 554-565.

Feng, G., Qu, S., Huang, Y., & Nix, W. D. (2007). An analytical expression for the stress field around an elastoplastic indentation/contact. *Acta Materialia*, *55*(9), 2929-2938.

Follansbee, P. S., & Sinclair, G. B. (1984). Quasi-static normal indentation of an elasto-plastic half-space by a rigid sphere—I: Analysis. *International Journal of Solids and Structures*, *20*(1), 81-91.

Gandhi, V. S., Ramesh, S., & Kumaravelan, R. (2012). Analysis of elastic-plastic contact performance of rigid sphere against a deformable flat-effect of strain hardness. *American Journal of Applied Sciences*, *9*(2), 240-245.

Ghaednia, H., Pope, S. A., Jackson, R. L., & Marghitu, D. B. (2016). A comprehensive study of the elasto-plastic contact of a sphere and a flat. *Tribology International*, *93*, 78-90.

Ghaednia, H., Wang, X., Saha, S., Xu, Y., Sharma, A., & Jackson, R. L. (2017). A review of elastic–plastic contact mechanics. *Applied Mechanics Reviews*, *69*(6), 060804.

Giannakopoulos, A. E., & Larsson, P. L. (1997). Analysis of pyramid indentation of pressure-sensitive hard metals and ceramics. *Mechanics of Materials*, *25*(1), 1-35.

Giannakopoulos, A. E., & Suresh, S. (1997a). Indentation of solids with gradients in elastic properties: Part I. Point force. *International Journal of Solids and Structures*, *34*(19), 2357-2392.

Giannakopoulos, A. E., & Suresh, S. (1997b). Indentation of solids with gradients in elastic properties: Part II. Axisymmetric indentors. *International Journal of Solids and Structures*, *34*(19), 2393-2428.

Giannopoulos, G. I., Georgantzinos, S. K., & Anifantis, N. K. (2010). A semi-continuum finite element approach to evaluate the Young's modulus of single-walled carbon nanotube reinforced composites. *Composites Part B: Engineering*, *41*(8), 594-601.

Gojny, F. H., Wichmann, M. H., Fiedler, B., Kinloch, I. A., Bauhofer, W., Windle, A. H., & Schulte, K. (2006). Evaluation and identification of electrical and thermal conduction mechanisms in carbon nanotube/epoxy composites. *Polymer*, *47*(6), 2036-2045.

Gorrasi, G., Milone, C., Piperopoulos, E., Lanza, M., & Sorrentino, A. (2013). Hybrid clay mineral-carbon nanotube-PLA nanocomposite films. Preparation and photodegradation effect on their mechanical, thermal and electrical properties. *Applied Clay Science*, *71*, 49-54.

Gourgiotis, P., & Zisis, T. (2016). Two-dimensional indentation of microstructured solids characterized by couple-stress elasticity. *The Journal of Strain Analysis for Engineering Design*, *51*(4), 318-331.

Green, I. (2005). Poisson ratio effects and critical valus in spherical and cylindrical Hertzian contacts. *Applied Mechanics and Engineering*, *10*(3), 451-462.

Gunes, R., Aydin, M., Apalak, M. K., & Reddy, J. N. (2011). The elasto-plastic impact analysis of functionally graded circular plates under low-velocities. *Composite Structures*, *93*(2), 860-869.

Gupta, M., & Wong, W. L. E. (2015). Magnesium-based nanocomposites: Lightweight materials of the future. *Materials Characterization*, *105*, 30-46.

Hallad, S. A., Banapurmath, N. R., Patil, A. Y., Hunashyal, A. M., & Shettar, A. S. (2016). Studies on the effect of multi-walled carbon nanotube–reinforced polymer-based nano-composites using finite element analysis software tool. *Proceedings of the Institution of Mechanical Engineers, Part N: Journal of Nanomaterials, Nanoengineering and Nanosystems*, *230*(4), 200-212.

Hardy, C. C. N. G. V., Baronet, C. N., & Tordion, G. V. (1971). The elasto-plastic indentation of a half-space by a rigid sphere. *International Journal for Numerical Methods in Engineering*, *3*(4), 451-462.

Hassanzadeh-Aghdam, M. K., & Mahmoodi, M. J. (2017). A comprehensive analysis of mechanical characteristics of carbon nanotube-metal matrix nanocomposites. *Materials Science and Engineering: A*, *701*, 34-44.

Hassanzadeh-Aghdam, M. K., Mahmoodi, M. J., & Ansari, R. (2019). Creep performance of CNT polymer nanocomposites-An emphasis on viscoelastic interphase and CNT agglomeration. *Composites Part B: Engineering*, *168*, 274-281.

Hernot, X., Bartier, O., Bekouche, Y., El Abdi, R., & Mauvoisin, G. (2006). Influence of penetration depth and mechanical properties on contact radius determination for spherical indentation. *International Journal of Solids and Structures*, *43*(14-15), 4136-4153.

Hertz, H. (1881). Über die Berührung fester elastischer Körper. *J reine und angewandte Mathematik*, *92*, 156.

Hou, P. F., Zhang, W. H., Tang, J. P., & Chen, J. Y. (2019). Three-dimensional exact solutions of elastic transversely isotropic coated structures under conical contact. *Surface and Coatings Technology*, *369*, 280-310.

Isaza, C., Sierra, G., & Meza, J. M. (2016). A novel technique for production of metal matrix composites reinforced with carbon nanotubes. *Journal of Manufacturing Science and Engineering*, *138*(2), 024501.

Jackson, R. L., & Green, I. (2005). A finite element study of elasto-plastic hemispherical contact against a rigid flat. *Journal of Tribology*, *127*(2), 343-354.

Jackson, R., Chusoipin, I., & Green, I. (2005). A finite element study of the residual stress and deformation in hemispherical contacts. *Journal of Tribology, 127*(3), 484-493.

Jackson, R.L. and Kogut, L. (2006). A comparison of flattening and indentation approaches for contact mechanics modeling of single asperity contacts. *Journal of Tribology, 128*(1), 209-212.

Jana, T., Mitra, A., & Sahoo, P. (2020). Unloading analysis of elastically and plastically graded hemispherical contact with rigid flat. *Tribology International*, *142*, 105973.

Jin, Z., Pan, E., Zhang, Z., & Liu, K. (2024). Conical indentation over a transversely isotropic and layered elastic half-space. *Mechanics of Materials*, 105081.

Johnson, K. L. (1985). Contact Mechanics. Cambridge University Press.

Jorgensen, O., Giannakopoulos, A. E., & Suresh, S. (1998). Spherical indentation of composite laminates with controlled gradients in elastic anisotropy. *International Journal of Solids and Structures*, *35*(36), 5097-5113.

Kadin, Y., Kligerman, Y., & Etsion, I. (2006). Multiple loading–unloading of an elastic–plastic spherical contact. *International Journal of Solids and Structures*, *43*(22-23), 7119-7127.

Khanna, V., Kumar, V., & Bansal, S. A. (2021). Mechanical properties of aluminium-graphene/carbon nanotubes (CNTs) metal matrix composites: Advancement, opportunities and perspective. *Materials Research Bulletin*, *138*, 111224.

Kim, D., Park, K., Kim, K., Miyazaki, T., Joo, S., Hong, S., & Kwon, H. (2019). Carbon nanotubes-reinforced aluminum alloy functionally graded materials fabricated by powder extrusion process. *Materials Science and Engineering: A*, *745*, 379-389.

Kim, S. H., Lee, B. W., Choi, Y., & Kwon, D. (2006). Quantitative determination of contact depth during spherical indentation of metallic materials—A FEM study. *Materials Science and Engineering: A*, *415*(1-2), 59-65.

Kirtania, S., & Chakraborty, D. (2014). Analysis of carbon nanotube-reinforced alumina matrix nanocomposites with a broken fiber. *Journal of Reinforced Plastics and Composites*, *33*(4), 389-398.

Kirtania, S., & Chakraborty, D. (2018). Determination of thermoelastic properties of carbon nanotube/epoxy composites using finite element method. *Journal of Materials Engineering and Performance*, *27*, 3783-3788.

Kogut, L., & Etsion, I. (2002). Elastic-plastic contact analysis of a sphere and a rigid flat. *Journal of Applied Mechanics*, *69*(5), 657-662.

Kogut, L., & Komvopoulos, K. (2004). Analysis of the spherical indentation cycle for elastic–perfectly plastic solids. *Journal of Materials Research*, *19*(12), 3641-3653.

Kokini, K., Choules, B. D., & Takeuchi, Y. R. (1997). Thermal fracture mechanisms in ceramic thermal barrier coatings. *Journal of Thermal Spray Technology*, *6*, 43-49.

Komvopoulos, K., & Ye, N. (2001). Three-dimensional contact analysis of elastic-plastic layered media with fractal surface topographies. *Journal of Tribology*, *123*(3), 632-640.

Kumar, A., Sharma, K., & Dixit, A. R. (2021). A review on the mechanical properties of polymer composites reinforced by carbon nanotubes and graphene. *Carbon Letters*, *31*(2), 149-165.

Kumar, S. (2023). Investigating effect of CNT agglomeration in CNT/polymer nanocomposites using multiscale finite element method. *Mechanics of Materials*, *183*, 104706.

Kwon, H., Estili, M., Takagi, K., Miyazaki, T., & Kawasaki, A. (2009). Combination of hot extrusion and spark plasma sintering for producing carbon nanotube reinforced aluminum matrix composites. *Carbon*, *47*(3), 570-577.

Larsson, P. L., Giannakopoulos, A. E., Soderlund, E., Rowcliffe, D. J., & Vestergaard, R. (1996). Analysis of Berkovich indentation. *International Journal of Solids and Structures*, *33*(2), 221-248.

Li, L., Etsion, I., Fanslau, E. B., & Talke, F. (2009). An Analysis of the Dimple/Gimbal Contact in a Hard Disk Drive Suspension. In *Proceedings of Joint Conference on Micromechatronics for Information and Precision Equipment,* The Japan Society of Mechanical Engineers, 105-106.

Lichinchi, M., Lenardi, C., Haupt, J., & Vitali, R. (1998). Simulation of Berkovich nanoindentation experiments on thin films using finite element method. *Thin Solid Films*, *312*(1-2), 240-248.

Liew, K. M., Lei, Z. X., & Zhang, L. W. (2015). Mechanical analysis of functionally graded carbon nanotube reinforced composites: a review. *Composite Structures*, *120*, 90-97.

Liu, Q., Fan, G., Tan, Z., Guo, Q., Xiong, D., Su, Y., Li, Z. & Zhang, D. (2021). Reinforcement with intragranular dispersion of carbon nanotubes in aluminum matrix composites. *Composites Part B: Engineering*, *217*, 108915.

Liu, T. J., & Wang, Y. S. (2008). Axisymmetric frictionless contact problem of a functionally graded coating with exponentially varying modulus. *Acta Mechanica*, *199*, 151-165.

Liu, Y. J., & Chen, X. L. (2003). Evaluations of the effective material properties of carbon nanotube-based composites using a nanoscale representative volume element. *Mechanics of materials*, *35*(1-2), 69-81.

Liu, Z. Y., Xiao, B. L., Wang, W. G., & Ma, Z. Y. (2012). Elevated temperature tensile properties and thermal expansion of CNT/2009Al composites. *Composites Science and Technology*, *72*(15), 1826-1833.

Lusti, H. R., & Gusev, A. A. (2004). Finite element predictions for the thermoelastic properties of nanotube reinforced polymers. *Modelling and Simulation in Materials Science and Engineering*, *12*(3), S107-S119.

Lyashenko, I. A., & Popov, V. L. (2020). The effect of contact duration and indentation depth on adhesion strength: Experiment and numerical simulation. *Technical Physics*, *65*, 1695-1707.

Lyashenko, I. A., Pham, T. H., & Popov, V. L. (2024). Effect of indentation depth on friction coefficient in adhesive contacts: Experiment and Simulation. *Biomimetics*, *9*(1), 52, 1-25.

Maji, P., Rout, M., & Karmakar, A. (2020). Free vibration response of carbon nanotube reinforced pretwisted conical shell under thermal environment. *Proceedings of the Institution of Mechanical Engineers, Part C: Journal of Mechanical Engineering Science*, *234*(3), 770-783.

Majumder, S., McGruer, N. E., Adams, G. G., Zavracky, P. M., Morrison, R. H., & Krim, J. (2001). Study of contacts in an electrostatically actuated microswitch. *Sensors and Actuators A: Physical*, *93*(1), 19-26.

Majumder, S., McGruer, N., & Adams, G. G. (2003). Contact resistance and adhesion in a MEMS microswitch. In *International Joint Tribology Conference* 37068, 79-84.

Megalingam, A., & Mayuram, M. M. (2014). Effect of surface parameters on finite element method based deterministic Gaussian rough surface contact model. *Proceedings of the Institution of Mechanical Engineers, Part J: Journal of Engineering Tribology*, *228*(12), 1358-1373.

Miyamoto, Y., Kaysser, W. A., Rabin, B. H., Kawasaki, A., & Ford, R. G. (Eds.). (2013). Functionally graded materials: design, processing and applications (Vol. 5). *Springer Science & Business Media.*

Moharrami, N., & Bull, S. J. (2014). A comparison of nanoindentation pile-up in bulk materials and thin films. *Thin Solid Films*, *572*, 189-199.

Nahas, M. N. (2017). Finite element modeling of carbon nanotubes and their composites. *Computational Finite Element Methods in Nanotechnology*. CRC Press, 291-309.

Nahas, M. N., & Alzahrani, M. A. (2012). Finite element analysis of the effective mechanical properties of a nano scale cubic element of epoxy reinforced with monolayer graphene. *Journal of Computational and Theoretical Nanoscience*, *9*(5), 707-710.

Nguyen, P. D., & Duc, N. D. (2024). A semi-analytical sinusoidal shear deformation theory for nonlinear dynamic response and vibration of CNT–FGM doubly curved shallow shells. *Acta Mechanica*, *235*(4), 2077-2112.

Nieto, A., Agarwal, A., Lahiri, D., Bisht, A., & Bakshi, S. R. (2021). *Carbon nanotubes: reinforced metal matrix composites*. CRC Press.

N'Jock, M. Y., Roudet, F., Idriss, M., Bartier, O., & Chicot, D. (2016). Work-of-indentation coupled to contact stiffness for calculating elastic modulus by instrumented indentation. *Mechanics of Materials*, *94*, 170-179..

Nouri, N., Ziaei-Rad, S., Adibi, S., & Karimzadeh, F. (2012). Fabrication and mechanical property prediction of carbon nanotube reinforced Aluminum nanocomposites. *Materials & Design*, *34*, 1-14.

Ogar, P., Ugryumova, E., Gorokhov, D., & Zhuk, A. (2021). Influence of the characteristics of hardenable material on elastoplastic flattening of spherical asperities. *Materials Today: Proceedings*, *38*, 1638-1643.

Olsson, E., & Larsson, P. L. (2016). A unified model for the contact behaviour between equal and dissimilar elastic–plastic spherical bodies. *International Journal of Solids and Structures*, *81*, 23-32.

Papadopoulos, P., & Solberg, J. M. (1998). A Lagrange multiplier method for the finite element solution of frictionless contact problems. *Mathematical and Computer Modelling*, *28*(4-8), 373-384.

Pau, M., Leban, B., & Baldi, A. (2006). Experimental analysis of contact for the indentation of a flat rounded punch. *International Journal of Solids and Structures*, *43*(25-26), 7959-7965.

Peng, H., Liu, Z., & Zhang, G. (2013). A study of overall contact behavior of an elastic perfectly plastic hemisphere and a rigid plane. *Proceedings of the Institution of Mechanical Engineers, Part J: Journal of Engineering Tribology*, *227*(3), 259-274.

Phani, P. S., & Oliver, W. C. (2019). A critical assessment of the effect of indentation spacing on the measurement of hardness and modulus using instrumented indentation testing. *Materials & Design*, *164*, 107563.

Phung-Van, P., Nguyen-Thoi, T., Luong-Van, H., & Lieu-Xuan, Q. (2014). Geometrically nonlinear analysis of functionally graded plates using a cell-based smoothed three-node plate element (CS-MIN3) based on the C0-HSDT. *Computer Methods in Applied Mechanics and Engineering*, *270*, 15-36.

Qin, J., Huang, Y., Xiao, J., & Hwang, K. C. (2009). The equivalence of axisymmetric indentation model for three-dimensional indentation hardness. *Journal of Materials Research*, *24*, 776-783.

Radhamani, A. V., Lau, H. C., & Ramakrishna, S. (2018). CNT-reinforced metal and steel nanocomposites: A comprehensive assessment of progress and future directions. *Composites Part A: Applied Science and Manufacturing*, *114*, 170-187.

Ramamurty, U., & Jang, J. I. (2014). Nanoindentation for probing the mechanical behavior of molecular crystals–a review of the technique and how to use it. *CrystEngComm*, *16*(1), 12-23.

Rashidifar, M. A., & Ahmadi, D. (2015). Vibration analysis of randomly oriented carbon nanotube based on FGM beam using Timoshenko theory. *Advances in Mechanical Engineering*, *7*(2), 653950, 1-10.

Rodríguez-Tembleque, L., García-Macías, E., & Sáez, A. (2018). CNT-polymer nanocomposites under frictional contact conditions. *Composites Part B: Engineering*, *154*, 114-127.

Rubel, R. I., Ali, M. H., Jafor, M. A., & Alam, M. M. (2019). Carbon nanotubes agglomeration in reinforced composites: A review. *AIMS Materials Science*, *6*(5), 756-780.

Saba, F., Zhang, F., Sajjadi, S. A., Haddad-Sabzevar, M., & Li, P. (2016). Pulsed current field assisted surface modification of carbon nanotubes with nanocrystalline titanium carbide. *Carbon*, *101*, 261-271.

Saito, Y., Tani, Y., Miyagawa, N., Mitsushima, K., Kasuya, A., & Nishina, Y. (1998). High yield of single-wall carbon nanotubes by arc discharge using Rh–Pt mixed catalysts. *Chemical Physics Letters*, *294*(6), 593-598.

Sarkar, S., & Das, P. K. (2014). Dry sliding wear characteristics of carbon nanotube/alumina nanocomposites under a sharp pyramidal indenter. *Ceramics International*, *40*(9), 13971-13978.

Sears, A., & Batra, R. C. (2006). Buckling of multiwalled carbon nanotubes under axial compression. *Physical Review B—Condensed Matter and Materials Physics*, *73*(8), 085410-11.

Selim, B. A., Zhang, L. W., & Liew, K. M. (2017). Impact analysis of CNT-reinforced composite plates based on Reddy's higher-order shear deformation theory using an element-free approach. *Composite Structures*, *170*, 228-242.

Sharma, A., & Jackson, R. L. (2017). A finite element study of an elasto-plastic disk or cylindrical contact against a rigid flat in plane stress with bilinear hardening. *Tribology Letters*, *65*, 1-12.

Sharma, S., & Singh, B. P. (2021). Mechanical Properties of Graphene–Carbon Nanotube Reinforced Hybrid Polymer Nanocomposites.

Shen, H. S. (2009). Nonlinear bending of functionally graded carbon nanotube-reinforced composite plates in thermal environments. *Composite Structures*, *91*(1), 9-19.

Shen, H. S., & Zhang, C. L. (2010). Thermal buckling and postbuckling behavior of functionally graded carbon nanotube-reinforced composite plates. *Materials & Design*, *31*(7), 3403-3411.

Shi, Z., Feng, X., Huang, Y., Xiao, J., & Hwang, K. C. (2010). The equivalent axisymmetric model for Berkovich indenters in power-law hardening materials. *International Journal of Plasticity*, *26*(1), 141-148.

Shin, S. E., Ko, Y. J., & Bae, D. (2016). Mechanical and thermal properties of nanocarbon-reinforced aluminum matrix composites at elevated temperatures. *Composites Part B: Engineering*, *106*, 66-73.

Shokrieh, M. M., & Rafiee, R. (2010). A review of the mechanical properties of isolated carbon nanotubes and carbon nanotube composites. *Mechanics of composite materials*, *46*, 155-172.

Shtaerman, I. Y. (1949). Contact problem of the theory of elasticity. *Gostekhizdat, Moscow*.
Sinclair, G. B., Follansbee, P. S., & Johnson, K. L. (1985). Quasi-static normal indentation of an elasto-plastic half-space by a rigid sphere—II. Results. *International Journal of Solids and Structures*, *21*(8), 865-888.

So, K. P., Kushima, A., Park, J. G., Liu, X., Keum, D. H., Jeong, H. Y., Yao, F., Joo, S.H., Kim, H.S., Kim, H. & Lee, Y. H. (2018). Intragranular dispersion of carbon nanotubes comprehensively improves aluminum alloys. *Advanced Science, 5*(7), 1800115, 1-8.

Song, W., Ovcharenko, A., Li, L., & Talke, F. E. (2013). Flattening of a deformable sphere by a rigid sphere during transient thermo-mechanical contact. *Wear*, *300*(1-2), 29-37.

Song, Z. G., Zhang, L. W., & Liew, K. M. (2016). Dynamic responses of CNT reinforced composite plates subjected to impact loading. *Composites Part B: Engineering*, *99*, 154-161.

Song, Z., & Komvopoulos, K. (2013). Elastic–plastic spherical indentation: deformation regimes, evolution of plasticity, and hardening effect. *Mechanics of Materials*, *61*, 91-100.

Song, Z., & Komvopoulos, K. (2014). An elastic–plastic analysis of spherical indentation: Constitutive equations for single-indentation unloading and development of plasticity due to repeated indentation. *Mechanics of Materials*, *76*, 93-101.

Soni, S. K., Thomas, B., & Kar, V. R. (2020). A comprehensive review on CNTs and CNT-reinforced composites: syntheses, characteristics and applications. *Materials Today Communications*, *25*, 101546, 1-37.

Soni, S. K., Thomas, B., Swain, A., & Roy, T. (2022). Functionally graded carbon nanotubes reinforced composite structures: An extensive review. *Composite Structures*, *299*, 116075, 1-22.

Suh, A. Y., & Polycarpou, A. A. (2005). Adhesive contact modeling for sub-5-nm ultralow flying magnetic storage head-disk interfaces including roughness effects. *Journal of Applied Physics*, *97*(10), 104328, 1-11.

Sun, Y., & Liew, K. (2008). The buckling of single-walled carbon nanotubes upon bending: the higher order gradient continuum and mesh-free method. *Computer Methods in Applied Mechanics and Engineering*, *197*(33-40), 3001-3013.

Suresh, S., Giannakopoulos, A. E., & Alcala, J. (1997). Spherical indentation of compositionally graded materials: theory and experiments. *Acta materialia*, *45*(4), 1307-1321.

Tabor, D. (1948). A simple theory of static and dynamic hardness. *Proceedings of the Royal Society of London. Series A. Mathematical and Physical Sciences*, *192*(1029), 247-274.

Taljat, B., & Pharr, G. M. (2004). Development of pile-up during spherical indentation of elastic–plastic solids. *International Journal of Solids and Structures*, *41*(14), 3891-3904.

Tamayo-Vegas, S., Muhsan, A., Liu, C., Tarfaoui, M., & Lafdi, K. (2022). The effect of agglomeration on the electrical and mechanical properties of polymer matrix nanocomposites reinforced with carbon nanotubes. *Polymers*, *14*(9), 1842, 1-17.

Tang, L.C., Wan, Y.J., Peng, K., Pei, Y.B., Wu, L.B., Chen, L.M., Shu, L.J., Jiang, J.X., & Lai, G.Q., (2013). Fracture toughness and electrical conductivity of epoxy composites filled with carbon nanotubes and spherical particles. *Composites Part A: Applied Science and Manufacturing, 45*, 95-101.

Thostenson, E. T., Ren, Z., & Chou, T. W. (2001). Advances in the science and technology of carbon nanotubes and their composites: a review. *Composites Science and Technology*, *61*(13), 1899-1912.

Tzeng, S. H., Tsai, J. L., & Chiu, Y. T. (2008). Characterizing the elastic properties of carbon nanotubes/polyimide nanocomposites. In *6th Asian-Australasian Conference on Composite Materials: Progress of Composites 2008 in Asia and Australasia, ACCM 2008* (pp. 80-83).

Ürk, D., Demir, E., Bulut, O., Çakıroğlu, D., Cebeci, F. Ç., Öveçoğlu, M. L., & Cebeci, H. (2016). Understanding the polymer type and CNT orientation effect on the dynamic mechanical properties of high volume fraction CNT polymer nanocomposites. *Composite Structures*, *155*, 255-262.

Váradi, K., Néder, Z., Friedrich, K., & Flöck, J. (1999). Finite-element analysis of a polymer composite subjected to ball indentation. *Composites Science and Technology*, *59*(2), 271-281.

Vasiliev, A. S., Volkov, S. S., Belov, A. A., Litvinchuk, S. Y., & Aizikovich, S. M. (2017). Indentation of a hard transversely isotropic functionally graded coating by a conical indenter. *International Journal of Engineering Science*, *112*, 63-75.

Wagih, A., & Fathy, A. (2016). Experimental investigation and FE simulation of nano-indentation on Al–Al2O3 nanocomposites. *Advanced Powder Technology*, *27*(2), 403-410.

Wagih, A., Attia, M. A., AbdelRahman, A. A., Bendine, K., & Sebaey, T. A. (2019). On the indentation of elastoplastic functionally graded materials. *Mechanics of Materials*, *129*, 169-188.

Wang, L., & Xiang, Y. (2013). 3D Finite element analysis of a single asperity tangential elastic-plastic deformation characteristics. *Journal of Applied Sciences*, *13*(21), 4688-4694.

Wang, M., Shen, J., Chen, B., Wang, Y., Umeda, J., Kondoh, K., & Li, Y. (2022). Compressive behavior of CNT-reinforced aluminum matrix composites under various strain rates and temperatures. *Ceramics International*, *48*(7), 10299-10310.

Wang, S., Yuan, W., Liang, X., & Wang, G. (2022). A new analytical model for the flattening of Gaussian rough surfaces. *European Journal of Mechanics-A/Solids*, *94*, 104578.

Wang, Y., Yang, G., Lei, X., Li, Q., Rong, L., Hu, X., & Wei, Y. (2019). Metal ductility evaluation by flattening test: The geometry dependence. *International Journal of Pressure Vessels and Piping*, *170*, 40-48.

Wei, C., & Yang, J. F. (2012). A finite element study on the hardness of carbon nanotubes-doped diamond-like carbon film. *Journal of Materials Research*, *27*(1), 330-338.

Wei, Y., Guo, R., Liu, Y., Dong, C., Li, D., Wan, A., & Zhao, G. (2020). Analytical calculation of the tooth surface contact stress of cylindrical gear with variable hyperbolic circular-arc-tooth-trace. *Symmetry*, *12*(8), 1318.

Wu, C. E., Lin, K. H., & Juang, J. Y. (2016). Hertzian load–displacement relation holds for spherical indentation on soft elastic solids undergoing large deformations. *Tribology International*, *97*, 71-76.

Xu, K., Chu, N. R., & Jackson, R. L. (2022). An investigation of the elastic cylindrical line contact equations for plane strain and stress considering friction. *Proceedings of the*

Institution of Mechanical Engineers, Part J: Journal of Engineering Tribology, *236*(9), 1889-1897.

Xue, T., Qin, X., Zhang, S., Wang, Z., & Bai, J. (2024, May). Free vibration analysis of CNT reinforced plates using higher order shear deformation theory. In *Journal of Physics: Conference Series, IOP Publishing, 2760*(1), 012022.

Yang, S., Yu, S., Ryu, J., Cho, J. M., Kyoung, W., Han, D. S., & Cho, M. (2013). Nonlinear multiscale modeling approach to characterize elastoplastic behavior of CNT/polymer nanocomposites considering the interphase and interfacial imperfection. *International Journal of Plasticity*, *41*, 124-146.

Yang, Y. Y., Munz, D., & Schaller, W. (1997). Effect of the stress jump at the interface of a joint on the failure behavior. *International Journal of Fracture*, *87*(4), L113-L118.

Yoo, S. J., Han, S. H., & Kim, W. J. (2013). Strength and strain hardening of aluminum matrix composites with randomly dispersed nanometer-length fragmented carbon nanotubes. *Scripta Materialia*, *68*(9), 711-714.

Yousefi, A. H., Memarzadeh, P., Afshari, H., & Hosseini, S. J. (2020). Agglomeration effects on free vibration characteristics of three-phase CNT/polymer/fiber laminated truncated conical shells. *Thin-Walled Structures*, *157*, 107077, 1-17.

Yu, W., Dai-Ning, F., Ai-Kah, S., & Bin, L. (2007). Effects of radius and orientation of single-walled carbon nanotubes on their nonlinear tensile deformation behaviour. *Chinese Physics Letters*, *24*(1), 248-251.

Yu, Z. Y., Tan, Z. Q., Fan, G. L., Lin, R. B., Xiong, D. B., Guo, Q., Su, Y. S., Li, Z. Q., & Zhang, D. (2018). Young's modulus enhancement and measurement in CNT/Al nanocomposites. *Acta Metallurgica Sinica (English Letters)*, *31*, 1121-1129.

Yuan, X., & Wang, Y. (2018). Radial deformation of single-walled carbon nanotubes adhered to solid substrates and variations of energy: Atomistic simulations and continuum analysis. *International Journal of Solids and Structures*, *144*, 145-159.

Yuan, Z., Han, Y., Zang, S., Chen, J., He, G., Chai, Y., Zhufang, Y. & Fu, Q. (2021). Analysis of the mechanical properties of TiN/Ti multilayer coatings using indentation under a broad load range. *Ceramics International*, *47*(8), 10796-10808.

Zare, Y., & Rhee, K. Y. (2018). A simple model for electrical conductivity of polymer carbon nanotubes nanocomposites assuming the filler properties, interphase dimension, network level, interfacial tension and tunneling distance. *Composites Science and Technology*, *155*, 252-260.

Zarei, H., Fallah, M., Bisadi, H., Daneshmehr, A., & Minak, G. (2017). Multiple impact response of temperature-dependent carbon nanotube-reinforced composite (CNTRC) plates with general boundary conditions. *Composites Part B: Engineering*, *113*, 206-217.

Zeinedini, A., Shokrieh, M. M., & Ebrahimi, A. (2018). The effect of agglomeration on the fracture toughness of CNTs-reinforced nanocomposites. *Theoretical and Applied Fracture Mechanics*, *94*, 84-94.

Zhan, G. D., Kuntz, J. D., Wan, J., & Mukherjee, A. K. (2003). Single-wall carbon nanotubes as attractive toughening agents in alumina-based nanocomposites. *Nature materials*, *2*(1), 38-42.

Zhang, H., Gao, C., Li, H., Pang, F., Zou, T., Wang, H., & Wang, N. (2020). Analysis of functionally graded carbon nanotube-reinforced composite structures: a review. *Nanotechnology Reviews*, *9*(1), 1408-1426.

Zhang, L. W., Lei, Z. X., & Liew, K. (2015). Buckling analysis of FG-CNT reinforced composite thick skew plates using an element-free approach. *Composites Part B: Engineering*, *75*, 36-46.

Zhang, T., Kumari, L., Du, G. H., Li, W. Z., Wang, Q. W., Balani, K., & Agarwal, A. (2009). Mechanical properties of carbon nanotube–alumina nanocomposites synthesized by chemical vapor deposition and spark plasma sintering. *Composites Part A: Applied Science and Manufacturing*, *40*(1), 86-93.

Zhao, B., Zhang, S., Wang, Q. F., Zhang, Q., & Wang, P. (2015). Loading and unloading of a power-law hardening spherical contact under stick contact condition. *International Journal of Mechanical Sciences*, *94*, 20-26.

Ziegler, T., & Kraft, T. (2014). Functionally graded materials with a soft surface for improved indentation resistance: Layout and corresponding design principles. *Computational Materials Science*, *86*, 88-92.

Zuberi, M. J. S., & Esat, V. (2015). Investigating the mechanical properties of single walled carbon nanotube reinforced epoxy composite through finite element modelling. *Composites Part B: Engineering*, *71*, 1-9.

Publications from the Thesis

This page is left blank intentionally

International Journal of Surface Engineering and Interdisciplinary Materials Science
Volume 10 • Issue 1

Flattening Cylindrical Contact Analysis of Single Walled Carbon Nanotube (SWCNT) Nanocomposite

Rakesh Bhadra, Jadavpur University, India
https://orcid.org/0000-0002-4661-8151

Tamonash Jana, Mallabhum Institute of Technology, India
https://orcid.org/0000-0002-4673-5534

Anirban Mitra, Jadavpur University, India*
https://orcid.org/0000-0003-3530-9123

Prasanta Sahoo, Jadavpur University, India

ABSTRACT

The present study examines the effects of changes in single-wall carbon nanotube (SWCNT) volume % in an Al reinforced nanocomposite under loading and unloading in a cylindrical flattening contact. Flattening action is provided by a rigid flat, which moves downward and upward to simulate the loading and unloading stages, respectively. The cylinder is modelled as a 2D quarter-circle, which consists of the embedded CNTs. Volume % of the nanotubes is varied by changing the wall thickness and number of CNTs, while the overall radius is kept fixed. Finite element model to perform a plane stress quasi-static analysis is created using ANSYS. The simulated results are compared with results from published studies to satisfactorily validate it. Various parameters, in the contact zone and in the vicinity of the CNTs, are presented as results. It is found that above a certain CNT thickness, higher volume percentage of CNTs result in higher contact force as well as contact area. Additionally, more matrix material in the asperity is found to yield plastically for higher volume percentage of CNTs.

KEYWORDS

Al-SWCNT, ANSYS, Carbon Nanotube, Contact Simulation, Finite Element Analysis, Flattening Contact, Plane Stress

INTRODUCTION

Selection of appropriate materials for a particular application is an important requirement in the context of modern industrial growth and use of advanced machineries, where, invariably there is relative motion between contacting surfaces of different machine parts. Contact phenomena are frequently

DOI: 10.4018/IJSEIMS.313629 *Corresponding Author

This page is left blank intentionally

Reports in Mechanical Engineering
Vol. 4, No. 1, 2023, pp. 121-130
ISSN: 2683-5894, DOI: https://doi.org/10.31181/rme040102082023b

Effect of CNT radius on flattening contact behaviour of CNT-Al nanocomposite: A numerical approch

Rakesh Bhadra[1,2], Tamonash Jana[1,3], Anirban Mitra[1] and Prasanta Sahoo[1]
[1]Department of Mechanical Engineering, Jadavpur University, Kolkata 700032, India
[2]Department of Mechanical Engineering, Tezpur University, Sonitpur 784028, India
[3]Department of Mechanical Engineering, IIEST, Shibpur 711103, India

Article Info

Article history:

Received June 24, 2023
Revised July 24, 2023
Accepted August 2, 2023

Keywords:

Contact Simulation,
Flattening,
Nanotubes and Nanocomposites,
FEM.

ABSTRACT

In the present paper, a flattening contact analysis of CNT-Al nanocomposite is presented for both loading and unloading phases. APDL code is used in ANSYS framework to create the FE model to analyse the contact behaviour between a frictionless cylinder (CNT-Al) and a rigid flat. The developed model has been validated against established results of certain problems with lesser complexity. The contact force, contact area, von Mises stresses and nodal displacements are extracted from the simulated solution. These parameters are noted at the end of the loading step and also once unloading is completed from a certain interference. It has been found that as CNT radius increases, the contact properties get decreased. It's also observed that beyond a certain CNT radius, the contact properties of CNT-Al nanocomposite materials start to resemble those of the matrix material and eventually fall below the matrix material.

Corresponding Author:

Anirban Mitra,
Department of Mechanical Engineering, Jadavpur University, Kolkata 700032, India.
Email: anirban.mitra@jadavpuruniversity.in

1. Introduction

Nanotechnology is one of the latest developments in the advancement of engineering and technological application. Contounous growth in nanocomposite applications in various domains establish its increasing importance and underscores its capabilities in enhancing material strength and capacity. In this regard, use of carbon nanotubes (CNTs) as rainforcement material in the nanocomposite, to obtain substantial improvements in material properties and its usefulness in arresting crack growth [Kirtania & Chakraborty, 2007], must be mentioned. A very interesting domain of application related to fluid mechanics has been recently brought forward, where, CNT embedded boundary layer is utilized for energy harvesting [He & Elazem, 2021]. The theory discussed in the paper relates to applications of nanosensors, thermal and nanocomposite materials, resonators, nanomechanical gears etc. In the field of solid mechanics, use of nanocomposites with embedded CNTs to mitigate problems related to contact is another area of application with potential. Contacting parts of machine elements (for example, gears, cams, bearings etc.), which are usually under rapid loading and unloading, are often susseptible to failure. At such contact interfaces there is asperity level contact resulting in high stresses being developed. Use of nanocomposites in such contact scenarios to improve the contact parameters is a possible solution and requires thorough research.

Loading and unloading contact analysis of cylinders/hemispheres with a rigid plate, that can be thought of as an imitation of a single asperity contact, is one of the foremost areas of research in the above-mentioned domain. Johnson (1985) developed an analytical model to understand the unloading contact behavior with a spherical indenter. The model's predictions were in-line with experimental observations reported by Tabor (1948). The analysis indicated that unloading perfectly followed an elastic path despite extremely high plastic

This page is left blank intentionally

Available online at www.sciencedirect.com

ScienceDirect

Procedia Structural Integrity 60 (2024) 149–164

Structural Integrity Procedia

www.elsevier.com/locate/procedia

Third International Conference on Structural Integrity 2023 (ICONS 2023)

Contact Analysis of CNT-FGM Nanocomposite Using Indentation Contact Model

Rakesh Bhadra[a,b*], Tamonash Jana[c], Anirban Mitra[a] and Prasanta Sahoo[a]

[a]*Department of Mechanical Engineering, Jadavpur University, Kolkata 700032, India*
[b]*Department of Mechanical Engineering, Tezpur University, Sonitpur 784028, India*
[c]*Department of Mechanical Engineering, Institute of Engineering and Management, University of Engineering and Management, Kolkata- 700091, India*

Abstract

In the present paper, carbon nanotube (CNT) reinforced functionally graded (FG) material matrix nanocomposite (CNT-FGM) is indented with a rigid conical indenter and the contact behaviour of the CNT-FGM nanocomposite is analyzed in the context of variation in gradation parameter and wall thickness of the CNTs. The study is conducted on the basis of finite element model, which is developed utilizing Ansys Parametric Design Language (APDL) codes in commercial finite element modelling platform, ANSYS. The material model is developed considering the CNTs are uniformly distributed in the graded matrix, whose elastic properties vary along the direction of indentation. The gradation model, corresponding to the matrix material, adopted for the present study is a power law function. In this study, elastically graded material (EGM)matrix CNT reinforced CNT-FGM nanocomposite has been examined, varying the elastic gradation parameter (+2, 0 and -2) of the matrix material. Additionally, effect of the variations in CNT wall thickness are explored, while maintaining other parameter constant in the nanocomposite. A frictionless contact between the CNT-FGM substrate and rigid indenter is simulated for both loading and unloading process. Prior to extracting pertinent results, the current model undergoes validation by comparing its outcomes with those published in the literature. It is observed that the contact force-displacement plots align satisfactorily for both sets of data. Various contact parameters, such as contact force, contact area, contact pressure distribution, stress distribution, and deformation behavior during the indentation contact, are then extracted from the analysis. The observation indicates that positive gradation parameter result in superior contact properties compared to negative gradation parameters as well as without gradation.

Keywords: Contact Simulation; Nanotubes; FGM: Composites; Indentation and contact force;

* *Corresponding author. Tel.: +91* 033 2414 6666
E-mail address: rakeshbhadra20@gmail.com

10.1016/j.prostr.2024.05.037

This page is left blank intentionally

Structures and Stress Analysis

Institution of MECHANICAL ENGINEERS

Journal of MECHANICAL ENGINEERING SCIENCE

Proc IMechE Part C: J Mechanical Engineering Science
2024, Vol. 238(4) 1125–1141

DOI: 10.1177/09544062231169138
journals.sagepub.com/home/pic
SAGE

Finite element based indentation contact analysis of SWCNT nano-composite

Rakesh Bhadra[1,2], Tamonash Jana[1,3], Anirban Mitra[1] and Prasanta Sahoo[1]

Abstract

The focus of the present study is to simulate the indentation type contact behaviour of single walled carbon nanotube (SWCNT) based nanocomposite. The contact system consists of a deformable Aluminium matrix, reinforced with a group of SWCNTs, and a conical indenter which is assumed as rigid. Downward and upward displacement is imparted on the conical indenter in order to simulate the loading and unloading phases of the contact. The model has been developed using APDL code on the ANSYS platform. Adequacy and validity of the model has been established by comparison with results from already published papers available in literature and the matching between the two sets of results is found to be excellent. In terms of results, contact forces, contact area, contact pressure and deformation behaviour are extracted from the analysis with varying wall thickness of CNTs. Detailed analysis of the obtained results has been carried out and it is found that sink in and pile up (in one particular scenario) behaviour is exhibited. It is also found that due to high deformation of the tubes at high indentation depth, there is material flow towards the axis of symmetry and creation of small elastic zones in the matrix material.

Keywords

Contact simulation, nanotubes, composites, indentation and contact force

Date received: 7 June 2022; accepted: 23 March 2023

Introduction

A composite material is obtained when two or more materials (often with drastically different properties) are combined together without changing the corresponding mechanical properties. If one of the phases of the composite material is in the nano-scale, the material is referred to as a nanocomposite. While in case of alloys there is combination of multiple phases to form a new substance, constituent materials of composite materials do not dissolve or mix into one another. Typically, the matrix phase and reinforcement phase features of composite materials are in harmony. A careful choice of matrix and reinforcements is essential in order to fit desired properties to the intended use.[1,2] The ability to adjust a material's properties is the most crucial feature of composite materials (one can design the required properties). To cater to various specialised applications and improve the mechanical properties, a wide range of reinforcing materials are employed, for example, SiC, B_4C, Y_2O_3, Al_2O_3, TiC, BN, ZnO and carbon nanotubes (CNTs).[3–14] Amongst them CNTs exhibit highly desirable mechanical properties, including a Young's modulus of 1 TPa, tensile strength of 200 GPa, strong thermal conductivity[15,16] and high aspect ratios between 30 and thousands.[17–19] Therefore, CNTs employed as reinforced materials enables significant enhancements to the mechanical properties of the composite.[20,21] As a result, since the beginning of the last decade, CNT-reinforced composites have been an important topic of research.[22]

A crucial first step in the design and study of components comprised of such materials is the evaluation of their mechanical properties. So, it is not a surprise that numerous studies employing various techniques to determine these features have been published over the years. Nahas[23] has described the fundamentals of

[1]Department of Mechanical Engineering, Jadavpur University, Kolkata, India
[2]Department of Mechanical Engineering, Tezpur University, Sonitpur, India
[3]Department of Mechanical Engineering, IIEST, Shibpur, India

Corresponding author:
Prasanta Sahoo, Department of Mechanical Engineering, Jadavpur University, 188 Raja S C Mallik Road, Kolkata 700032, India.
Emails: psjume@gmail.com; prasanta.sahoo@jadavpuruniversity.in

This page is left blank intentionally

IOP Publishing Phys. Scr. 99 (2024) 105050 https://doi.org/10.1088/1402-4896/ad7aa5

Physica Scripta

PAPER

RECEIVED
9 February 2024

REVISED
10 July 2024

ACCEPTED FOR PUBLICATION
13 September 2024

PUBLISHED
25 September 2024

Loading-unloading contact analysis of functionally graded carbon nanotube reinforced composite (FG-CNTRC)

Rakesh Bhadra[1,2], **Tamonash Jana**[3], **Anirban Mitra**[1] and **Prasanta Sahoo**[1]

[1] Department of Mechanical Engineering, Jadavpur University, Kolkata 700032, India
[2] Department of Mechanical Engineering, Tezpur University, Sonitpur 784028, India
[3] Department of Mechanical Engineering, Institute of Engineering and Management, University of Engineering and Management, Kolkata, 700091, India

E-mail: psjume@gmail.com **and** prasanta.sahoo@jadavpuruniversity.in

Keywords: contact simulation, nanotubes, composites, FG-CNTRC, contact force

Abstract

The present work deals with a finite element based spherical indentation contact analysis of a functionally graded carbon nanotube reinforced composite (FG-CNTRC) substrate. The gradation in the composite is achieved by varying the distribution of the reinforced CNTs within the matrix material, which is considered to be aluminium in the present study. The finite element modelling and analysis has been performed in finite element software ANSYS platform. The model's validity has been convincingly substantiated through a comparison with the findings of already published relevant articles from the literature. In the present study, a detailed investigation is conducted for three types of CNT distribution in the substrate: increasing, decreasing, and uniform density with depth. The investigation aims to examine the influence of these distributions on different contact behavioral parameters e.g. contact force, contact area, contact stresses etc The analysis would pave a way for modelling and fabricating appropriate FG-CNTRC substrate for a desired as well as damage resistant surface contact behavior.

1. Introduction

Carbon nanotubes (CNTs) have emerged as outstanding reinforcement material for composites, owing to their exceptional mechanical, electrical, thermal and vibrational properties. As far as mechanical properties are concerned, CNTs have Young's modulus of around 1 TPa, tensile strength of 200 GPa, high aspect ratios between 30 and thousands and fundamental natural frequencies of the order of Terahertz (arising out of enhanced elastic modulus along with extremely small diameter) [1–4]. CNTs have been demonstrated to impart strong anisotropic characteristics due to their exceptionally high aspect ratio. It leads to the possibility that specific distribution of these tubes within a matrix material can be utilized to obtain materials with properties tailored to specific applications. As reinforcements, carbon nanotubes (CNTs) are already proven to significantly enhance the composite material's strength, stiffness, and fracture toughness. Hence, it is no surprise that CNT-reinforced nanocomposites have garnered significant attention since the start of the previous decade [5] and continue to captivate researchers with their potential to revolutionize various industries, including aerospace, automotive, electronics and energy sectors [6]. Utilizing industry-standard fabrication techniques, CNT-based nanocomposites with metal and polymer as matrix material have been fabricated and investigated by large number of researchers [6]. It has been conclusively demonstrated that volume percentage of CNTs significantly affects the mechanical, thermal and electrical properties of the nanocomposites [7–11].

Extensive investigations have been carried out pertaining to CNT-reinforced nanocomposites, highlighting the noteworthy potential of carbon nanotube (CNT) and polyimide nanocomposites within a diverse spectrum of application domains. In order to investigate the mechanical attributes of this innovative material, a multi-scale Finite Element Method (FEM) simulation methodology had been employed to decipher the behaviour of CNT within the nanocomposite matrix [12, 13]. Furthermore, Giannopoulos *et al* conducted a similar Finite

This page is left blank intentionally

Physica Scripta

PAPER

RECEIVED
30 June 2025

REVISED
11 September 2025

ACCEPTED FOR PUBLICATION
16 September 2025

PUBLISHED
29 September 2025

Carbon nanotube (CNT) reinforced functionally graded material matrix composite (CNTR-FGMMC) under flattening contact

Rakesh Bhadra[1], **Tamonash Jana**[2], **Anirban Mitra**[3,*] and **Prasanta Sahoo**[3]

[1] Department of Mechanical Engineering, Tezpur University, Sonitpur - 784028, India
[2] Department of Mechanical Engineering, Institute of Engineering and Management, University of Engineering and Management, Kolkata, 700091, India
[3] Department of Mechanical Engineering, Jadavpur University, Kolkata - 700032, India
[*] Author to whom any correspondence should be addressed.

E-mail: anirban.mitra@jadavpuruniversity.in

Keywords: flattening, contact simulation, nanotubes, composites, FGM-CNT, contact force

Abstract

In industrial machines and machine elements, it is quite common to find contact between surfaces under various loading conditions. Interaction between such contacting surfaces during loading and subsequent unloading and the responses of the contact system are important in terms of the longevity and sustainability of the components. The present work studies flattening contact of a carbon nanotube (CNT) reinforced functionally graded material (FGM) matrix nanocomposite (CNTR-FGMMC) using a finite element-based cylindrical contact model. It focuses on the effect of gradation parameter or index of the functionally graded matrix material. The FGM is treated as an elastically-graded material, where both the modulus of elasticity and tangent modulus vary while the yield strength remains constant. The finite element model has been tested for convergence and validity by comparison with established results from systems with lesser complexity. The flattening analysis is conducted by varying elastic inhomogeneity/gradation parameters while maintaining a constant wall thickness of CNTs. Stress and deformation behaviours, including contact force and contact area, throughout the loading and unloading phases as gradation parameters vary. Additionally, the analysis encompasses an examination of energy losses attributed to plasticity. The study reveals that the gradation parameter plays a significant role in contact behaviour.

1. Introduction

The interaction between contact surfaces during loading and unloading is an important aspect in determining the longevity of contact-engaged components. Rapid stress increases during loading, followed by sudden decrease during unloading, can lead to micro-crack formation, which poses challenges for interconnected machine components. In the context of modern micro and nanotechnology advancements, such as MEMS microswitches [1, 2], AFM systems [3] and magnetic storage devices [4, 5], a flattening-based single asperity contact analysis is a first step towards comprehensive understanding of such a complex contact phenomenon.

Contact analysis has a history of more than a century of pioneering research work and a steady stream of work has been ongoing throughout pushing the boundaries of the domain. In the late 19th century, Hertz [6] correlated force, contact area and deformation in contact models, proposing an elliptical nature for the contact surface. The fundamental assumptions of the theory are: (i) the surfaces are smooth and frictionless, (ii) deformations are purely elastic, and (iii) the contact area is much smaller than the dimensions of the bodies. A flattening contact between a cylindrical asperity and a rigid flat, can be conveniently based on Hertzian contact theory [7]. Subsequent researchers extended this theory to address both macro and micro contact issues.

Johnson [8] expanded the knowledge by presenting equations for contact radius and deformation in circular contact, as well as parameters like half-bandwidth and maximum contact pressure for parallel cylinders. Ghaednia *et al* [9] explored the integration of the yield strength ratio into elastic-plastic contact modeling,

This page is left blank intentionally

Contact Analysis of Functionally Graded Carbon Nanotubes Reinforced Composite (FG-CNT)

Rakesh Bhadra, Tamonash Jana, Anirban Mitra, and Prasanta Sahoo

Abstract The primary focus of this study is to examine how the arrangement of carbon nanotubes (CNTs) within a functionally graded nanocomposite (FG-CNT) impacts its behavior. A finite element model for contact, based on spherical indentation, is created using APDL code within the ANSYS platform. The analysis involves three different distribution patterns: uniform distribution (FG-UD), distribution with decreasing order (FG-V), and distribution with increasing order (FG-Λ) from the contact surface toward the base. The model's accuracy is confirmed by comparing its results with existing literature. Key parameters such as contact force, contact area, stress distribution, and deformation characteristics are extracted from the contact model. Through a detailed investigation, it is found that the FG-V distribution pattern exhibits enhanced contact properties.

Keywords Carbon nanotubes · Nanocomposites · FG-CNT · FEM · Indentation contact simulation

1 Introduction

In contemporary engineering applications, Functionally Graded Materials (FGMs) have gained widespread acceptance and application across various domains, including tribology, biomechanics, nanotechnology, sensor technology, thermal barrier coatings for turbine blades, and optical/electrical applications [1]. The popularity of FGMs is attributed to their exceptional thermal and mechanical properties,

R. Bhadra (✉) · T. Jana · A. Mitra · P. Sahoo
Department of Mechanical Engineering, Jadavpur University, Kolkata 700032, India
e-mail: rakeshbhadra20@gmail.com

R. Bhadra
Department of Mechanical Engineering, Tezpur University, Sonitpur 784028, India

T. Jana
Department of Mechanical Engineering, Institute of Engineering and Management (IEM), University of Engineering and Management, Kolkata 700091, India

P. Sahoo and T. K. Barman (eds.), *Advances in Materials, Manufacturing and Design*, Lecture Notes in Mechanical Engineering,
https://doi.org/10.1007/978-981-97-6667-3_59

Rakesh Bhadra
14-07-2025